Biochemical and Genetic Studies of

UDP-2,3-Diacylglucosamine Hydrolysis in Lipid A Biosynthesis

by

Hayley E. Young

Department of Biochemistry
Duke University

Date:_____

Approved:

_____
Pei Zhou, Supervisor

_____
Teresa A. Garrett

_____
Meta J. Kuehn

_____
Dewey G. McCafferty

_____
Thomas J. McIntosh

Dissertation submitted in partial fulfillment of
the requirements for the degree of Doctor
of Philosophy in the Department of
Biochemistry in the Graduate School
of Duke University

2014

ABSTRACT

Biochemical and Genetic Studies of

UDP-2,3-Diacylglucosamine Hydrolysis in Lipid A Biosynthesis

by

Hayley E. Young

Department of Biochemistry
Duke University

Date:_____

Approved:

_____
Pei Zhou, Supervisor

_____
Teresa A. Garrett

_____
Meta J. Kuehn

_____
Dewey G. McCafferty

_____
Thomas J. McIntosh

An abstract of a dissertation submitted in partial
fulfillment of the requirements for the degree
of Doctor of Philosophy in the Department of
Biochemistry in the Graduate School of
Duke University

2014

Abstract

The outer-leaflet of the outer membrane of Gram-negative bacteria is composed of lipopolysaccharide (LPS), which is attached to the membrane via a hexa-acylated saccharolipid called lipid A. The fourth step of lipid A biosynthesis involves the cleavage of the pyrophosphate group of UDP-2,3-diacyl-GlcN to form lipid X; this step is carried out by LpxH in *E. coli* and the majority of β- and γ-proteobacteria. LpxH has been previously characterized, however sample impurity and non-optimized assay conditions hindered meaningful conclusions. The enzyme was suggested to contain signature motifs found in the calcineurin-like phosphoesterase (CLP) family of metalloenzymes, however the extent of biochemical data fails to demonstrate a significant level of metal activation in LpxH assays. We report cloning, purification, and detailed enzymatic characterization with a highly purified sample of *H. influenzae* LpxH (HiLpxH). HiLpxH shows over 600-fold stimulation of activity in the presence of Mn^{2+}. Furthermore, EPR studies reveal the presence of a Mn^{2+} cluster in LpxH. Finally, point mutants of residues in the conserved metal-binding motifs of the CLP family greatly inhibit HiLpxH activity, highlighting their importance in enzyme function. Overall, through optimized purification and assay methods, our work unambiguously establishes LpxH as a membrane-associating CLP containing a Mn^{2+} cluster coordinated by conserved residues. These results set the scene for further structural investigation of the enzyme and for design of novel antibiotics targeting lipid A biosynthesis.

Several species of Gram-negative bacteria lack LpxH orthologs, yet retain other lipid A biosynthetic enzymes and still produce lipid A. An unrelated protein, LpxI, is responsible for UDP-DAGn hydrolysis is several such organisms. Interestingly, some bacteria, such as the human pathogen *Chlamydia trachomatis,* have neither LpxH nor LpxI orthologs, suggesting the presence of a third UDP-DAGn hydrolase. Through implantation of a novel complementation screen that used a *C. trachmatis* genomic library and a conditional-lethal *lpxH* mutant *E. coli* strain, we were able to identify an open reading frame encoding an new enzyme capable of lipid X production. Due to its ability to complement UDP-DAGn hydrolase function *in vivo* and catalyze the formation of lipid X *in vitro*, we have designated the enzyme LpxG. Further biochemical analysis with purified LpxG revealed it facilitates hydrolysis through attack on the α phosphate of its substrate and is activated by Mn^{2+} *in vitro.* LpxG is in the same CLP superfamily as LpxH, however it shows very little homology to LpxH or LpxI. Identification of LpxG improves our understanding of the lipid A biosynthetic pathway in *C. trachomatis.* More broadly, as limited genetic tools are available for the study of the prevalent pathogen, it provides an advantageous method for the functional screening of other *C. trachomatis* genes.

Dedication

To my father, whose infectious curiosity guided me towards science at a young age and will forever be a source of inspiration.

To my mother, whose encouragement and conviction has made every obstacle seem surmountable.

To my family, who are truly unending sources of love and support. Their work ethic, selflessness, and integrity have influenced all of my achievements.

To my mentor Pei Zhou, who graciously accepted the responsibility of my guidance. His patience, optimism, and tenacity have been invaluable to my graduate pursuits.

To my mentor Professor Christian H. R. Raetz, whose critical eye for data and experimental design has shaped my development as a scientist. I am extremely proud to be part of his legacy.

Contents

List of Tables

List of Figures

List of Abbreviations

CMC - Critical micelle concentration

CLP - Calcineuin-like phosphoesterase

DDM - Dodecyl maltoside

EDTA - Ethylenediaminetetraacetic acid

EPR - Electron paramagnetic resonance

HEPES - 4-(2-hydroxyethyl)-1-piperazineethanesulfonic acid

Kdo - 3-deoxy-D-*manno*-oct-2-ulosonic acid

LPS - Lipopolysaccharide

LOS - Lipooligosaccharide

ORF - Open reading frame

SDS-PAGE - Sodium dodecyl sulfate-polyacrylamide gel electrophoresis

TLC - Thin-layer chromatography

TLR4 -Toll-like receptor 4

TX-100 - Triton X-100

UDP-DAGn - UDP-2,3-diacylglucosamine

UDP-GlcNAc - UDP-*N*-acetylglucosamine

Acknowledgements

The presented work would not have been possible without the contributions of my colleagues and friends. Thank you to the past members of the Raetz laboratory, especially Dr. Hak Suk Chung, Dr. Louis Metzger, and Dr. Ryan Emptage, for their experimental guidance, intellectual input, and friendship. I also extend my gratitude to Ali Masoudi, Dr. Chuljn Lee, and Dr. Jinshi Zhao for their scientific and emotional support through the transition to the Zhou lab.

Electron paramagnetic resonance experiments were carried out and analyzed by Dr. Alex Smirnov, Dr. Tatyana Smirnova, and Matthew Donohue at North Carolina State University. Mass spectrometry was completed by Dr. Ziquang Guan at Duke University. The lab of Dr. Raphael Valdiva assisted with *Chlamydia trachomatis* studies, providing bacterial samples, open reading frame library, and helpful discussions. This research was funded by N.I.H. grant GM51310 to C.R.H. Raetz and P. Zhou

.

1. Introduction

It is estimated that the global population of bacteria is greater than 10^{30} (1), making these prokaryotes the most prevalent organisms on the planet. Bacteria play a variety of different roles in nature and occupy a gamut of environmental niches, ranging from the human body to deep ocean vents. Current research has even proved that the metabolic power of these organisms can be harnessed and employed for bioremediation (2) or modified to generate efficient biotechnological tools (3). Despite their usefulness, bacteria are also responsible for causing infection and disease of host organisms, often colonizing the respiratory system, gastrointestinal tract, and skin. An increasing number of these infections are being acquired in a hospital setting; in the United States, infections encountered in the hospital or a health care facility affect more than 2 million patients, cost $4.5 billion, and contribute to 88,000 deaths in hospitals annually (4,5). Due to the genetic plasticity of these pathogens, many have developed resistance to currently available antibiotic treatment. A 2013 CDC report estimated that 2 million Americans per year fall ill as a result of antibiotic resistant bacteria, with at least 23,000 of those infections resulting in death.

Due to their threat to human health, as well as their applications to biotechnology, it is advantageous to ascertain more information about bacteria. A more complete understanding of the properties of these organisms will yield information that

can be used to better human life. The work presented in the following chapters is aimed at such a goal and is targeted at the elucidating bacterial processes.

1.1 Classification of Gram-negative Bacteria

Bacteria are often classified by the structure of their outer membrane through use of the Gram staining procedure. Gram-positive bacteria are surrounded by an inner lipid bilayer that is encapsulated by a thick meshwork of sugars and amino acids (Fig.1, left). This structure, termed the peptidoglycan, traps crystal violet during the Gram staining procedure. Conversely, Gram-negative bacteria have a much thinner peptidoglycan that is surrounded by a second lipid bilayer, designated the outer membrane (Fig. 1, right). Because of the thinner peptidoglycan, the crystal violet can be washed away and the bacteria can be dyed by another substance, resulting in a negative Gram test.

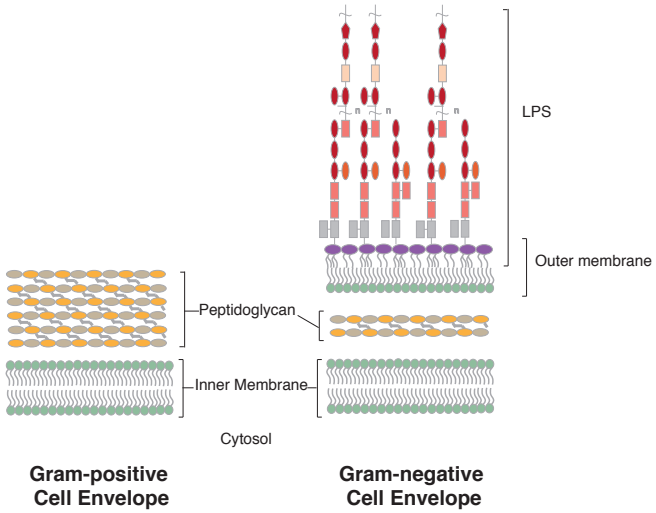

Figure 1: Gram Classification of Bacterial Cell Envelope

1.2 Lipolysaccharide

Besides a less substantial peptidoglycan, a defining characteristic of Gram-negative bacteria is the presence of an outer membrane (Fig. 2). The inner membrane in both Gram-positive and Gram-negative organisms is a symmetric lipid bilayer composed of phospholipids such as phosphotidylglycerol and phosphotidylethanolamine (6). These lipids are also found on the inner leaflet of the outer membrane in Gram-negatives, however the outer leaflet is comprised of lipopolysaccharide (LPS) (6). LPS, also known as endotoxin, is a complex molecule consisting of a long chain of sugars anchored into the membrane by a saccharolipid; it can be sub-divided into three parts: O-antigen, core region, and lipid A. LPS plays an important role in protection of organisms from the environment, especially in a host organism where they encounter low pH, bile, antimicrobial peptides, and proteins of the complement system (6,7). In some Gram-negative bacteria, O-antigen and part of the core region is present, resulting in the designation of the outer membrane moiety as LOS (lipid oligosaccharide) instead of LPS (8). While the identity of sugars comprising LPS can vary across species (core region) and even serotype (O-antigen region), the overall structure remains conserved (7).

1.2.1 O antigen region

The most distal region of LPS, the O-antigen, is also the most variable portion of the molecule (7) (Fig. 2). In some species, it is a linear chain of sugar repeats, while in

others, it is modified with phosphorylations and glycosidic branches. Variations in the O-antigen are seen within the same organism, with non-uniform chain lengths and branch sites forming LPS heteropolymers. This variation appears to be modal, and a distinct LPS profile is usually detectable for specific organisms (7).

The O-antigen plays an important role in protecting the cell from its outside environment. It can also assist in the evasion of host immune responses, protecting the bacteria from the complement system and altering its sensitivity to neutrophil response and bactericidal and permeability-increasing proteins (9). Identity of the O-antigen often designates the serotype of a bacterial species, as it often is a target for production of host antibodies. There are 170 O-serotypes of *Escherichia coli*, speaking to the immense diversity of the O-antigen. Laboratory strains such as *E. coli* K-12 lack O-antigen.

Genes contained in the *rfb* locus usually carry out the synthesis of the O-antigen (10). These encoded enzymes are glycosyl trasferases that employ sugar nucleotides as substrates; they function in the cytosol or on the periphery of the inner membrane. The growing polysaccharide is assembled on the membrane carrier undecaprenyl phosphate (UndP, C_{55}) that is also used in synthesis of peptidoglycan and lipid A modification (11). The formation of undecaprenyl pyrophosphate-linked glycose through transfer of a sugar-1-phosphate residue to UndP traps energy in the pyrophosphate bond. This energy is later used to drive the ligation reaction to core lipid A after polymerization.

The *rfb* genes are not essential for bacterial survival, particularly in a laboratory setting, however they do enhance survivability in the host.

1.2.2 Core Region

The core region is found proximal to the O-antigen region (Fig. 2). In *E. coli*, it is subdivided into an inner and outer core, with the outer core being the site of O-antigen attachment. In many mucosal pathogens, specifically *Neiserria gonohorroae* (8) and *Chlamydia trachomatis (12),* there is no outer core and the inner core extends into branches; these branches serve to determine serological specificity in such organisms. The structure of inner and outer core seems to be well conserved in Gram-negative bacteria on the genus and sometimes the family level (7). In fact, similarity can be seen in the inner core of highly divergent species, with two 3-deoxy-D-*manno*-oct-ulosonic acid (Kdo) comprising this region in nearly all Gram-negative bacteria (7).

Similar to the O-antigen, the core plays an important role in protecting Gram-negative bacteria from their extracellular environment. Bacteria with mutations in core synthesis enzymes show changes in hydrophilicity, resulting in hypersensitivity to hydrophobic dyes, detergents, hydrophobic antibiotics, fatty acids, phenols, and polycyclin hydrocarbons (13). Such mutants have also been noted for leaky outer membranes, releasing proteins into the cytosol unless high concentrations of Mg^{2+} are present in growth media. Some bacteria, such as *Salmonella* and *Pseudomonas*, modify their core LPS sugars with phosphorylations. Divalent cations bridge these

phosphorylations on neighboring LPS, creating a strong protective barrier for the cell. In *Pseudomonas aeruginosa*, such phosphorylations are required for viability (14).

Also like O-antigen synthesis enzymes, core synthesis enzymes are glycosyltransferases that use sugar nucleotide donors (10). In *E. coli*, these proteins are often peripherally associated with the inner leaflet of the inner membrane and directly add carbohydrate moieties to Kdo_2 lipid A. As discussed below, the Kdo portion of the inner core is usually incorporated by KdtA (WaaA) before the completion of lipid A synthesis. The rest of the core is assembled by enzymes found in the *waa* operon working in sequence. Outer core synthesis genes are often non-essential in a laboratory setting. Inner core synthesis, however, does seem to be important for bacterial viability. This is presumably due to the specificity of the transport machinery that exports lipid A across the inner membrane (see below).

1.2.3 Lipid A

Lipid A serves as the hydrophobic anchor to LPS (Fig. 2). Its acylated di-glucosamine structure is highly conserved throughout LPS-containing Gram-negative bacteria (6). Besides indirectly shielding organisms through attaching the protective O-antigen and core region to the membrane, lipid A also had a direct role in defense. The presence of many saturated hydrocarbon chains on lipid A reduce the fluidity of outer membrane. Lipid A is usually phosphorylated, permitting cation bridging between

negatively charged LPS molecules to strengthen the impermeability of the outer membrane.

In addition to a role in permeability, lipid A has been implicated in other bacterial processes. It has been postulated that lipid A is required for the proper folding and function of proteins in the outer membrane. Specifically, the crystal structure of receptor FhuA revealed a non-covalently attached LPS molecule making contact with the protein in the lipid A region (15). Additionally, the outer-membrane protease OmpT has been shown to rely on lipid A for activity (16). Lipid A is also hypothesized to play a role in outer membrane vesiculation in *Porphyromonus gingivalis* and *Pseudomonas aeruginosa*, either through protein sorting, vesicle formation, or interaction with factors influencing vesicle formation (17,18).

Lipid A synthesis is required for viability in nearly all Gram-negatives, even in a laboratory setting (6). Many organisms can tolerate non-threatening growth environments in the absence of O-antigen and core region, but the enzymes synthesizing lipid A cannot be deleted. A noted exception is *Neiserria meningitidis*: deletion of the first gene of lipid A biosynthesis results in a viable organism (19). This mutant does duplicate slowly, however, and only exhibits growth in a laboratory setting. Another notorious pathogen, *Chlamydia trachomatis,* can be inhibited in lipid A synthesis during replication, however this inhibition results in a loss of infectious progeny (20). Additionally, colistin-resistant *Acinetobacter baumannii* have been reported to lack LPS

due to mutations in genes of the lipid A biosynthetic pathway (21). While these *A. baumannii* variants are viable, they do show increased sensitivity to host cationic antimicrobials (22). Thus, lipid A has proved essential for growth and/or infection in a host environment for all LPS-containing Gram-negative bacteria, making its biosynthesis (carried out by the Raetz pathway, as described below) a promising target for the development of antibiotics.

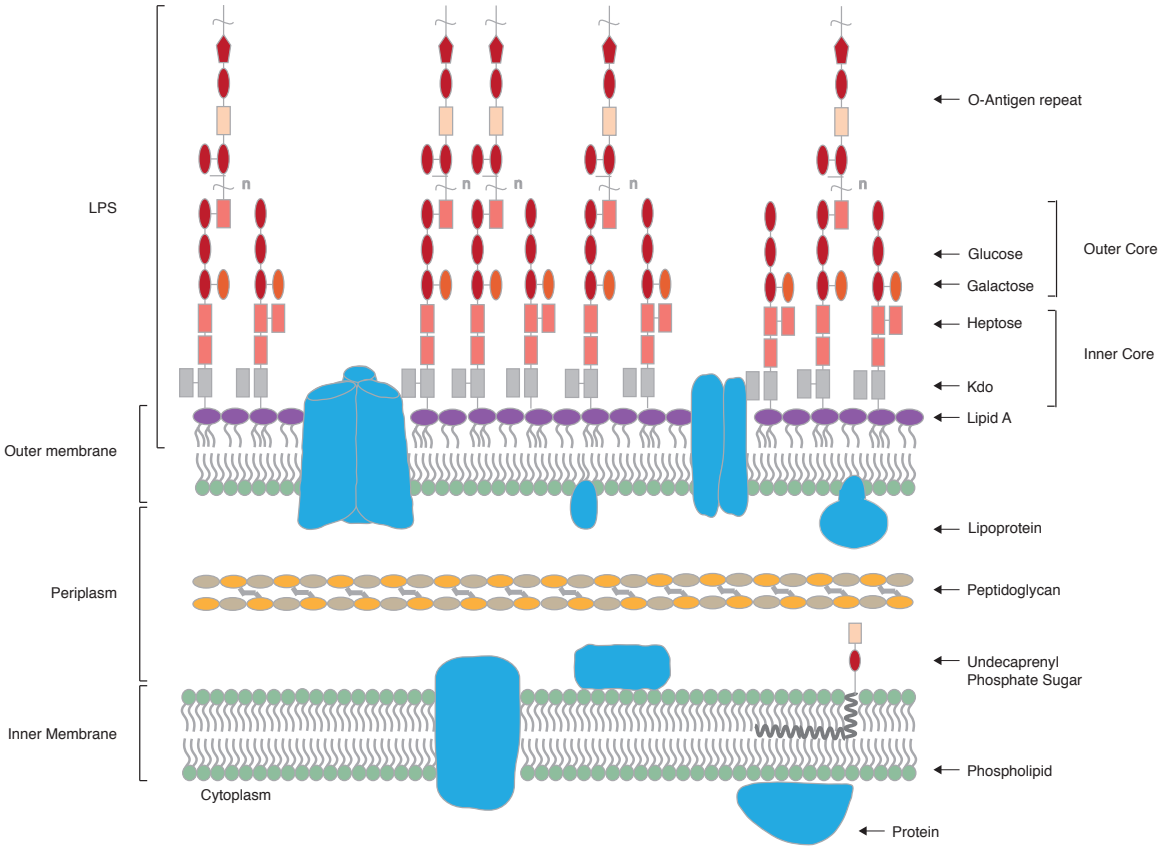

Figure 2: Structure of *Escherichia coli* Cell Envelope

The Gram-negative model organism *E. coli* exhibits the canonical dual membrane structure. The inner membrane is composed of: phospholipids (green), specifically phosphotidylglycerol and phosphotidylethanolamine; proteins (blue), which span the membrane or be associated with the periplasmic or cytosolic face; and undecaprendyl phosphate (gray), which serves to shuttle sugars into the periplasm. A meshwork of sugars and amino acids are cross-linked in the periplasm to form the peptidoglycan (yellow). The outer membrane is an asymmetric bilayer comprised of phospholipids in the inner leaflet and lipopolysaccharide (LPS) in the outer leaflet. Proteins (blue) contained in the outer membrane may be periplasmic-facing, or membrane spanning, serving as porins, channels, and transporters. LPS is made up of a long chain of sugars (red) anchored into the outer membrane by lipid A (purple).

1.3 Lipid A and the Immune Response

Lipid A also plays a crucial role in Gram-negative infection of all vertebrates and assortment of invertebrates (23). Upon invasion of a host, bacteria shed their LPS molecules, which are subsequently recognized by soluble LBP (LPS binding protein) and trafficked to immune cells (24) (Fig. 3). LBP-LPS then interacts with the monocyte differentiation antigen CD14, facilitating the delivery of the LPS to the MD2-Toll-Like Receptor 4 (TLR4) complex on the surface of monocytes, lymphocytes and endothelial cells (25). This complex is a known pattern recognition receptor (PRR) that is an important part of the innate immune system. In the case of TLR4, the activating pattern is the lipid A moiety of LPS (26). Recognition of lipid A is advantageous to the immune system, as this is the most invariant portion of LPS, permitting sensitivity to many Gram-negative organisms.

Interaction of lipid A with MD2-TLR4 triggers receptor dimerization (Fig. 3). This dimerization elicits two response pathways mediated by interaction of signaling proteins with TLR4's cytoplasmic TIR (toll interleukin receptor) domain (27). In the myeloid differentiation primary response protein 88 (MYD88) pathway, NF-κB is induced to upregulate the transcription of pro-inflammatory cytokines such as TNF (tumor necrosis factor), interleukin 6 (IL-6), and IL-2. The TRIF (TIR domain-containing adaptor inducing interferon-β) pathway leads to the upregulation of interferon β (INF-β) and interferon response proteins, such as IFN-γ-induced protein, RANTES, and

granulocyte colony-stimulating factor (G-CSF). These serve to mount the host's adaptive immune response. TRIF signaling occurs after the MD2-TLR4 complex is endocytosed (28,29).

Both aspects of the TLR4-inducing signaling cascade is meant to clear the host of infection through inflammation, cytokine release, recruitment of effector cells, phagocytosis, cytotoxicity, and activation of the complement system (30). However, if the system is over-stimulated, these responses can result in tissue damage, organ failure, or sepsis (29). The latter represents a severe and often fatal inflammatory response of the body to the overwhelming presence of infection and is characterized by organ failure. Thus, in addition to species-specific infection pathologies, sepsis can also be a detrimental outcome of Gram-negative infection.

While lipid A in its hexacylated form is a potent activator of the TLR4 system, modified structures of lipid A dramatically alter the immune response (26,31-33). Studies with lipid A structure variants have revealed that removal of the 1-phosphate prevents complete interaction with TLR4, resulting in the inability of the TIR domain to fully induce the MYD88 pathway (26). Likewise, removal of the secondary acyl chains to yield a tetra-acylated product (lipid IV_A) precludes full interaction with MD2, also resulting in reduction of MYD88 signaling (26). This ability to use structural modification of lipid A to separate the inflammatory response (MYD88) from the adaptive immune response (TRIF) has led to the development of lipid-A based

adjuvants (28). Specifically, a chemically detoxified mixture of lipid A from *Salmonella enterica* susp. Serovar Minnesota, which is primarily composed of 3-O-deacyl-4'-monophosphoryl lipid A, has been approved by the FDA as a vaccine adjuvant. This adjuvant, known as MLP, is a TLR4 agonist and has been effectively used to elicit an immune response in cancer vaccines against human papilloma virus (34). Other work has shown that *Salmonella* can be genetically modified to produce a non-toxic yet strongly immunogenic form of lipid A for use as a whole-cell vaccine (31,32). Further research on the interactions between lipid A and TLR4 could greatly facilitate development for a variety of vaccines.

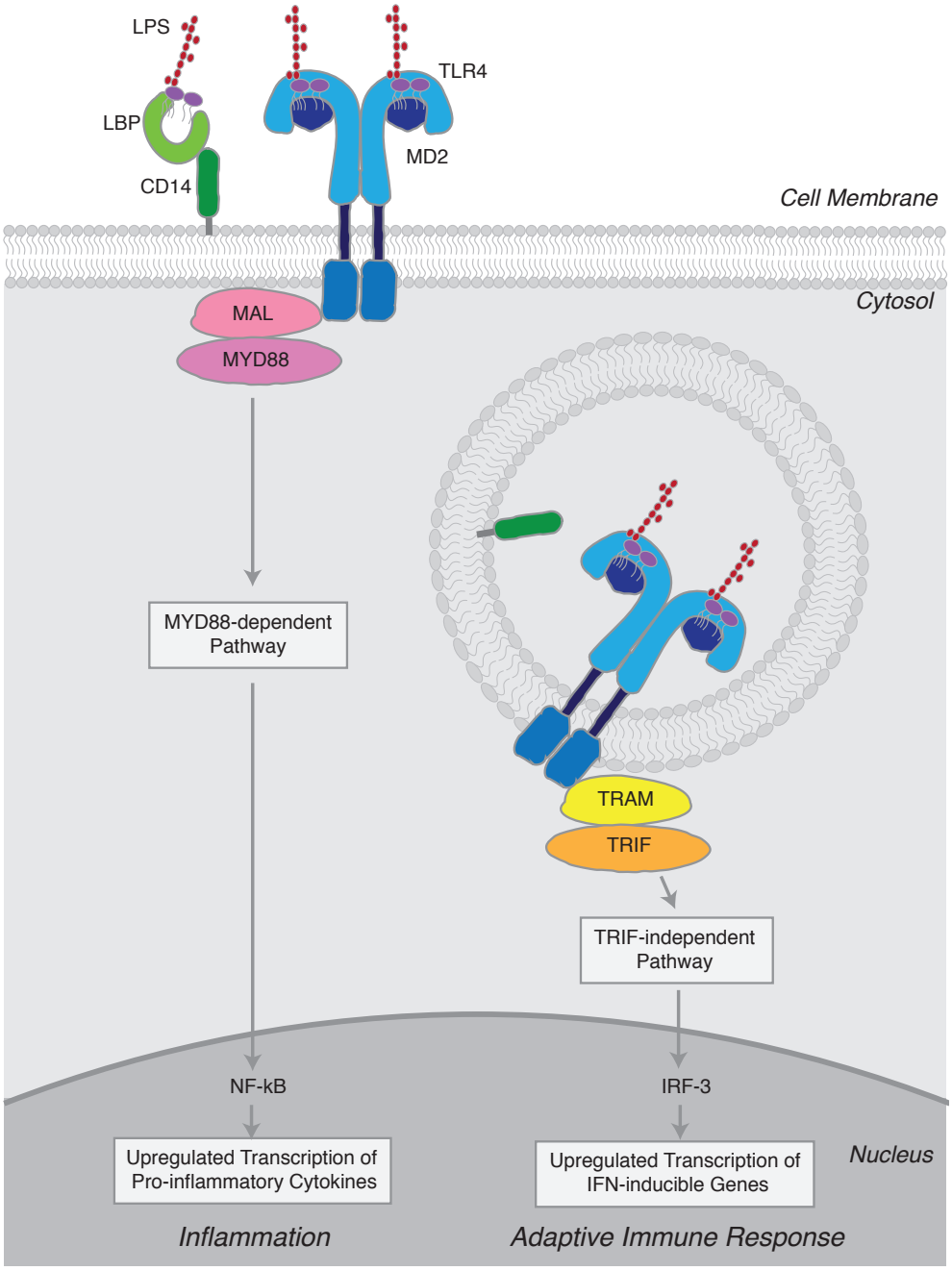

Figure 3: LPS-mediated Immune Response

Caption continues on next page.

Figure 3: In the event of Gram-negative infection, lipid binding protein (LPB) associates with LPS shed from bacteria. CD14 on the surface of immune and endothelial cells facilitates the transfer of LPS to the MD2-TLR4 complex. Subsequent dimerization elicits structural changes in the cytosolic domain of TLR4, leading to cell signaling cascades. In the MYD88-dependent pathway, MAL and MYD88 initiate NF-κB signaling to upregulate transcription of cytokines that leads to an inflammatory response. Alternatively, the TRIF pathway can be triggered after the TLR4-MD2 dimerized complex is endocytosed. This results in the upregulation of interferon-inducible genes by IRF-3, leading to activation of the adaptive immune system. Figure modified from (29).

1.4 Raetz Pathway of Lipid A Biosynthesis

The essentiality, conservation, and immunogenic properties of lipid A make it an intriguing target for the treatment of infections, as inhibitors of its synthesis would be toxic to pathogens, target a broad spectrum of bacteria, and could reduce the chance of sepsis in infected hosts. Thus, the biosynthesis of lipid A, as carried out by the Raetz pathway (Fig. 4) is of particular relevance to study of Gram-negative bacteria. While the pathway is highly conserved in most Gram-negative bacteria, it has been most thoroughly studied in *E. coli.* In this organism, the reactions carried out by the nine constitutive lipid A biosynthetic enzymes take place in the cytosol, membrane periphery, and inner leaflet of the inner membrane.

1.4.1 Cytosolic Steps

The beginning steps of the Raetz pathway are carried out by soluble proteins. In the first step, the acyltransferase LpxA catalyzes the addition of a *R*-3-hydroxymyristate to the 3 position of UDP-N-acetyl-glucosamine (UDP-GlcNAc), employing ACP as the acyl donor (35). In some species, the dehydrogenase GnnA and transaminase GnnB

modify UDP-GlcNAc before its use in lipid A biosynthesis (36,37). This generates a diamino form of the sugar nucleotide in which the 3-OH group is substituted for an amine. Select bacteria have LpxA orthologs that are specific for the diamino precursor, while others can incorporate both the modified and unmodified sugar (37).

As the LpxA reaction is unfavorable, the second step, catalyzed by LpxC, is the committed step of the pathway (38). LpxC is a zinc-dependent enzyme that deacetylates the glucosamine ring of its substrate. Next, LpxD acylates the newly modified nitrogen substituent at the 2 position of the sugar ring (39). LpxD is similar in both sequence and structure to LpxA and also utilizes ACP as the hydrocarbon donor. The third reaction yields UDP-2,3-diacylglucosamine (UDP-DAGn).

1.4.2 Peripheral Steps

The fourth the fifth steps of the Raetz pathway are thought to occur at the periphery of the inner membrane; the enzymes responsible for these reactions are not embedded within the lipid bilayer, but do indicate membrane association. In the fourth step of the pathway in E. coli, LpxH hydrolyzes the pyrophosphate bond in UDP-DAGn to generate UMP and 2,3-diacyl-glucosamine-1-phosphate (lipid X) (40). Many Gram-negative bacteria do not contain orthologs for LpxH and instead employ the unrelated yet functionally identical enzyme LpxI to catalyze UDP-DAGn hydrolysis (discussed below) (41). In both LpxH- and LpxI-containing pathways, the subsequent metabolic step relies on the glycosyl transferase LpxB to join lipid X with a second molecule of

UDP-DAGn (42). This yields UDP and disaccharide mono-phosphate (DSMP); the formation of DSMP is characterized by a β,1′-6 linkage between the glucosamine units, which is a hallmark of the structure of lipid A.

1.4.3 Membrane-bound Steps

After being produced by LpxB, DSMP is phosphorylated at the 4′-position by the P-loop kinase LpxK (43). This enzyme is integrated into the inner membrane and generates a tetracylated product referred to as lipid IV_A. At this point, a portion of the inner core is added to the 6′ hydroxyl moiety of lipid IV_A by membrane-bound KdtA (WaaA) (44). In *E. coli*, KdtA is bi-functional and attaches two units of Kdo, thus producing Kdo_2-lipid IV_A; KdtA orthologs in other bacterial species can be mono- or tri-functional (45). Finally, in the last steps of the pathway, trans-membrane proteins LpxL and LpxM add secondary lauryl and myristyl moieties to the hydroxyl group on the 2′ and 3′ acyl chains, respectively (45,46). This generates the final hexacylated product, Kdo_2-lipid A.

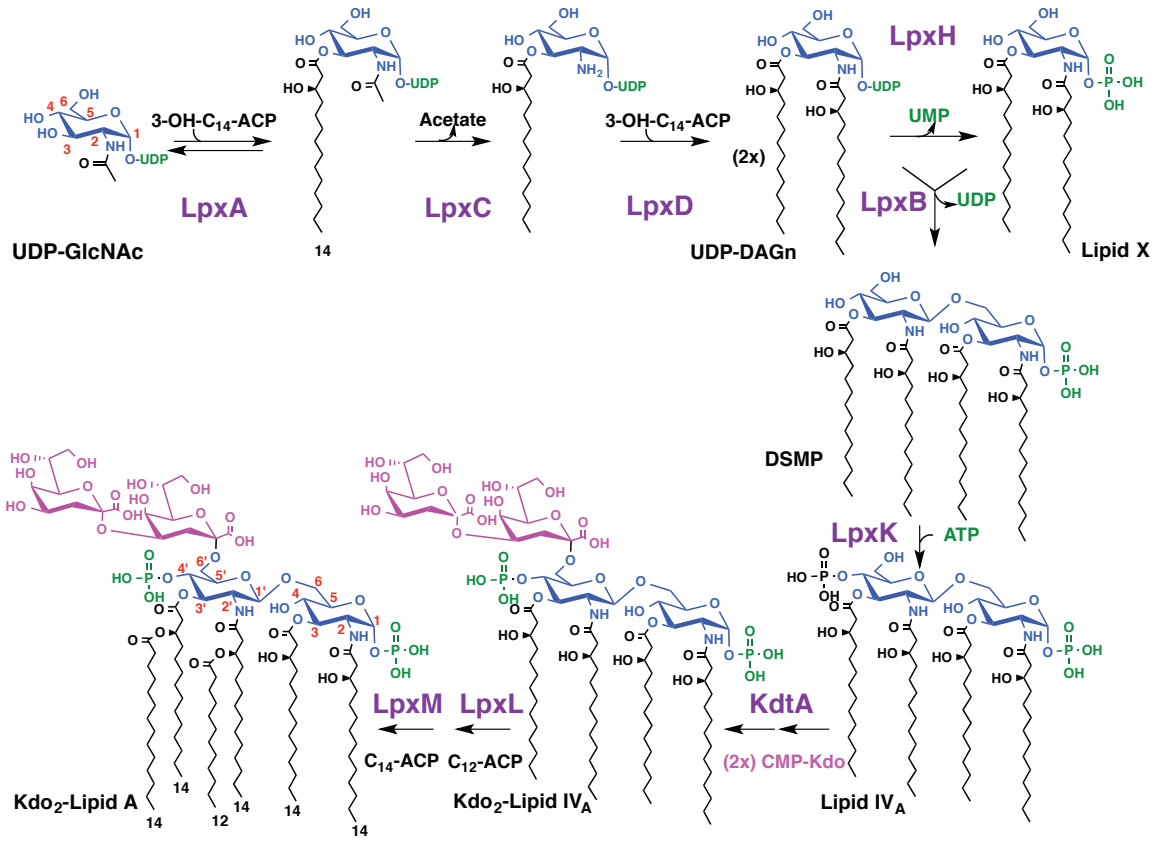

Figure 4: Raetz Pathway of Lipid A Biosynthesis

In *E. coli,* the constitutive synthesis of hexacylated Kdo_2-lipid A is carried out by the nine denoted Lpx enzymes that comprise the Raetz pathway. A majority of the pathway is conserved in nearly all Gram-negative bacteria.

1.5 Lipopolysaccharide Transport to the Outer Membrane

After its synthesis, Kdo_2-lipid A decorated with additional core sugars by glycosyl transferases in the inner leaflet of the inner membrane. It is then transported across the inner membrane by MsbA (Fig. 5). This enzyme is an ABC transporter that presumably uses energy from ATP hydrolysis to flip core LPS into the periplasmic surface of the inner membrane (47,48). It has been postulated that the 1 and 4′

phosphate groups of lipid A serve as important contacts between MsbA and its substrate (49). Genetic studies have revealed that over-expression of MsbA can compensate for *kdtA* deletion in *E. coli,* yielding a viable strain whose LPS consists solely of lipid IV_A. This suggests that while the transporter has lower affinity for the tetra-acylated precursor that lacks core sugars, it can still flip the molecule across the membrane (50). Mutations earlier in the pathway cannot be compensated by MsbA over-expression, indicating the importance of the phosphate moieties for flippase function. Interestingly, *msbA* deletion can be compensated by a point mutation in *yhjD* (51). Although the function of *yhjD* is not known, it is hypothesized that alteration of this gene activates an independent transport pathway.

While the core region and lipid A are transported together, the O-antigen of LPS moves separately across the membrane, employing the lipid carrier undecaprenyl phosphate (Fig. 5). There are three pathways by which this may occur (7). In the Wzy-dependent pathway, individual O-antigen units are polymerized in the cytosol and then flipped to periplasm by Wzx. Once there, Wzy links them into repeating units and then Wzz generates modal distribution of chain lengths by regulating continued branching by Wzy or ligation to the lipid A core. Alternatively, an ABC-transport mediated pathway can be utilized for linear O-antigens: once the O-antigen is assembled on the undecprenyl phosphate, an ABC transporter flips the molecule into the periplasm.

Finally, in the synthase dependent pathway, there is simultaneous polymerization and transfer of the O-antigen chain across membrane.

Once in the periplasm, the O-antigen is linked to the core region of lipid A by the ligase WaaL to generate the mature form of LPS (52). This LPS molecule is then transported across the periplasm and into the outer membrane by the Lpt proteins (Fig. 5). While the exact mechanism of the system is not known, the small periplasmic protein LptA is hypothesized to chaperone LPS across the periplasm (53). The method of this accompaniment is unclear, however it has been suggested that LptA forms a slightly helical linear filament that spans the periplasm to facilitate transport of the hydrophobic molecule across the aqueous environment (53). LptC, LptF, and LptG are found in the inner membrane and are thought to serve as an anchor point for LptA (54,55). LptB, a cytoplasmic protein, contains an ATP-binding cassette and is thus postulated to interact with LptG and LptF to assist in the acquisition of energy to fuel LPS transport (53,56). After traversing the periplasm, LPS is incorporated into the outer surface of the outer membrane by the beta-barrel protein LptD and its partner lipo-protein LptE. It is not known whether LPS is incorporated into the inner leaflet of the outer membrane and then flipped across the lipid bilayer or transported directly to the outer leaflet in a channel mechanism (56,57).

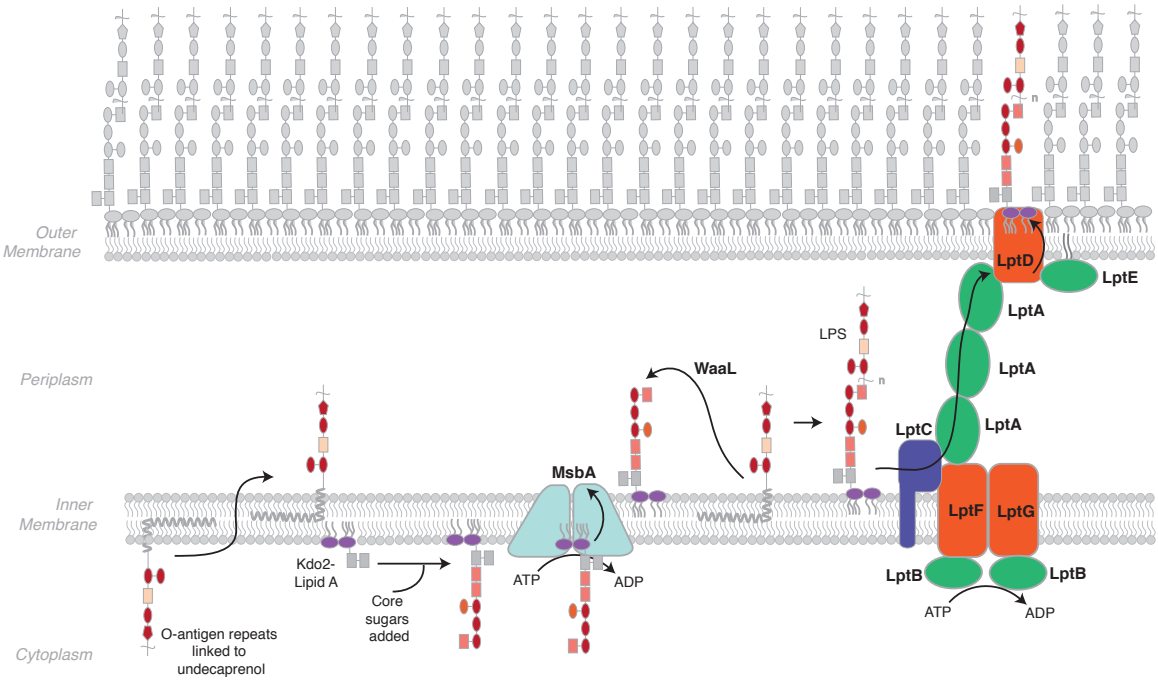

Figure 5: Export of LPS to the Outer Membrane

The distal O-antigen portion of LPS is synthesized on undecaprenyl phosphate on the cytosolic face of the inner membrane; the lipid serves as a carrier to transfer the carbohydrate chain to the periplasmic leaflet. After completion of the Raetz pathway in the cystosol and inner leaflet of the inner membrane, additional sugars are added to Kdo_2-lipid A to form core lipid A. Through ATP hydrolysis, the ABC transporter MsbA flips core lipid A into the outer leaflet of the inner membrane. There, WaaL ligates the O-antigen to the outer core, creating mature LPS. Next, the Lpt transport system facilitates the movement of LPS across the periplasm by chaperone LptA and inner membrane-associated proteins LptCBFG. Finally, LptD and its protein partner LptE deliver LPS to the cell surface.

1.6 Lipid A Modification

While the final product of the Raetz pathway is Kdo_2-lipid A, many bacteria employ enzymes that modify the molecule after its synthesis (Fig. 6). These alternations assist bacteria in adapting to their environment, as changes in lipid A structure can mediate membrane permeability and interfere with the host's ability to detect LPS (29).

Modifications are usually only required for a portion of the bacterial life cycle; thus, such enzymes are often under translational and post-translational control. In the presence of antimicrobial peptides or in depletion of cations, *E. coli, S. typhimurium,* and *P. aeruginosa* employ the PhoPQ and PmrAB systems to upregulate proteins that strengthen the integrity of the outer membrane through modification of lipid A (58,59). Modification enzymes can also be regulated directly through substrate availability (60) and small peptide inhibitors induced by stress response systems (61-63). Furthermore, indirect regulation can occur through action of other modification proteins, as chemical alterations of lipid A by one enzyme can reduce another modification enzyme's affinity for the molecule (64).

Modifications to the carbohydrate moieties of Kdo_2-lipid A (Fig. 6) are often employed to increase membrane integrity, particularly for protection from cationic antimicrobial peptides released by bacterial hosts. Such modifications usually occur in the outer leaflet of the inner membrane after MsbA has flipped lipid A to the periplasm. In *E. coli* and *Salmonella,* the enzyme ArnT can add 4-amino-4-deoxy-L-arabinose (aminoarabinose) to the 4' phosphate group of core lipid A in the periplasmic side of the inner membrane (65). The aminoarabinose substrate of ArnT is synthesized in the cytosol and then transferred to the periplasm via undecaprenyl phosphate (66). Other modifications include attachment of phosphoethanolaime to the 1 phosphate of core-lipid A by EptA (67);. In absence of ArnT activity, this modification can additionally

occur at the 4′ phosphate (68). A related enzyme, EptB, also decorates core-lipid A with phosphoethanolamine, albeit on the outer Kdo residue (69).

Specific enzymes can similarly tailor the acylation state of Kdo_2-lipid A (Fig. 6). Such proteins serve to alter membrane fluidity and assist in evasion of the host immune response, as six hydrocarbon chains are necessary for full TLR4 activation. PagP, an outer membrane beta-barrel protein, can add a palmitate to the hydroxyl group on the 2-position acyl chain through use of a phospholipid donor (70). In *Salmonella typhimurium* and other inter-cellular pathogens, the outer membrane lipase PagL removes the *R*-3-hydroxymyristol chain at the 3 position of lipid A (71). This organism also contains another outer membrane lipase LpxR which removes the 3′-acyloxyacyl substituent from Kdo_2-lipid A (72). Other acyl modification can occur at the outer leaflet of the inner membrane by LpxO; this protein hydroxylates the 3′ secondary acyl chain of Kdo_2-lipid A (73).

In addition to those listed above, there are numerous additional enzymes that modify lipid A (29). Some of these enzymes are found in a wide variety of Gram-negative bacteria, while others are very specific to certain species. Modification of the structure of lipid A can be extremely helpful for bacterial survival. However, it may also make the organism more susceptible to other environmental stressors.

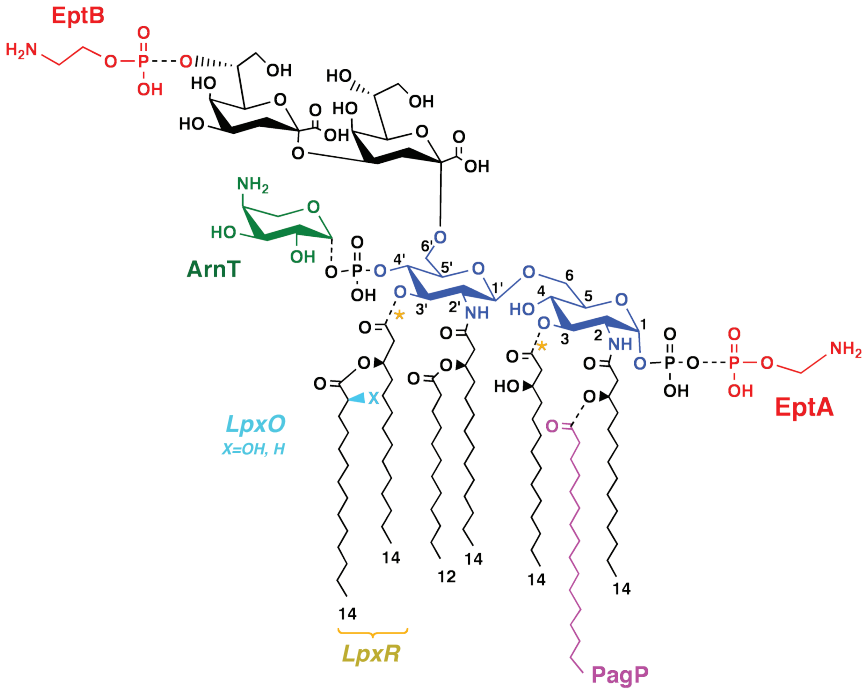

Figure 6: Common Modifications of Lipid A in *E. coli* and *Salmonella*

The final product of the Raetz pathway, Kdo_2-lipid A, can be modified to assist bacterial environmental adaptation. These modifications can include phosphethanolamine additions (red) to the carbohydrate head group by EptA and EptB. ArnT can also catalyze the attachment of 4-amino-4-deoxy-L-arabinose (aminoarabinose) to the 4′ phosphate (green). An additional palmitate moiety (pink) may be added to the hydroxyl group on the 2 acyl chain by outer membrane protein PagP. Outer membrane lipases PagL and LpxR remove the *R*-3-hydroxymyristol chain at the 3 postion and the 3′-acyloxyacyl substituent, respectively (marked with yellow asterisk). Hydroxylation of the 3′ secondary acyl chain of Kdo_2-lipid A (light blue) is catalyzed by LpxO. Enzymes not present in common laboratory strain *E. coli* K-12 are italicized. Figure modified from (6).

1.7 Lipid A Biosynthesis and Antibiotic Development

The antibiotics used to treat Gram-negative infections include inhibitors of cellular processes, such as protein synthesis and DNA replication and repair (74). Also included are those altering the cell envelope such as vancomycin and drugs of the β-lactam family that act by preventing proper peptidoglycan assembly (74). However, all

of these classes of antibiotics are becoming ineffective as the prevalence of resistant and multi-drug resistant Gram-negative bacteria is rapidly growing, especially in hospitals and long-term care facilities (75,76). Other pathways required for bacterial growth, such as the Raetz pathway, are potential avenues for the development of new drugs. Presently, there has been significant investigation on inhibitors of LpxC, encompassing hydroxamate (77), hydantoin (78), and sulfonamide (79) derivatives. Other compounds from a uridine-based library have also been identified as effective inhibitors of early Lpx enzymes (80); they are assumed to compete with the enzyme's substrate by mimicking the UDP moiety. Studies elucidating the structures, kinetic parameters, and substrate specificity of Raetz pathway enzymes may facilitate the design of additional inhibitory compounds that could be optimized for use as antibiotics.

1.8 Conservation of Lipid A Biosynthesis

1.8.1 Evolution of Raetz Pathway Enzymes

While the lipid A pathway of *E. coli* is often used as a standard model for production of the saccharolipid, recent bioinformatic studies have revealed it may represent a highly evolved form of synthesis (81). Comparison of bacterial genomes representing the 20 highly divergent phyla of Gram-negative organisms revealed that only a sub-group of γ-Proteobacteria (termed Group II) contains the nine Lpx enzymes seen in *E. coli.* These bacteria are largely enteric, encountering harsh conditions in their

gastrointestinal environment. This likely increases selective pressure for an optimized pathway for lipid A synthesis.

The similarity of the lipid A pathway in different organisms appears to correlate with bacterial phylogeny, as movement away from Group II γ-Proteobacteria corresponds with loss of Lpx orthologs (81) (Fig. 7). The LpxM ortholog does not emerge outside of Group II ϒ-Proteobacteria. The enzyme responsible for the fourth step of the *E. coli* pathway, LpxH, is only present in γ, β, and ε Proteobacteria; it is replaced by a functional analog, LpxI, in α- and ζ-Proteobacteria as well as other bacteria phyla (Fig. 8). Interestingly, there are phyla such as Chlamydiae that lack orthologs for LpxI or LpxH, suggesting the existence of a third UDP-DAGn hydrolase. Presence of LpxK, KdtA, and LpxL seems to be correlated, as most bacteria appear to contain none or all of these enzymes. Despite the variance in conservation of the later portion of the Raetz pathway, the early enzymes LpxA, LpxC, LpxD, and LpxB are highly preserved across nearly all Gram-negative phyla. Their genes are often found in a *lpxD-lpxC-fabZ-lpxA-lpxB* operon, with *fabZ* encoding an enzyme of phospholipid biosynthesis. These four Lpx enzymes may represent a primordial form of the lipid A pathway (81).

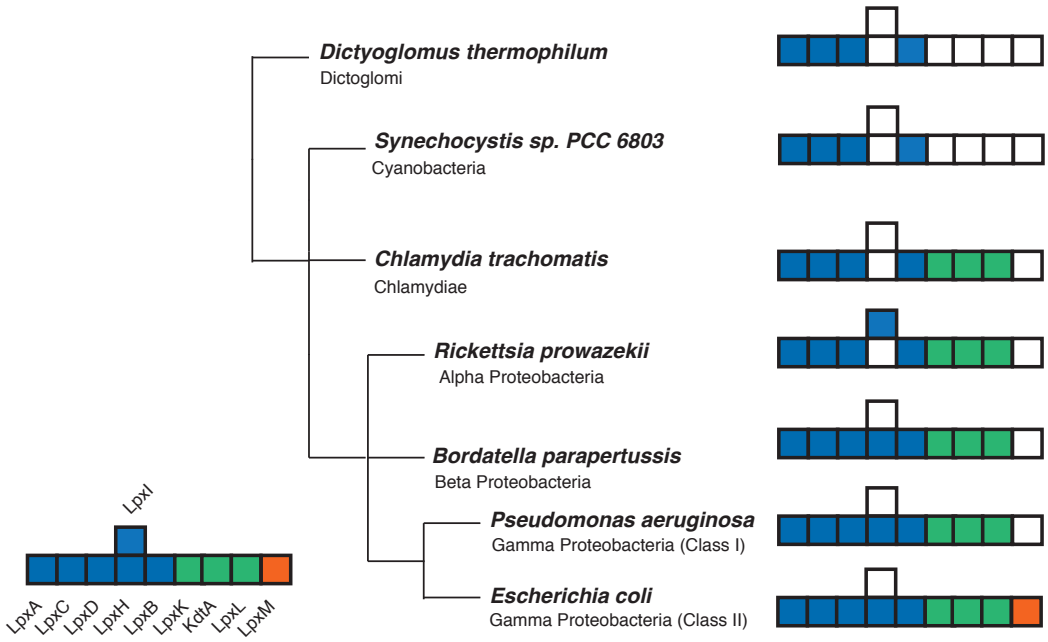

Figure 7: Conservation of Lipid A Biosynthetic Enzymes

The presence of lipid A biosynthetic enzymes in a diverse sample of Gram-negative bacteria is depicted through use of block key, with a colored square denoting the presence of the corresponding Lpx enzyme. Bacterial species are organized based on 16S rRNA phylogeny, however distance is not to scale. Phylum is denoted below each species. The block key is ordered the same as the Raetz pathway, beginning with LpxA on the left and ending with LpxM on the right. Figure was created based on data presented in (81).

1.8.2 Distribution of UDP-DAGn Hydrolase Orthologs

Considering the prevalence of third (LpxD) and fifth (LpxB) enzymes of the Raetz pathway across Gram-negative bacteria, it is intriguing that the fourth enzyme is not also highly conserved. As mentioned, two unrelated enzymes have been shown to function as the UDP-DAGn hydrolase required in the fourth step of lipid A biosynthesis: LpxH and LpxI. LpxH orthologs appear to be confined to classes of Proteobacteria, however an LpxH homolog with 42% similarity does exist in bacteria outside of this

phylum (40,81) (Fig. 8). Bioinformatic studies suggest that this homolog, designated LpxH2, may be an ancestor to LpxH, with the former undergoing gene duplication to create the latter. Such an event is not rare in the evolution of the lipid A pathway. The similarity of LpxA and LpxD in both sequence and structure suggest they originated through gene duplication. Furthermore, LpxL shows evidence of multiple gene duplications, including one that resulted in evolution of LpxM.

Both LpxH and LpxH2 are part of the calcineurin-like phosphatase (CLP) family and show presence of the conserved DXHX$_{\sim 25}$GDXXDRX$_{\sim 25}$GNH(D/E) motif (40). In LpxH orthologs, however, the last histidine of the motif is replaced with arginine; this may attribute to optimized UDP-DAGn hydrolase function. Interestingly, some Proteobacteria like *Pseudomonas aeruginosa* contain both LpxH and LpxH2 orthologs, indicating *lpxH2* was retained after duplication. Investigation has shown that *P. aeruginosa lpxH2* cannot complement *lpxH* function in *E. coli* (82). This suggests that in the case of dual-existence of the proteins, LpxH2 may have evolved a different function, allowing LpxH to be fully responsible for UDP-DAGn hydrolysis. Some species containing LpxI also display LpxH2 orthologs, as is seen in *Sinorhizobium meliloti*. Curiously, LpxH2 from this species appears to play the role of a phospholipase C (83). Overall, this implies that if LpxH2 exists in the presence of LpxH or LpxI, it does not function in lipid A biosynthesis. It remains to be determined if LpxH2 orthologs from organisms lacking *lpxH* and *lpxI* can function as UDP-DAGn hydrolases in the synthesis

of lipid A. Nonetheless, the existence of LpxH2 in phyla lacking LpxH or LpxI presents possible candidates for the fourth step of the Raetz pathway in these organisms.

The other known UDP-DAGn hydrolase, LpxI, shares no homology with LpxH, indicating that they evolved separately to carry out their enzymatic functions (41). LpxI is found within Proteobacteria as well as other phyla, but never in the same organism as LpxH orthologs. Overall, bacteria exhibiting LpxI orthologs represent more ancestral species of bacteria (Fig. 8). The gene encoding LpxI is found to cluster between *lpxA* and *lpxB* in the *lpxC-fabZ-lpxA-lpxB* operon. Taken together, this indicates that LpxI may have evolved earlier than LpxH to perform the fourth step of lipid A biosynthesis (41).

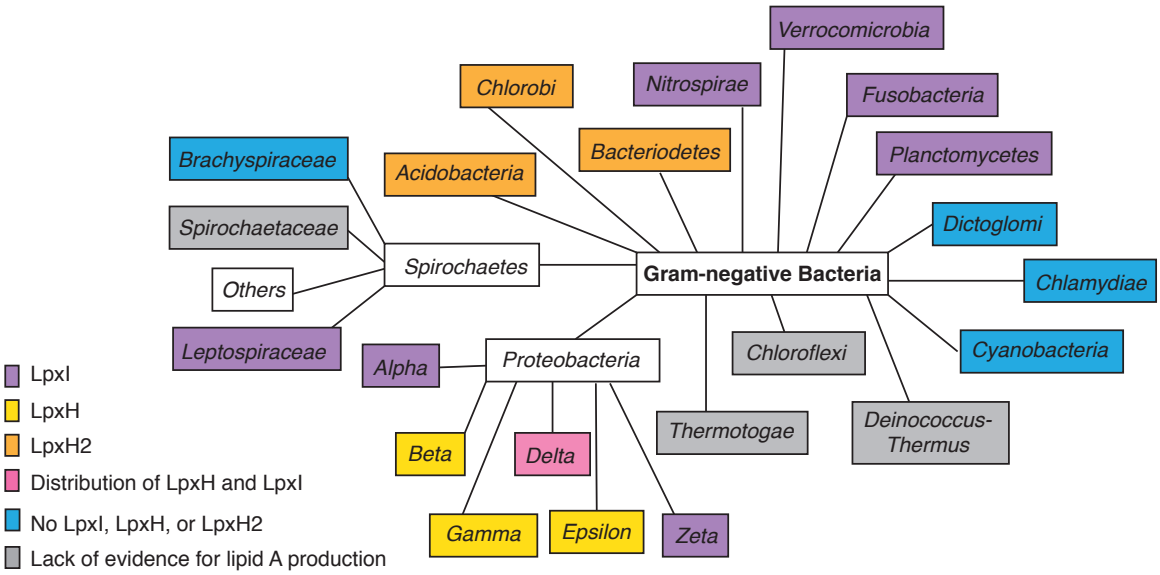

Figure 8: Distribution of UDP-DAGn Hydrolases in Gram-Negative Bacteria

The names of fifteen Gram-negative bacterial phyla are listed, radiating out from the marked center box. Proteobacteria is further subdivided into classes to better illustrate the distribution of UDP-DAGn hydrolases. Likewise, the Spirochaetes phylum is divided into families. Representative bacterial species from each classification were used to determine the presence of UDP-DAGn hydrolases LpxI and LpxH, or the related protein LpxH2. Outcomes are denoted by box color according to the key. Classifications were only given the LpxH2 designation if neither LpxH nor LpxI orthologs were present; this diagram does not account for the existence of LpxH2 in organisms also containing LpxH or LpxI. While bioinformatic analysis suggests that LpxH2 may function as the UDP-DAGn hydrolase in denoted phyla, no biochemical evidence supports this claim. Box color was additionally utilized to denote the absence of LpxI, LpxH, or LpxH2 orthologs despite the presence of other lipid A enzymes (blue). The lack of any Lpx genes or evidence of lipid A production is also marked (gray). Data presented in (81) and (41) was used to create the diagram

1.8.3 Unanswered Questions and Recent Developments

Organization of bacteria by conservation of Raetz pathway enzymes aligns well with the traditional phylogeny based on 16S rRNA sequences, however exceptions do

exist (81) (Fig. 8). In the Spirochaetes phylum, the family Spirochaetaceae shows no evidence of lipid A synthesis genes, however sister-families Leptospiraceae and Brachyspiraceae display strong Lpx orthologs. Furthermore, Leptospiraceae contains LpxI whereas Brachyspiraceae displays no evidence of LpxI, LpxH, LpxH2.

The absence of a candidate UDP-DAGn hydrolase as seen in Brachyspiraceae is also evident in other phyla (Fig. 8). Cyanobacteria and Dictogolomi have LpxADCB orthologs but no candidate UDP-DAGn hydrolase. In Chlamydiae, seven of the Lpx enzymes are present, but there is no evidence for LpxH, LpxI, or LpxH2. This strongly suggests the presence of an undiscovered UDP-DAGn hydrolase that plays a role in lipid A biosynthesis.

Recently, another Lpx enzyme was discovered in α, δ, ζ-Proteobacteria as well as Fusobacteria, Chlamydiae, Acidobacteria, and Spirochaetes (84). This protein, LpxJ, serves the same function as LpxM but is unrelated in sequence and distribution, as LpxM is not found outside of Proteobacteria. Such a relationship is similar to that between LpxI and LpxH. Discovery of LpxJ further supports the evolutionary divergence of the Raetz pathway.

1.9 UDP-Diacylglucosamine Hydrolysis

Discovery that UDP-DAGn hydrolysis played a role in the lipid A biosynthetic process was facilitated through the discovery of lipid X (Fig. 9). While searching for *E. coli* mutants defective in phospholipid biosynthesis, researchers isolated strain MN7,

which harbored temperature sensitive mutations in the phosphatidylglycerophosphate synthase gene *pgsA* and a second gene, termed *pgsB (85).* Characterization of MN7 through ^{32}P-labeling and subsequent 2D-TLC revealed temperature-dependent accumulation of two previously unknown phosphate-containing lipids, termed lipid X and lipid Y (86). After determination of the structure of lipid X by NMR, it was hypothesized that two molecules of lipid X were joined together to yield the diacyglucosamine backbone of the lipid A moiety of LPS (87,88). The linkage of sugars is often facilitated by the presence of a nucleotide moiety that serves to activate the substrate. Thus, it was postulated that a nucleotide-derivative of lipid X may be a lipid A precursor (89). Indeed, additional ^{32}P labeling of MN7 indicated temperature-dependent accumulation of a modified form of lipid X containing a UMP moiety on the 1-phosphate, corresponding to what is now known as UDP-DAGn. Pulse-labeling experiments revealed that UPD-DAGn was a precursor to lipid X, yielding the conclusion that some sort of hydrolysis reaction served to generate the latter from the former. Conversion of UDP-DAGn to lipid X was detectable in crude extracts of *E. coli*, supporting the existence of an UDP-DAGn hydrolase (90).

The discoveries of the genes that are known to encode the UDP-DAGn hydrolase activity important for lipid A biosynthesis, *lpxH* and *lpxI*, are discussed below. Another *E. coli* protein, Cdh, has been shown to have UDP-DAGn hydrolase activity *in vitro*, however it does not play a role in lipid A biosynthesis. Cdh is a promiscuous hydrolase

first characterized to act on CDP-diacylglycerol, an intermediate in phospholipid biosynthesis (91-93). While it can produce lipid X *in vitro*, it is not necessary for cell viability, indicating it is not involved in the essential lipid A pathway. Furthermore, when *cdh* is knocked out, UDP-DAGn hydrolase activity is still present in crude lysates of *E. coli*. Cdh is also predicted to be periplasmic facing (94), and as lipid A biosynthesis has been demonstrated to take place in the cytoplasm and inner leaflet of the inner membrane (95), the enzyme would not have proper access to UDP-DAGn to produce lipid X *in vivo*.

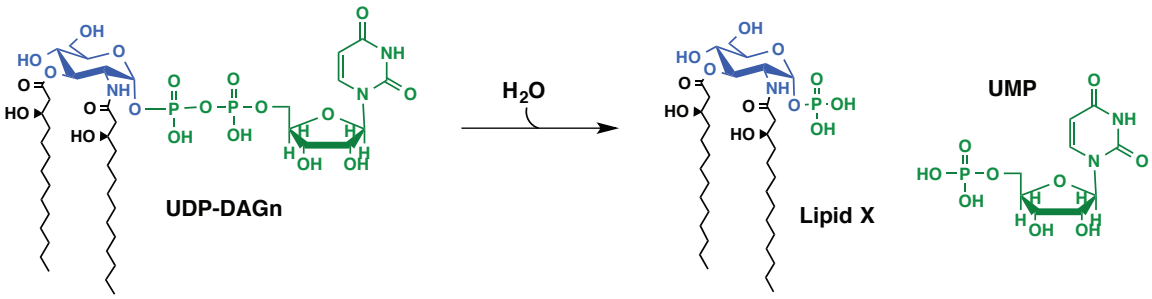

Figure 9: Hydrolysis of UDP-2,3-Diacylglucosamine to Generate Lipid X

1.9.1 LpxH

1.9.1.1 Discovery

While *lpxI* has been suggested to evolve earlier, *lpxH* was the first UDP-DAGn hydrolase gene to be discovered. To identify the gene responsible for lipid X production in *E. coli*, a Kohara phage library was used to infect a Cdh deletion strain and resulting lysates were assayed for UDP-DAGn hydrolase activity (40). One clone, corresponding

to *ybbf*, displayed ~10-fold enhanced activity over background. This candidate gene, renamed *lpxH*, was tested independently for lipid X production *in vitro* and was confirmed to have UDP-DAGn hydrolase activity. Over-expression of LpxH corresponded to an accumulation of lipid X in cell-free extracts over vector control. Deficiency in the enzyme, mediated through temperature-controlled expression, resulted in accumulation of UDP-DAGn. Complete knockout of *lpxH* without complementation was not possible, denoting the essentiality of the gene's activity. It was thus concluded that *lpxH* encoded the enzyme responsible for the fourth step of the Raetz pathway (40).

1.9.1.2 Characterization

Basic characterization of LpxH was carried out using a crude ~60% homogenous sample obtained through dye affinity chromatography (40). Its mechanism of hydrolysis was determined through ^{31}P NMR analysis of reaction products generated in the presence of $H_2{}^{18}O$; a shift in the UMP spectrum corresponded to the presence of the heavy oxygen atom, correlating to a hydrolytic attack on the α phosphate of UDP-DAGn. Kinetic studies indicated an apparent K_M of 60 μM and apparent V_{max} of 10 μm/min/mg. The protein displayed a pH optimum of ~8.0 and showed sensitivity to detergent *in vitro*, with activity decreasing in the presence of Triton X-100. While this characterization of LpxH yielded general information about the enzyme, the lack of a

homogenous sample prevented definitive conclusions to be made about its enzymatic properties.

Bioinformatic analysis reveals that LpxH contains a motif signature of the calcineurin-like phosphoesterase (CLP) superfamily. This motif, DXHX$_{\sim 25}$GDXXDRX$_{\sim 25}$GNH(D/E), is found in enzymes that utilize a di-metal cluster for catalysis. While addition of Mn^{2+} showed stabilization of LpxH during purification (40), metal dependency of the enzyme was not reported in the literature. Furthermore, the type of chemistry performed by LpxH, cleavage of a pyrophosphate bond in a nucleotide moiety, is not canonical for CLP enzymes. These dilemmas demand further biochemical characterization of LpxH.

1.9.2 LpxI

1.9.2.1 Discovery

Upon discovery of *lpxH,* it was noted that orthologs of the gene were not found in all Gram-negative bacteria. Specifically lacking were α- and δ-Proteobacteria and thermophiles and extremophiles like *Aquifex*, all of which contain very strong homologs for both LpxD and LpxB and are known to produce lipid A. In order to identify a possible UDP-DAGn hydrolase in these organisms, a bioinformatic approach was employed (41). As mentioned above, *lpxDCAB* are clustered together in many organisms. Sequence analysis revealed a gene of unknown function between *lpxA* and *lpxB* in several bacteria species lacking LpxH. The *Caulobactor crescentus* homolog of this

gene, designated *lpxI,* was cloned and expressed in *E. coli.* Presence of the *C. crescentus* protein corresponded to >1000 fold increase in UDP-DAGn hydrolysis over vector control. This hydrolase activity was not observed in the presence of CDP-diacylglycerol, indicating specificity of LpxI the lipid A precursor. Furthermore, *lpxI* was able to complement an *lpxH* deletion in *E. coli.* Together, this provided definitive evidence that *lpxI* encoded for a UDP-DAGn hydrolase (41).

1.9.2.2 Characterization

With use of affinity chromatography, LpxI was purified to >90% homogeneity and enzymologically characterized (41). It was determined to have an apparent K_M of 105 μM and apparent V_{max} of 69 μmol/min/mg. Surface dilution kinetics were not detectable: detergent concentration had little effect on lipid X production *in vitro*. Activity was shown to be metal dependent, as EDTA addition abrogated activity *in vitro*. Mg^{2+} was found to increase LpxI-mediated hydrolysis 10-fold, while Mn^{2+} and Co^{2+} stimulated the protein 6-fold over no metal controls. The hydrolytic mechanism for LpxI was also determined with use of $H_2{}^{18}O$. Mass spectrometry analysis of LpxI reaction products generated in the presence of the isotopically labeled water indicated a mass shift in the lipid X species that corresponded to ^{18}O addition. The UMP species showed no sign of such shift, suggesting that unlike LpxH, LpxI employs hydrolytic attack at the β phosphate of UDP-DAGn to form lipid X.

1.9.2.3 Structure

In addition to LpxI's biochemical properties, the structural characteristics of the protein have also been reported (96). The 2.55 Å structure of *C. crescentus* LpxI reveals a novel fold, with two distinct domains being connected by a flexible linker (Fig. 10). Density for the LpxI product lipid X is clearly seen in the N-terminal domain and existence of the molecule is supported by the observation that the protein co-purifies with stoichiometric amounts of the lipid. This N-terminal section of the protein, designated LXD (lipid X binding domain), shows presence of a lipid-binding cleft that encapsulates the acyl chains of lipid X. Hydrophobic residues lining the cleft presumably drive the association of the product with the LXD as the diacyl glucosamine head group of lipid X is solvent exposed.

The C-terminal domain of LpxI contains 11 absolutely conserved polar residues, some of which are required for activity. Thus, this domain is termed ICD, representing LpxI catalytic domain. An alanine point mutation of an aspartate residue in ICD (D225A) abrogates hydrolytic activity, and its over-expression corresponds to an accumulation of UDP-DAGn substrate. Furthermore, the 3.0 Å crystal structure of the D225A variant of LpxI reveals the presence of UDP-DAGn (Fig. 10), indicating co-purification of the lipid nucleotide with the enzyme (96). Like in the wild-type structure with lipid X, the LXD of the mutant structure surrounds the acyl chains of the lipid nucleotide. The head group of the substrate molecule, however, is not solvent exposed,

but shrouded by the ICD. This results in a "closed" confirmation of LpxI in which the LXD and ICD are positioned 70° closer together than seen in the wild type "open" form. The overall structures of the individual domains remain the same in both forms, with the only change being in the linker region. This conformation change is not likely to be an artifact of crystal packing, as the sedimentation velocity of wild type LpxI in solution is slower than that of the mutant form.

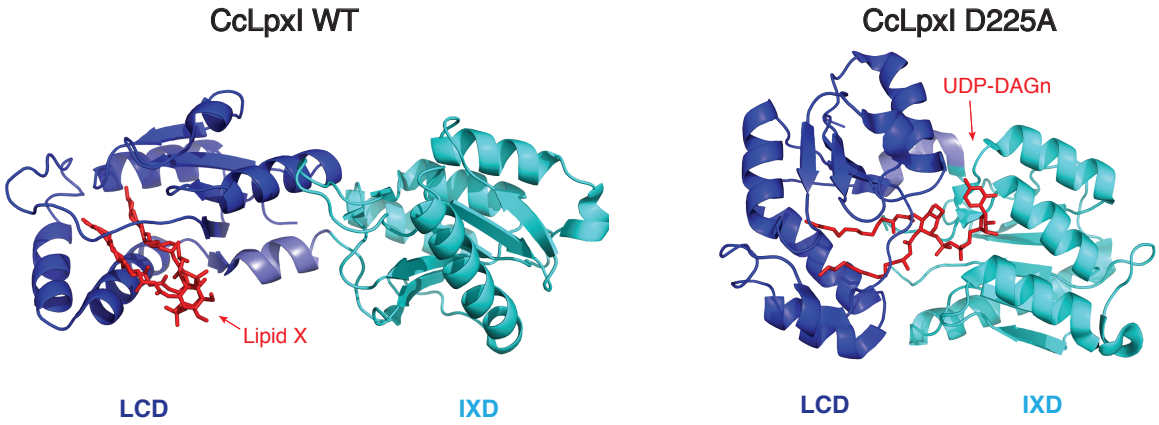

Figure 10: Structures of LpxI

The 2.55 Å structure of wild-type LpxI from *C. crescentus* (CcLpxI WT, PDB code 4GGM) is depicted on the left. The N-terminal lipid X binding domain (LXD, blue) is connected to the C-terminal LpxI catalytic domain (ICD, cyan) through a linker region (periwinkle). The LpxI reaction product lipid X (red) was also present in the structure. The 3.0 Å structure of the D225A mutant of LpxI from *C. crescentus* (CcLpxI D225A, PDB code 4J6E) is depicted on the right. UDP-DAGn (red), the LpxI reaction substrate, is evident in the mutant structure.

Capturing the enzyme with both its substrate and product led Metzger and colleagues to propose a model for LpxI-mediated UPD-DAGn hydrolysis (96) (Fig. 11). Structural and biochemical data suggests the protein likely functions a dimer through its catalytic cycle. Since lipid X is bound to purified LpxI in a stoichiometric ratio, the

enzyme likely holds onto its product in the LXD after catalysis, yielding a "resting" state. Release of lipid X may be triggered by presence of UDP-DAGn that binds to the ICD through interactions with the lipid head group of the substrate. The LXD then discharges the lipid X so it can accommodate the acyl chains of UDP-DAGn. In this resulting closed conformation, cleavage of the pyrophosphate bond occurs. LpxI subsequently extends back into its resting state form, transferring the newly formed lipid X to the LXD. The large conformational shift in this model may be driven by the energy released in UDP-DAGn hydrolysis.

The present LpxI macromolecular model explains *in vitro* catalysis, however other factors may play a role in lipid X production *in vivo.* Specifically, the release of lipid X could be mediated through the presence of other lipid A enzymes (96). Very little information is known about how proteins in the Raetz pathway communicate throughout the metabolic process. It is possible that interaction of LpxI with the proceeding LpxD or succeeding LpxB could trigger certain steps of lipid X production.

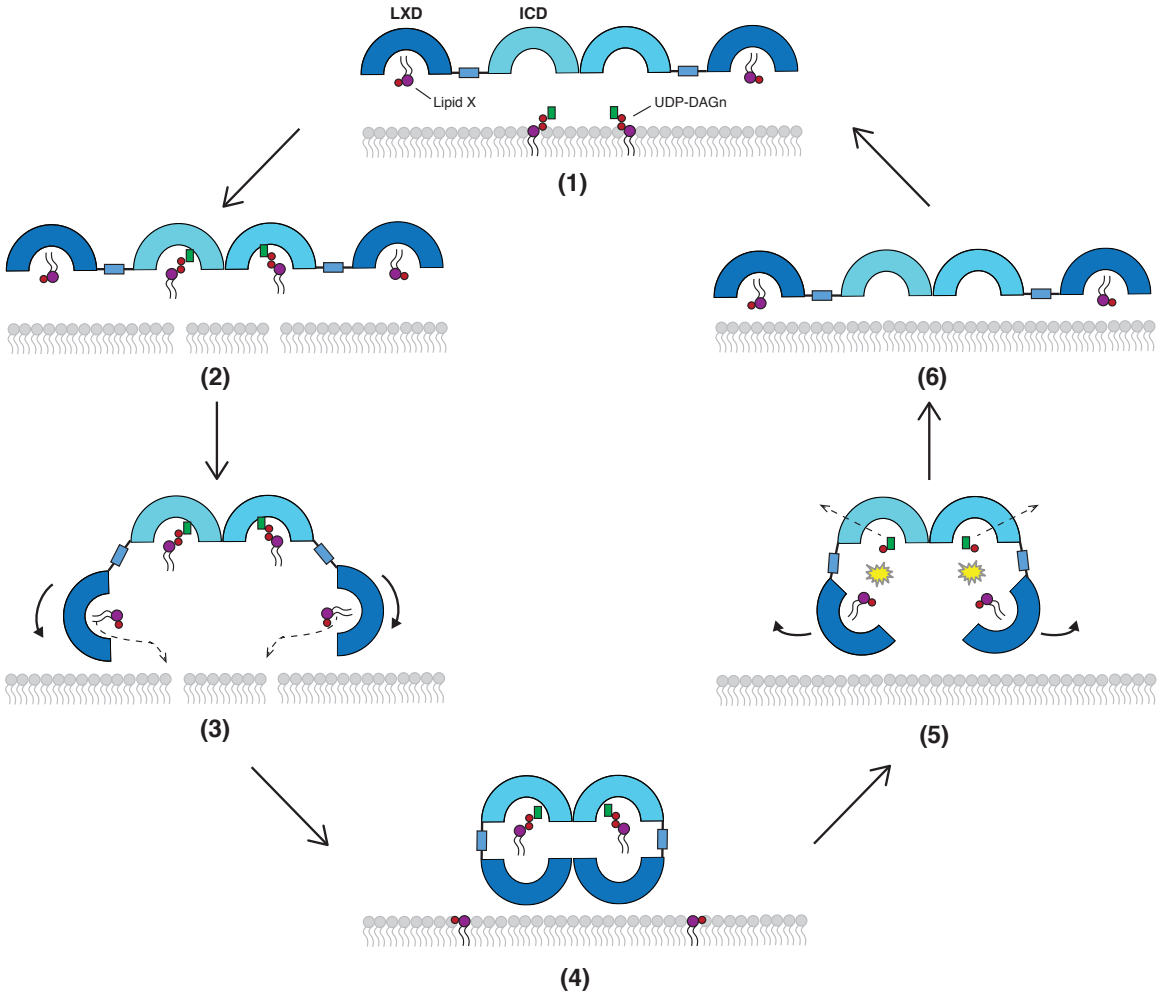

Figure 11: Model for LpxI Catalysis

Schematic representation of a possible method for production of lipid X by LpxI, as modified from Metzger, *et al.* (96). The lipid bilayer (gray), lipid X (purple and red) and UDP-DAGn (lipid X with green representing the UMP moiety) are shown. LpxI is depicted as a dimer and is colored by domain as in Fig. 10. (1) The cycle begins when lipid X-bound LpxI encounters UDP-DAGn substrate. (2) The ICD binds the head group of UDP-DAGn. (3) Lipid X is released from the LXD, which coincides with a hinge-like conformational shift. (4) The closed confirmation of LpxI is achieved when the LXD encapsulates the acyl chains of UDP-DAGn. (5) Hydrolysis of the pyrophosphate bond occurs; released energy drives a reverse conformational change. (6) LpxI reopens, transferring the newly formed lipid X to the LXD.

1.9.3 Relationship between LpxH and LpxI

As previously discussed, LpxI and LpxH are never found in the same organism. They are completely unrelated in sequence, with LpxH orthologs belonging to the CLP family (discussed below) and LpxI orthologs comprising their own unique class of enzymes. Furthermore, these proteins use different hydrolytic mechanisms to catalyze the formation of lipid X. Despite these differences, both proteins are able to complete the same transformation of UDP-DAGn to lipid X, with *lpxI* being able to complement *lpxH in vivo.* Thus, these UDP-DAGn hydrolases represent a pair of transformational analogs, as they generate the same product using different chemistry (97). Transformational analogs commonly represent convergent evolution, a phenomenon commonly observed with hydrolases (98,99). Study of these enzymes, both individually as well as in the context of the lipid A pathway, may provide insight into why nature has evolved to use extremely different enzymes for the same process.

1.10 Calcineurin-Like Phophoesterases

The calcineurin-like phosphoesterase (CLP) superfamily (Pfam00149) represents a group of metal-dependent phosphoesterases that contain a highly conserved DXH(X)$_{\sim 25}$GDXXDR(X)$_{\sim 25}$GNHD/E motif. The enzymes of this family hydrolyze a variety of phosphate substrates, including lipids (sphingomyelin phosphodiesterases (100)), proteins (serine/threonine phosphatases (101)), and nucleotide phosphates (DNA polymerases (102), 5′-nucleotidases, 3′-5′ exonucleases (103)). Also included are the

purple acid phosphatases (PAPs) (104); their function is unclear, but it is suspected they serve to dephosphorylate bone matrix in mammals and mobilize organic phosphate esters from the soil in plants (103). Proteins of this family often adopt a β-α-β-α-β secondary structure (Fig. 12).

CLP enzymes are known to perform catalysis using divalent and/or trivalent metal cofactors and an ordered shell of water molecules (103,105). The metal cofactors often include Fe^{2+}, Fe^{3+}, Zn^{2+}, Mn^{2+}, and/or Mg^{2+} and can be found in hetero- or homonuclear pairs (103). CLP proteins have been shown to have different affinities for each of their cofactors (*33)*, and in some cases, substrate binding is required for the binding of the lower-affinity metal (103,106). Structures of CLP enzymes reveal that metal binding occurs shallowly beneath the surface of proteins, permitting solvent accessibility to the active site (Fig. 11). It has been postulated that the metal ions serve to bridge an oxide that performs a nucleophilic attack, stabilize the formation of a phosphorane intermediate, or coordinate a nucleophilic hydroxyl group to allow for deprotonation (105,106).

A distinct feature of the metal ions found in CLP enzymes is their close proximity to one another within the protein (Fig. 12). Such clustering of cofactors is beneficial for the catalysis, as the proximity of the metal ions in an active site allows for a symmetric delocalization of charge that is not possible with only one metal (107). This delocalized distribution over two metals permits them to act like a unit in stabilizing

transition states of concerted mechanisms that facilitate the concurrent anionic ligand addition and anionic ligand dissociation. In the case of hydrolases, this stabilization of the transition state lowers the activation barrier for both nucleophilic attack by the activated water and phosphoester bond cleavage. Additionally, it has been reported that having two close Mn^{2+} ions in an active site increases the Lewis acidity of the metals, allowing them to have a higher affinity for ligands such as H_2O (107).

The residues of the CLP family motif play an important role in enzyme function. The functional groups of these amino acids directly serve as ligands to the ions and perform secondary coordination of waters and amino acids that in turn coordinate the metals, as observed in the structure of bacteriophage λ protein phosphatase (Fig. 12). The two metal cofactors are often bridged by a carboxylate group; such an orientation is a common structural motif in binuclear enzymes (103,107).

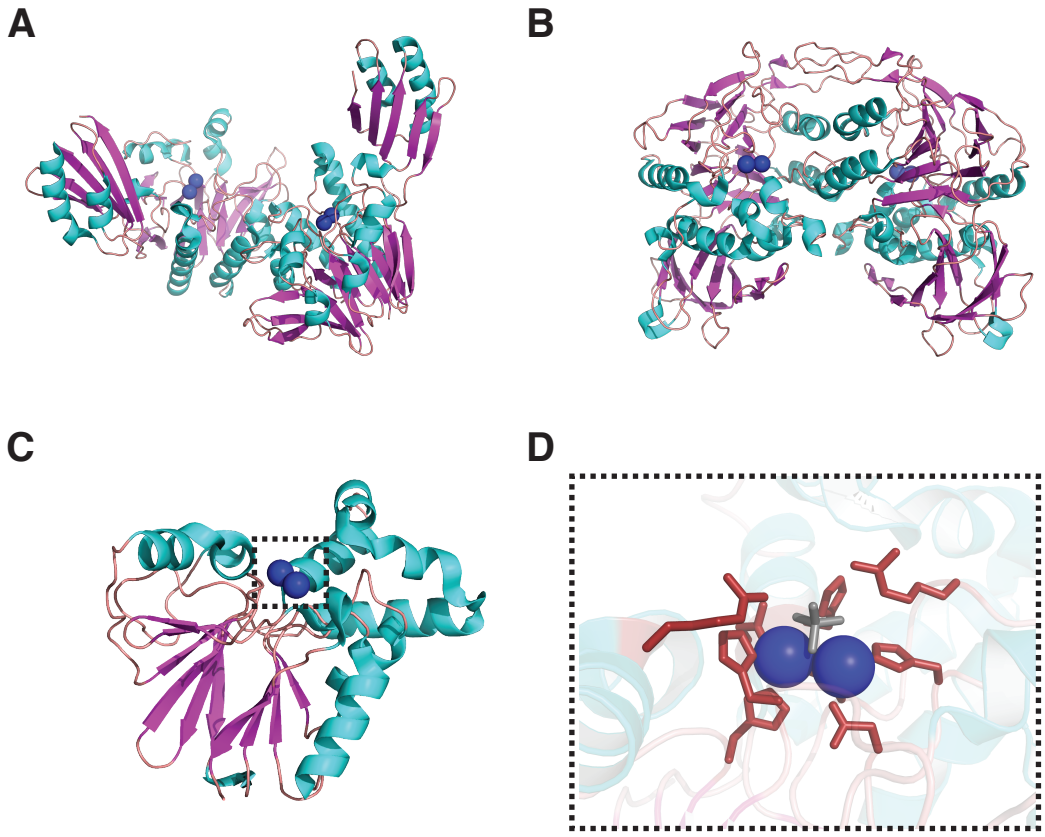

Figure 12: Structures of Representative CLP Enzymes

The crystal structures of (A) *Pyrococcus furtosis* Mre11 (PDB code 1II7), (B) sweet potato purple acid phosphatase (PDB code 1XZW), and (C) Bacteriophage λ Ser/Thr protein phosphatase (PDB code 1G5B) are shown as representatives of the CLP superfamily. Blue spheres represent metal ions. (D) Active site of Bacteriophage λ Ser/Thr protein phosphatase, as marked in (C) by dashed box. The residues of the conserved CLP motif (red) serve as a scaffold for the two metal ions (blue). Phosphate substrate analog is shown in gray.

1.11 Chlamydia trachomatis

Many well-known Gram-negative pathogens, such as *E. coli*, *Salmonella*, *Yersinia pestis*, *Vibrio cholerae*, and *Helicobacter pylori* are part of the Proteobacteria phylum. However, the phylum Chlamydiae also encompasses several bacterial species that are

threats to human health, specifically *Chlamydia trachomatis.* This obligate intracellular pathogen is the world's leading cause of infectious blindness and sexually transmitted bacterial infection (108). Ocular infections of *C. trachomatis* are responsible for conjuctival disease, which can develop into trachoma (blindness). Colonization of the bacteria in the genital tract can induce inflammation, edema, and mucosal discharge; neglect of treatment may lead to salpingitis, pelvic inflammatory disease, ectopic pregnancies, infertility, and increased susceptibility to infection with other sexually transmitted pathogens like HIV (109).

1.11.1 Life Cycle

Like other members of Chlamydiae, *C. trachomatis* exhibits a biphasic life cycle comprised of two morphological forms: the elementary body (EB) state and the reticulate body (RB) state (Fig. 13) (109). Infection begins when bacteria in the EB form attach and invade host epithelial cells. Once inside the phagocytic compartment, EBs produce proteins that mediate the formation of an inclusion. This inclusion quickly dissociates from the endolysosomal pathway, avoiding degradation by the lysosome.

After inclusion formation, EBs begin to differentiate into the RB form, which is the metabolically active and replicative state of *C. trachomatis.* This transition does not occur simultaneously in all EBs within the inclusion. Once in the RB morphology, bacteria begin to divide via binary fission, expanding the inclusion. At this halfway point of the infection, some of the RBs begin to convert back into the EB state. These

newly formed EBs are released through the mutually exclusive processes of cell lysis or extrusion to initiate new rounds of the infection.

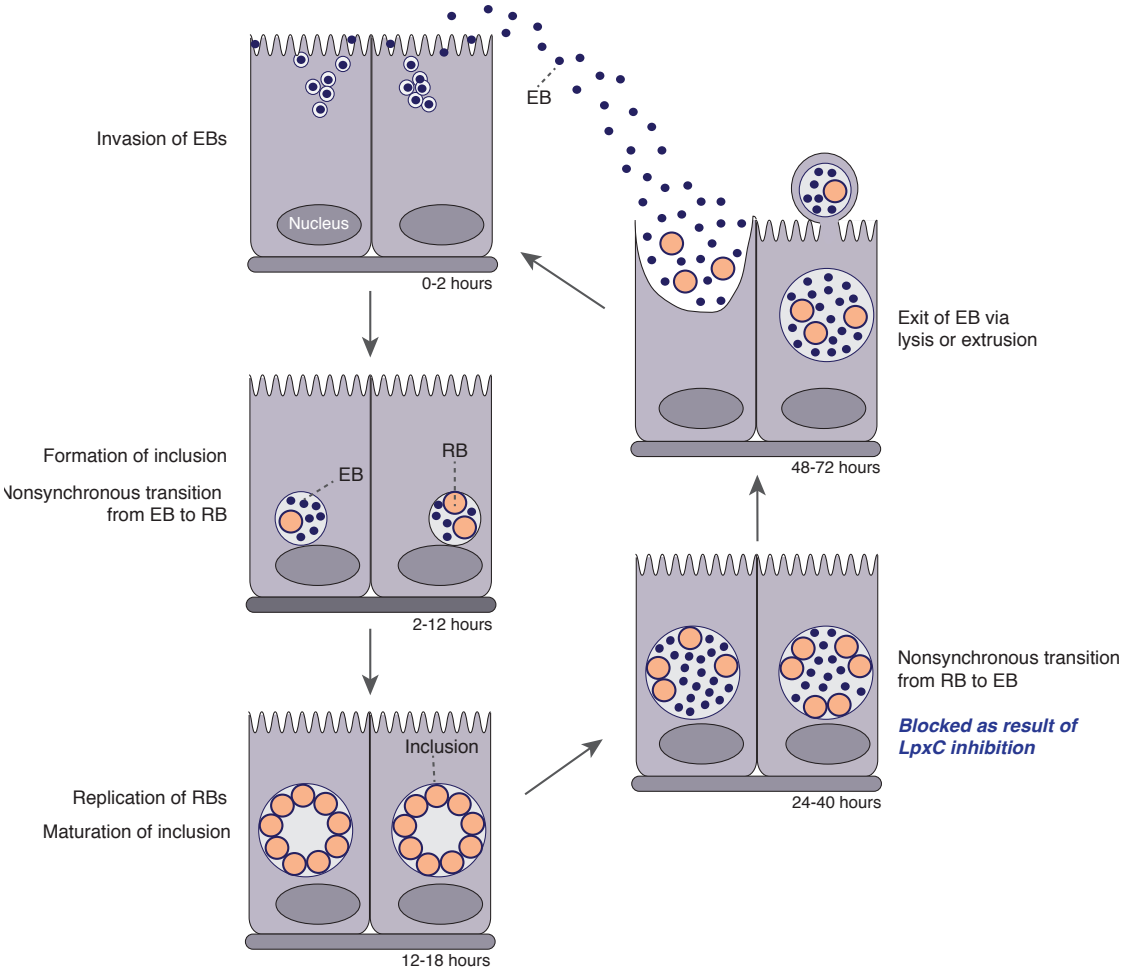

Figure 13: The Bi-Phasic Life Cyle of *Chlamydia trachomatis*

Infection begins when *C. trachomatis* in the EB form (dark blue) invade host epithelial cells (purple). After endocytosis, EBs hijack the endosomal pathway to generate a membrane-bound inclusion (denoted). At this time, EBs begin to differentiate into the RB form (peach). Subsequent replication of RBs increases the size of the inclusion. RBs then initiate transition back to the EB form. This process is blocked in the presence of inhibitors targets at the lipid A biosynthetic enzyme, LpxC. In the final stage of infection, newly formed EBs leave the cell through lysis or extrusion, restarting the infection cycle. Time scale of events is denoted below each step. This figure was modified from (109).

1.11.2 Lipooligosaccharide

1.11.2.1 Structure

Being a Gram-negative species, *Chlamydia trachomatis* has a dual-membrane cell envelope. Recent labeling experiments have demonstrated that the bacteria contain a sparse peptidoglycan (108). The proteins of the outer membrane of *C. trachomatis* EBs are highly cross-linked, providing structural integrity necessary for successful infection of host cells (110,111). Also in the outer membrane is lipooligosaccharide (LOS), an LPS-like species that displays a short, branching core but lacks additional outer core or O-antigen. *C. trachomatis* lipid A is penta-acylated, missing a 3′ secondary hydrocarbon chain compared to the corresponding *E. coli* molecule; it also displays longer acyl chains at the 2, 2′, and 2′-3-OH positions and lacks 3-hydroxyl moieties on the 3 and 3′chain (Fig. 14) (12). The branched core of *C. trachomatis* LOS is comprised of three Kdo residues attached to the lipid A backbone (12).

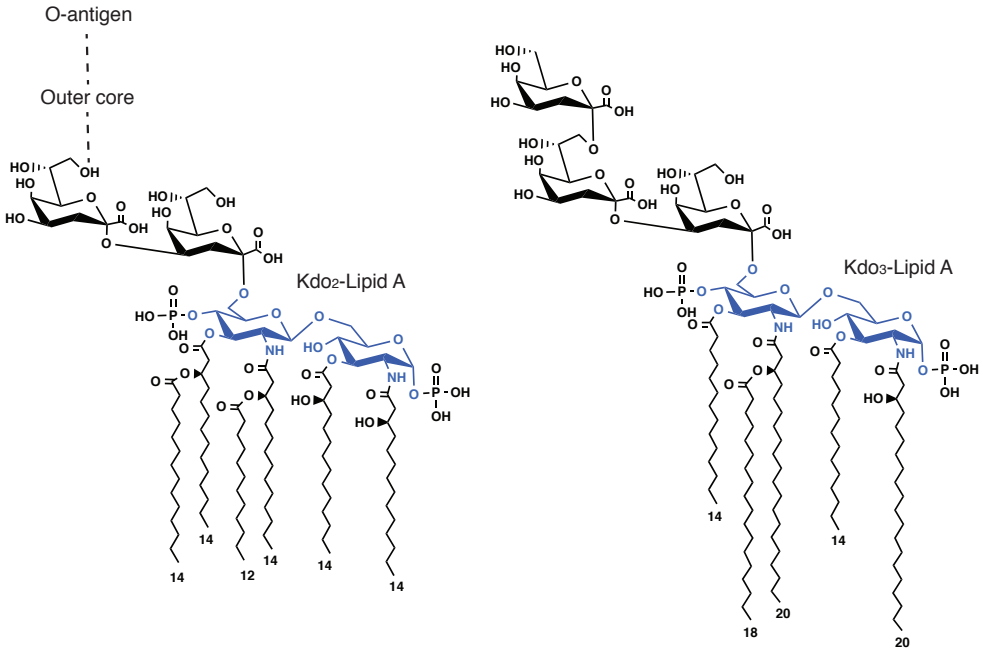

Figure 14: Structural Comparison of *E. coli* and *C. trachomatis* Lipid A
Shown are the lipid A moieties of *E. coli* LPS (left) and *C. trachomatis* LOS (right). The *E. coli* molecule represents the canonical Kdo_2 lipid A species that is the end product of the Raetz pathway. The lipid A moiety of *C. trachomatis* LOS is pentacylated, exhibits longer hydrocarbon chains than *E. coli,* and contains an third Kdo residue. While additional outer core and O-antigen regions are attached to Kdo_2 lipid A in the mature form of *E. coli* LPS, no further addition is made to *C. trachomatis* LOS.

1.11.2.1 Function

The role of LOS in *C. trachomatis* has been partially elucidated through determining the effects of inhibiting its synthesis (20). Small molecules known to abrogate LpxC, the third enzyme of the LOS biosynthesis, were employed to treat *C. trachomatis* infection in HeLa cells. It was observed that the bacteria were still able to replicate normally inside of HeLa cells, forming inclusions of standard morphology that

were filled with RBs. This was in contrast to the antibacterial effect seen in a similar intercellular *Salmonella entercia* serovar Typhimurium infection. The RBs from inhibitor-treated *C. trachomatis* lacked detectable LOS (as determined through use of an LOS-specific antibody), indicating that blockage of LpxC activity was in fact preventing synthesis of the molecule. Thus, it was concluded LOS is not required for *C. trachomatis* survival during beginning infection stages that involve intracellular replication (20).

While inhibitor-treated *C. trachomatis* infections formed normal inclusions in size and integrity, the population of each inclusion displayed a much higher RB to EB ratio compared to that seen in untreated infections. This translated to inclusions composed primarily of RBs, with the occasional EB appearing misshapen. Furthermore, *C. trachomatis* harvested from inhibitor-treated cultures showed a dramatic decrease in their ability to establish secondary infections, corresponding to the reduced level of EBs. Overall, this suggested that while LOS is not necessary for the transition of *C. trachomatis* from EB to RB or for replication of RBs, it is required for morphological conversion of RB form to EB form (20).

The importance of LOS in *C. trachomatis'* development to an infectious form might be due to the molecule's relationship with outer membrane proteins. As previously mentioned, the proteins in the outer membrane of *C. trachomatis* EBs are highly cross-linked, creating a sheath that gives the cell structure and protection

(110,111). The protein OmcB forms part of this formidable barrier (112); it is developmentally regulated for the late stages of the bacteria's life cycle for expression during the transition of the osmotically fragile RB to a rigid EB (113). *C. trachomatis* that were blocked for LOS synthesis displayed a decrease in OmcB despite presence of other constitutive outer membrane proteins (20). This decrease was not ubiquitous, as other developmentally regulated proteins that are involved in nucleoid condensation were evident at normal levels. Thus, it is possible that presence of LOS is important for proper expression or stability of OmcB (20). As the protein is important for maintaining the integrity of the EB, the inability of OmcB to function due to absence of LOS arrests *C. trachomatis* in the RB state.

As LOS inhibition correlates to inability of *C. trachomatis* to transition to the EB state, it may be employed for use as a therapeutic tool. It is already been shown that small molecules abrogating the activity of LpxC are effective in restricting the amount of infectious bacterial progeny in culture (20); inhibitors to other Raetz pathway enzymes would likely have the same effect. Such molecules could translate into treatments for *C. trachomatis* infections. Halting the bacteria in the RB state would not only prevent the spread of the pathogen to other cells, but it would also allow more time for infected cells to mount an immune response. This could assist in acquisition of cell-mediated immunity, which may be helpful to the host in the instance of subsequent *C. trachomatis* infection.

1.11.2.2 Conservation of Raetz Pathway

The similarity in the overall structures of lipid A from both *E. coli* and *C. trachomatis* corresponds with the conservation of Raetz pathway enzymes in these organisms (Fig. 15). The primary difference between the two molecules is the secondary acyl chain at the 3′ position (Fig. 15). In *E. coli*, LpxM catalyzes the addition of this moiety; *C. trachomatis* lacks such an ortholog, accounting for the nonappearance of the 3′ secondary acyl chain. This is not rare, as LpxM is only conserved within some γ proteobacteria. The presence of other acyl chains in the lipid A molecules is reflected in the conservation of LpxA, LpxD, and LpxL in both bacteria. Likewise, existence of the disaccharide backbone and 4′ phosphate group can be rationalized by occurrence of LpxB and LpxK, respectively. The Kdo residues attached to the backbone can be attributed to their respective KdtA orthologs. Furthermore, LpxC is present in both Gram-negatives. Thus, the only difference between the Raetz pathway of *E. coli* and *C. trachomatis* (albeit LpxM, as discussed above) appears to be in LpxH.

Considering the presence of other Lpx enzymes in *C. trachomatis* and the structure of the final lipid A product, the absence of LpxH does not indicate lack of UDP-DAGn hydrolase activity in the bacteria. Rather, it suggests that an alternative enzyme is serving to function in place of LpxH in the Raetz pathway. Other bacteria lacking LpxH employ its functional analog, LpxI, to serve as the fourth enzyme of lipid A biosynthesis. However, *C. trachomatis* does not display an ortholog for LpxI, implying

that the bacterial species contains an unidentified protein capable of UDP-DAGn hydrolysis.

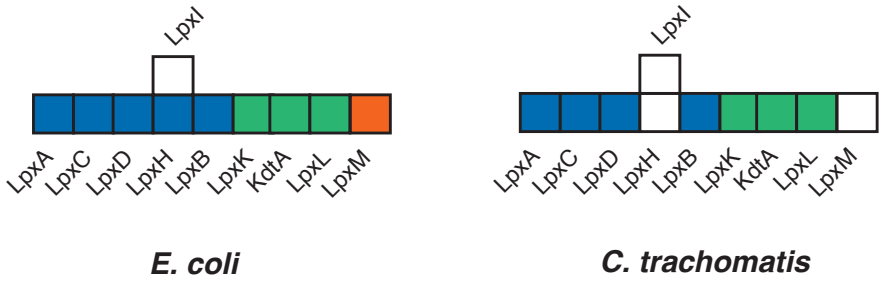

Figure 15: Genetic Comparison of *E. coli* and *C. trachomatis* Lipid A Biosynthesis
Key block showing the presence of Lpx orthologs encoding lipid A biosynthetic activities in *E. coli* and *C. trachomatis.* Absence of color correlates with absence of protein within the genome of the respective bacteria.

1.11.3 Genetics

C. trachomatis as a relatively small genome, being ~ 1 Mb in size. Comparison with other bacterial genomes reveals the absence of key biosynthetic pathways; this is likely due to the ability to *C. trachomatis* to obtain a variety of metabolites from its host (114). Some of the existing *C. trachomatis* pathways are missing canonical enzymes and utilize unique proteins in their place (115,116). Despite the small size of the genome, there are many *C. trachomatis* open reading frames that have unknown functions.

Functional characterization of the *C. trachomatis* genome is difficult due to the lack of genetic tools available for the bacteria (109). The obligate intracellular nature, unique life cycle, and incomplete understanding of host interaction make it impossible to use common molecular biology techniques for study of *C. trachomatis.* However, it is

known that the bacteria can undergo DNA exchange with one another in laboratory culture (117,118). Furthermore, chimeric *C. trachomatis* plasmids can be transformed into EBs and show evidence of recombinant gene expression (119). Very recently, this technique was optimized for controllable expression with use of the Tetracyline repressor and anhydrotetracycline (120).

In the absence of precise, direct genetic methods, other techniques for the functional assessment of *C. trachomatis* genes have been developed (109). Gain-of-function approaches involve expressing *C. trachomatis* genes in a heterologous system and subsequently monitoring of any changes in host function (121,122). Alternatively, for loss-of-function approaches, *C. trachomatis* are randomly mutagenized and then screened for desired genotype or phenotype. As random mutagenesis often causes multiple genomic lesions in a single strain, any unwanted mutations in isolated bacteria can be removed through genetic exchange with other *C. trachomatis* strains (123). This allows isolation of *C. trachomatis* with single mutations that can be utilized to assess corresponding gene functions.

1.12 Contributions of This Work to the Field

The work presented in the subsequent chapters serves to further elucidate enzymological and genetic aspects of UDP-DAGn hydrolysis in lipid A biosynthesis. As mentioned above, initial characterization of LpxH was hampered by sample impurity and a lack of a robust UDP-DAGn hydrolase assay, making it difficult to draw definitive

conclusions about the enzyme's properties. Chapter 2 addresses this issue with the purification of the *H. influenzae* ortholog of LpxH (HiLpxH) and development of an optimized *in vitro* assay for LpxH activity. With use of an ~90% homogenous protein sample and new dynamic method for hydrolytic assessment, we report a significant increase in apparent V_{max}. Additionally, we show a more dramatic pH profile of LpxH and present evidence that it does not obey surface dilution kinetics as previously reported.

While initial studies of LpxH bioinformatically identified the protein as a CLP metalloenzyme, there was a dearth of supporting biochemical evidence. Armed with a homogenous sample of LpxH and a robust *in vitro* assay, we report the metal dependency of HiLpxH in Chapter 3. The enzyme shows ~600 fold activation in the presence of Mn^{2+}. Furthermore, through EPR spectroscopy, we show evidence of a di-Mn^{2+} cluster in the enzyme. Mutagenesis additionally suggests that the residues of the CLP motif in HiLpxH play an important role in activity. Overall, this analysis definitively indicates that LpxH does function as a CLP enzyme.

The hydrolysis of UDP-DAGn is likely ubiquitous in lipid A biosynthesis, however some Gram-negative bacteria, such *Chlamydia trachomatis,* have neither an LpxH nor LpxI ortholog to facilitate this process. In Chapter 4, we discuss the design and implementation of a screen aimed to identify the unknown UDP-DAGn hydrolase in *C. trachomatis.* The strategy employs an *E. coli* strain with a temperature-controlled

expression of *lpxH* to screen a *C. trachomatis* open reading frame (ORF) library for functional complementarity. Successful completion of the method identified a candidate ORF, Ct461, that is capable of lipid X production *in vivo* and *in vitro.* We conclude that Ct461 encodes for LpxG, a unique UDP-DAGn hydrolase. This portion of work not only elucidates the genetic nature of UDP-DAGn hydrolysis in *C. trachomatis* but also serves as a model for the implementing functional analysis of unknown genes in genetically intractable bacteria.

In Chapter 5, we present the initial characterization of the newly identified UDP-DAGn hydrolase LpxG. With use of a purified protein sample and mass spectrometry, we demonstrate that LpxG facilitates hydrolysis through attack on the α-phosphate of UDP-DAGn. Based its homology to CLP metalloenzymes, we investigated the metal dependence of CtLpxG and found Mn^{2+} stimulates enzyme activity 35-fold. Additionally, we provide initial evidence that CtLpxG behaves like as CLP enzyme, as a point mutation in the conserved metallophosphoesterase motif abrogates activity. Finally, we compare the ability of LpxG, LpxH, and LpxI to perform UDP-DAGn hydrolysis *in vivo* using heterologous expression in *E. coli*; LpxG seems to be the least efficient functional ortholog, which may reflect an ancestral or adaptive evolution of the *C. trachomatis* lipid A pathway. The work in this chapter provides a foundation for more detailed enzymatic characterization of LpxG and allows for initial biochemical and bioinformatic comparison of the new hydrolase to its known functional orthologs.

2. Optimized Purification and Enzymological Characterization of the UDP-2,3-diacylglucosamine Hydrolase LpxH

2.1 Introduction

In *E. coli*, the pathway for lipid A biosynthesis consists of nine enzymes, each of which catalyzes a separate step (7). Nearly all of these nine enzymes are highly conserved throughout Gram-negative bacteria (81). However, an exception to the universal nature of the pathway is the fourth step that involves the hydrolysis of UDP-2,3-diacylglucosamine (UDP-DAGn) to yield UMP and 2, 3-diacylglucosamine 1-phosphate (more commonly known as lipid X) (Fig. 9). This reaction, thought to be the first membrane-associating step of the pathway, can be carried out by either LpxH (40,82) or LpxI (41). These two enzymes share no sequence similarity, are never found in the same organism, and attack different phosphates in their catalysis of UDP-DAGn hydrolysis (41). Despite these differences, *lpxI* can complement an *lpxH* knockout in *E. coli* (41), indicating that LpxI and LpxH have the same function within the context of the lipid A pathway.

In early efforts to characterize LpxH, the *E. coli* ortholog (EcLpxH) was over-expressed and purified. It was noted that the enzyme behaved like a peripheral membrane protein, partitioning to both the membrane and the cytosol during cell-extract fractionation. A Green-19 dye affinity column was employed to extract over-expressed EcLpxH from cell lysate. While this method did result in a 13-fold

enhancement in UDP-DAGn specific activity, it produced an EcLpxH sample that was only 60% homogenous. It was noted that incubating the sample with $MnCl_2$ after elution from the Green-19 column coincided with an increase in activity. Subsequent purification steps were attempted, however the protein proved to be unstable and lost activity during later isolation efforts.

Activity assessment during initial purification of LpxH was carried out through use of an *in vitro* autoradiographic thin-layer-chromatography (TLC)-based assay. Specifically, the enzyme sample was incubated with buffer and substrate doped with [β-^{32}P]-UDP-DAGn, then samples of the reaction were spotted on a silica TLC plate at various time intervals. The β position of the substrate's radiolabel permits the retention of the ^{32}P-marker after the molecule is hydrolyzed to lipid X. Thus, it is possible to quantify the percentage of substrate conversion using autoradiography.

In addition to tracking UDP-DAGn hydrolase activity during the identification and purification of LpxH, the autoradiographic assay was also used for enzymatic characterization. The catalytic activity of partially purified EcLpxH was assessed for pH dependence; activation was observed at pH 8.0, however the dynamic range of the results was too low to make any definitive conclusions about enzyme behavior. As the enzyme works on a lipid substrate and showed the properties of a peripheral membrane protein, LpxH hydrolysis was also tested over a range of detergent concentrations. Activity seemed to decrease as the level of detergent in the assay increased, leading to

the conclusion that LpxH obeyed surface dilution kinetics. Finally, the K_M and V_{max} of LpxH were determined to be 61.7 μM and 17.2 μmol $min^{-1}mg^{-1}$, respectively.

While the initial purification and characterization of EcLpxH provided important information about the function and basic properties of the UDP-DAGn hydrolase, a lack of sample purity and low protein activity prevented more detailed insight about the protein. To circumvent these problems, a more stable ortholog, better purification scheme, and more robust assay were necessary. Here we report the cloning and purification the *Haemophilus influenzae* ortholog of LpxH (HiLpxH) to near homogeneity and the identification of optimized UDP-DAGn hydrolase assay conditions. With this sample of enhanced purity and a more dynamic method of *in vitro* catalytic assessment, we are able to re-evaluate the enzymatic properties of LpxH. We observe a 1000-fold increase in observed activity under our optimized conditions, corresponding to an significant increase in the observed V_{max}. Additionally, we report a strong reliance of activity on basic assay conditions. Finally, we show that HiLpxH does not display surface dilution kinetics, as previously reported. Overall, our development of a more efficient purification scheme paired with our new understanding of the fundamental properties of LpxH set the scene for further enzymatic characterization and structural studies, which could both be important in the development of inhibitors.

2.2 Materials and Methods

2.2.1 Chemicals and Reagents

Reagents for bacterial growth included yeast extract, tryptone, and Bacto agar, and were purchased from Difco (Detroit, MI). The 4-(2-hydroxyethyl)-1 piperazineethanesulfonic acid (HEPES), phosphate-buffered saline (PBS) components, HCl, salts, ampicillin, isopropyl-β-D-thiogalactoside (IPTG), fatty acid-free bovine serum albumin (BSA), ethylenediaminetetraacetic acid (EDTA), and dithiothreitol (DTT) were purchased from Sigma-Aldrich (St. Louis, MO). Methanol, chloroform, pyridine, and acetic acid were obtained from EMD Science (Gibbstown, NJ). Radioactive γ-^{32}Pi was purchased from PerkinElmer (Waltham, MA). The plasmids used in this study were purified using Qiagen Mini-Prep kits (Qiagen, Valencia, CA) according to the manufacturer's protocol. DNA fragments were purified using QIAquick Spin kits. Sequencing was carried out by Eton Bioscience, Inc (Research Triangle Park, NC). Unless otherwise noted, protein concentration was determined either by BCA Assay or Bradford Assay (Thermo Scientific, Waltham, Massachusetts) depending on compatibility with buffer components. Both of these methods were carried out as described by the manufacturer.

2.2.2 Cloning of *H. influenzae lpxH*

Amplification of *lpxH* (HI0375) from *H. influenzae* genomic DNA (ATCC, Rockville, MD) was accomplished using polymerase chain reaction (PCR) with primers

Hih_F and Hih_R that were 50 base pairs upstream and downstream of *lpxH*. (Table 1) To facilitate eventual ligation of the gene product into an expression vector, we used primers (Integrated DNA Technologies, Coralville, IA) that allowed for the incorporation of *Nde*1 and *Xho*I restriction sites to the 5' and 3' ends of *lpxH* and the elimination of the stop codon at the end of the gene. The PCR reaction was carried out using a Mastercycler Gradient Thermocycler (Eppendorf, Hamburg, Germany) with the reagents and protocol of the KOD Hot Start Kit (EMD Chemicals, Gibbstown, NJ), however the reaction was additionally supplemented with 3% (w/v) dimethyl sulfoxide. Sequencing of the resulting product using the original primers was used to ensure proper amplification.

To generate an expression vector with a C-terminal His_{10} tag that was cleavable by Tobacco Etch Virus (TEV) protease, 33 additional nucleotides were added to pET21b (Novagen/EMD Chemicals) to encode for the 7 amino acids of the protease site (ENLYFQG) (124) and the 4 additional histidine residues needed to elongate the affinity tag. This was accomplished using QuikChange (Stratagene, La Jolla, CA) mutagenesis with 21TEV_F and 21TEV_R primers (Integrated DNA Technologies) that were designed to insert the additional nucleotides 3' to the *XhoI* restriction site in pET21b. The reaction was carried out using the manufacturer's protocol with an additional supplement of 3% (w/v) dimethyl sulfoxide and 1 M betaine. Following nucleotide insertion, the resulting plasmid, p21t10, was confirmed by sequencing with T7_Forward and T7_Reverse (Table

1) and transformed into chemically competent DH5α cells (Invitrogen). Additionally, p21t10 was transformed into chemically competent *E. coli* C41(DE3) to create the vector control expression strain VC_T10.

Insertion of amplified *H. influenza lpxH* into p21t10 was accomplished by digestion of both the PCR fragment and the vector with *Nde*1 and *Xho*I (New England Biolabs) under conditions described by the manufacturer. After treatment of p21t10 with antarctic phosphatase (New England Biolabs) under conditions described by the manufacturer, digested *lpxH* was inserted into the plasmid with T4 ligase (Invitrogen) as directed by the manufacturer. The ligation product, pHiHt10, was transformed into chemically competent C41(DE3) *E. coli* to generate the expression strain HiH_t10. Sequencing with T7 forward and reverse primers confirmed the appropriate insertion of *H. influenzae lpxH* into p21t10.

Table 1: Primers Used in the Characterization of HiLpxH

Name	Purpose	Primer sequence (5'-3' orientation)
21TEV_F	To add a TEV cleavage site and 4 additional histidines to pET21b	GGCCGCACTCGAGGAAAACCTGTACTT CCAGAGCCATCATCATCATCACCACCAC CACC
21TEV_R	To add a TEV cleavage site and 4 additional histidines to pET21b	GGTGGTGGTGGTGATGATGATGATGGC TCTGGAAGTACAGGTTTTCCTCGAGTGC GGCC
Hih_F	To amplify *H. influenzae lpxH*, confers 5' *Nde1* site	GCGAACTCCATATGAAACATAGCTATTT TATTTC
Hih_R	To amplify *H. influenzae lpxH*, eliminates stop codon with 3' *XhoI* restriction site	GCTGATGTCTCGAGATCTTTAATAAAAC C
T7 forward	To sequence segments of DNA cloned into pET21b and pTEV10	TAATACGACTCACTATAGGG
T7 reverse	To sequence segments of DNA cloned into pET21b and pTEV10	CTAGTTATTGCTCAGCGGTG

Table 2: Plasmids Used in the Characterization of HiLpxH

Plasmid	Description	Source
pET21b	high-copy expression vector containing a T7 promoter, Amp^R	Novagen
p21t10	modified pET21b vector encoding C-terminal TEV-protease cleavage site followed by a His_{10} tag, Amp^R	this work
pHiHt10	p21t10 containing *H. influenzae lpxH,* Amp^R	this work
pKJB2	$pET21a^+$ plasmid containing *E. coli lpxH*, Amp^R	(40)
pHiHt10	p21t10 containing *H. influenzae lpxH,* Amp^R	this work

Table 3: *E. coli* Strains Used in Characterization of HiLpxH

Strain	Description	Source
DH5α	F^- *Δ(argF-lacZYA)U169 deoR phoA supE44 Φ80 Δ(lacZ)M15 gyrA96 relA1 endA1 thi-1 hsdR17 recA1*λ^-	Invitrogen
C41(DE3)	F^- *ompT hsdS*$_B$ (r_B^- m_B^-) *gal dcm* (DE3)	(125)
VC_t10	C41(DE3) harboring p21t10, Amp^R	this work
HiH_t10	C41(DE3) harboring pHiHt10, Amp^R	this work

2.2.3 Protein Localization

Two samples of cell-free extract from HiH_t10 (obtained as described below) corresponding to 6 mg of total protein were brought to a volume of 1 mL with the appropriate stock solutions to yield final solution concentrations of 200 mM NaCl, 20 mM HEPES pH 8.0, and either 0% or 1.5% w/v of TX-100. These samples were then incubated for 1 h at 4 °C, then subjected to ultracentrifugation at 100,000 × *g* for 45 min. Resulting supernatants were collected as cytosolic fractions and pellets were resuspended in 200 mM NaCl and 20 mM HEPES pH 8.0 to obtain membrane fractions. The fractions were analyzed for the presence of HiLpxH by both SDS-PAGE and the optimized UDP-DAGn hydrolase activity assay, as described below.

2.2.4 Protein Expression and Purification

A typical prep of HiLpxH began with inoculating an overnight culture of LB with a single colony of HiH_t10. This overnight culture was subsequently used to inoculate 3 L of LB (10 g tryptone, 5 g yeast extract, 10 g NaCl per liter) supplemented

with 100 μg/mL of ampicillin to an OD_{600} of 0.02. Cultures were incubated at 30 °C with aeration at 220 rpm until they reached OD_{600} of 0.7-0.8, then induced for expression by the addition of 1 mM IPTG and grown for an additional 4 to 5 hours until the OD_{600} reached ~4. Cells from the growths were pelleted by centrifugation at 5,000 × *g*, washed with 140 mL of cold PBS, and then stored at -80 °C. For lysis, the frozen pellet was thawed, resuspended in 80 mL of ice cold 20 mM HEPES pH 8.0, and passed twice through a French pressure cell (SIM-AMINCO; Spectronic Instruments) at 18,000 psi. The debris from the resulting lysate was removed by centrifugation at 10,000 × *g* and the subsequent supernatant was collected as cell-free extract and stored at -80 °C.

Cell-free extract was thawed and diluted to 5 mg/mL with 20 mM HEPES pH 8.0. A stock solution of 10% (w/v) Triton X-100 (Thermo Scientific), was used to bring the cell-free extract to a final detergent concentration of 1.5% (w/v). All subsequent steps were carried out at 4 °C. The resulting solution was then mixed by inversion for 1 h and then subjected to ultracentrifugation at 100,000 × *g* for 45 min. The supernatant was removed and diluted with the appropriate stocks to make a 450 mL solution of ~3 mg/mL protein, 20 mM HEPES pH 8.0, 200 mM NaCl, 20 mM imidazole, and 0.5% Triton X-100. This solution was then loaded by gravity onto a packed column of 20 mL of Ni-NTA resin (Qiagen) that had been pre-equilibrated in 20 column volumes of load buffer (20 mM HEPES pH 8.0, 200 mM NaCl, 20 mM imidazole, 0.1% TX-100). The loaded column was next washed with an additional 10 column volumes of load buffer

followed by a 15 column volume wash with load buffer supplemented with 30 mM imidazole (final imidazole concentration 50 mM). To exchange HiLpxH out of detergent, the column was subjected to a 50 column volume wash with a solution of 20 mM HEPES pH 8.0, 200 mM NaCl. Elution of the protein was accomplished by a 7 column volume wash with a solution of 20 mM HEPES pH 8.0, 200 mM NaCl, and 400 mM imidazole. Samples from each wash of the column were analyzed by SDS-PAGE to ensure proper fractionation.

After elution, a TEV-protease reaction was used to cleave the C-terminal His_{10} tag. The eluted protein was diluted to a volume of 200 mL with the appropriate stock solutions to yield a sample with final concentrations of 2 mM DTT, 2 mM EDTA, 20 mM HEPES pH 8.0, 200 mM NaCl, 300 mM imidazole, and ~0.015 mg/mL (~1/50 of the HiLpxH concentration) of TEV protease. The protease used was prepared as described in the literature (124) and cleavage was monitored using SDS-PAGE. After overnight incubation, the reaction was concentrated to a final volume of 50 mL using 15 mL Amicon Ultra 10K molecular weight cutoff centrifuge concentrators (Millipore, Billerica, MA) and then dialyzed overnight against 8 L of 20 mM HEPES pH 8.0 and 200 mM NaCl. Remaining TEV protease and any uncleaved HiLpxH was removed from the sample by passage over a 5 mL Ni-NTA column pre-equilibrated with 20 column volumes of a solution containing 20 mM HEPES pH 8.0, 200 mM NaCl, and 20 mM imidazole. The flow-through was collected and then concentrated using Millipore

conical spin concentrations to a final concentration of ~8 mg/mL. The final protein sample, which contained HiLpxH followed by the residual TEV cleavage site residues of ENLYFQ, was analyzed by SDS-PAGE to confirm purity and stored at -80 °C in 15 μL aliquots.

2.2.5 Synthesis of Radioactive Substrate

^{32}P-labeled UDP-2,3-diacylglucosamine (UDP-DAGn) was prepared as previously described (41) with some modifications. Firstly, the 50 μL 0.2 M 1-H-tetrazole in acetonitrile in the morpholidate reaction was replaced with 20 μL 0.1 M dicyanoimdiazole in acetonitrile (Sigma Aldrich). Secondly, after the product of the morpholidate reaction was dried under N_2, it was extracted with a single phase Bligh-Dyer (126) with volumes of 0.5 mL methanol, 0.25 mL chloroform, and 0.2 mL PBS. The mixture was centrifuged to pellet debris and the supernatant was transferred to a 2 mL polypropylene tube and dried under N_2. The radioactive substrate was then resuspended in 100-170 μL of 20 mM HEPES pH 8.0 containing 0.02% Triton X-100 and sonicated for 2 min. One final centrifugation step was used to pellet any insoluble material. The supernatant containing the final [β-^{32}P] UDP-DAGn was transferred to a new tube and stored at -20 °C. These extra extraction steps removed contaminating impurities that interfered with the linearity of our assays.

2.2.6 Optimized *In Vitro* Assay for UDP-DAGn Hydrolase Activity

General autoradiographic assays for hydrolase activity were similar to that previously described (40) with optimized modifications. Reactions mixtures were a final volume of 15 μL in 0.6 mL polypropylene tubes and contained 20 mM HEPES pH 8.0, 0.5% (w/v) BSA, 0.05% (w/v) Triton X-100, 1 mM $MnCl_2$, 100 μM UDP-DAGn (prepared as previously described (127), 1,000 cpm/μL [β-^{32}P] UDP-DAGn, and enzyme. Previous studies of *E. coli* LpxH reported a small enhancement in enzyme stability and activity when the protein was purified with $MnCl_2$ (40); therefore, $MnCl_2$ was incorporated into the assay. All reaction components besides the enzyme were mixed to a volume of 12 μL and equilibrated at 30 °C for 10 min, after which 3 μL of enzyme was added to start the reaction. Unless otherwise noted, enzyme samples were diluted in a buffer identical to the assay mixture but lacking any lipid substrate. Aliquots of 1.5 μL were taken from the reactions at various time intervals and spotted onto 20 cm × 20 cm glass-backed silica gel thin layer chromatography (TLC) plates (EMD Chemicals, Darmstadt, Germany). These plates were developed in a 25:15:4:2 chloroform: methanol: water: acetic acid tank system, dried, exposed to phosphoscreens, scanned, and quantified as previously described (40).

2.2.7 Comparison of *In Vitro* Assays

Comparison of In Vitro Assays. To assess the effectiveness of the optimized *in vitro* assay, *E. coli* LpxH (EcLpxH) cell-free extract, HiLpxH cell-free extract, and purified

HiLpxH were analyzed for activity under both the original and the improved assay conditions. To prepare the EcLpxH cell-free extract, *E. coli* C41(DE3) was transformed with pKJB2 (40), a pET21a$^+$ plasmid containing *E. coli lpxH*. A 250 mL culture of the resulting strain was grown at 30 °C in LB media and induced for expression with IPTG at mid-log phase. After 5 h cells were harvested and lysed to generate cell-free extract using the method described above. The same procedure was carried out in parallel with strain HiH_t10 to prepare the HiLpxH cell-free extract. Purified HiLpxH was isolated by the aforementioned technique. Activity assessment under original conditions was conducted as previously reported with the final protein concentrations in the assay for EcLpxH cell-free extract, HiLpxH cell-free extract, and HiLpxH being 1.8, 4.5, and 8.5 μg/mL respectively. Samples were also tested under the optimized *in vitro* conditions with protein concentrations of 45 ng/mL EcLpxH cell-free extract, 110 ng/mL HiLpxH cell-free extract, and 1.7 ng/mL HiLpxH.

2.2.8 Kinetic Parameters, pH Optimum, and Detergent Dependence of HiLpxH

To determine the K_M and V_{max} of HiLpxH with respect to UDP-DAGn, purified HiLpxH was assayed under standard conditions except the concentration of UDP-DAGn was varied from 20 to 400 μM. The velocities from each of these reactions were plotted against substrate concentration and, using KalediaGraph (Synergy Software, Reading PA), the resulting curve was fit to the Michaelis-Menten equation. In order to maintain

linear conversion at various substrate concentrations, the HiLpxH in the assay was varied from 6 to 63 pM.

To assess the effect of pH on HiLpxH activity, purified protein was assayed under standard conditions except 20 mM HEPES pH 8.0 was replaced with a triple buffer system containing 100 mM sodium actetate, 50 mM bis(2-hydroxyethyl)iminotris-(hydroxymethyl)hexane, and 50 mM TRIS at a pH from 4.0 to 9.0. KaledíaGraph was used to fit a single-limb pK_a curve (Eq. 1) to the resulting data. The enzyme concentration of HiLpxH needed to see linear activity in the assay at different pH values ranged from 30 pM to 372 nM.

$$v = \frac{C}{1 + [H]/K_a}$$

Equation 1: pK_a Determination

To monitor the detergent dependence of HiLpxH, the Triton X-100 concentration in the standard assay was varied from 0 to 18 mM (1.2 % w/v). Purified HiLpxH was diluted in the standard buffer lacking Triton X-100, added to the reactions covering the mentioned range of detergent concentrations, and assayed for activity. Reported total detergent concentrations accounted for the small amount of detergent (0.01 mM, 0.0007% w/v) present in both the [β-^{32}P] UDP-DAGn and the non-radioactive UDP-DAGn. Linear activity could be observed at final enzyme concentrations of 30 pM and 6 pM.

2.2 Results

2.2.1 Expression and Purification of HiLpxH

Previous studies of LpxH were performed using the *E. coli* ortholog. However, purification attempts with this version of the protein proved cantankerous, as the enzyme did not maintain activity over time, suggesting it may be unstable upon isolation. In an effort to circumvent this issue, we turned to an UDP-DAGn hydrolase ortholog from another species: *Haemophilus influenzae*. Additionally, as dye affinity chromatography did not yield protein of high purity, we sought to employ a more efficient method of purification using Ni-NTA chromatography.

With the aforementioned motivations in mind, the gene encoding LpxH from *H. influenzae* was amplified from genomic DNA and cloned into a modified pET21b expression vector designed to yield a protein product that was tagged at the C-terminus with an 8-residue TEV protease cleavage site followed by 10 histidine residues. (It should be noted that there is a high frequency of conserved residues at the N-terminus of LpxH orthologs, thus a C-terminal tag was chosen to prevent any inadvertent alterations to the integrity of the N-terminal region). Transformation of this plasmid into *E. coli* C41 resulted in strain HiH_t10. When HiH_t10 was grown at 30 °C in the presence of IPTG, the over-expression of a 27 kD protein matching the molecular weight of the predicted protein product was evident when compared to a vector control strain VC_T10 via SDS-PAGE (Fig. 16A).

When over-expressed in *E. coli* C41, HiLpxH partitioned to both the membrane and the cytosolic fractions, as indicated by SDS-PAGE and activity assay (Fig. 16B). This membrane association of the protein is similar to the behavior reported for EcLpxH (40). To increase the yield of protein for purification, the cell-free extract from HiH_t10 was incubated with Triton X-100 to solubilize any HiLpxH that may be associated with the membrane, resulting in recovery of nearly all the LpxH activity to the soluble fraction (Fig. 2B). This additional isolation step was not explored in the purification of EcLpxH.

Following detergent treatment, Ni-NTA chromatography was used to isolate the His_{10}-tagged HiLpxH. Any remaining detergent from the initial solubilization step was removed with an extensive wash with buffer lacking detergent or imidazole after the protein was loaded onto the Ni-NTA column. The initial Ni-NTA step resulted in a 10-fold increase in specific activity (Table 4) and yielded protein that was ~90% pure by SDS-PAGE (Fig. 16C). Following dialysis to remove imidazole, cleavage of the His-tag, and subsequent clean-up with another Ni-NTA column, the final protein sample showed marginal increase in purity by gel, but a 6-fold enhancement in specific activity. This corresponded to a dramatic increase in total active units (480%, Table 4), suggesting that although the inclusion of an affinity tag facilitated protein purification, its presence inadvertently impaired the enzyme activity. Overall, we were able to consistently recover ~30 mg of HiLpxH per 1 L of HiH_t10 culture. This final protein sample was ~95% pure (Fig. 2C) and exhibited a 60-fold increase in specific activity (Table 4).

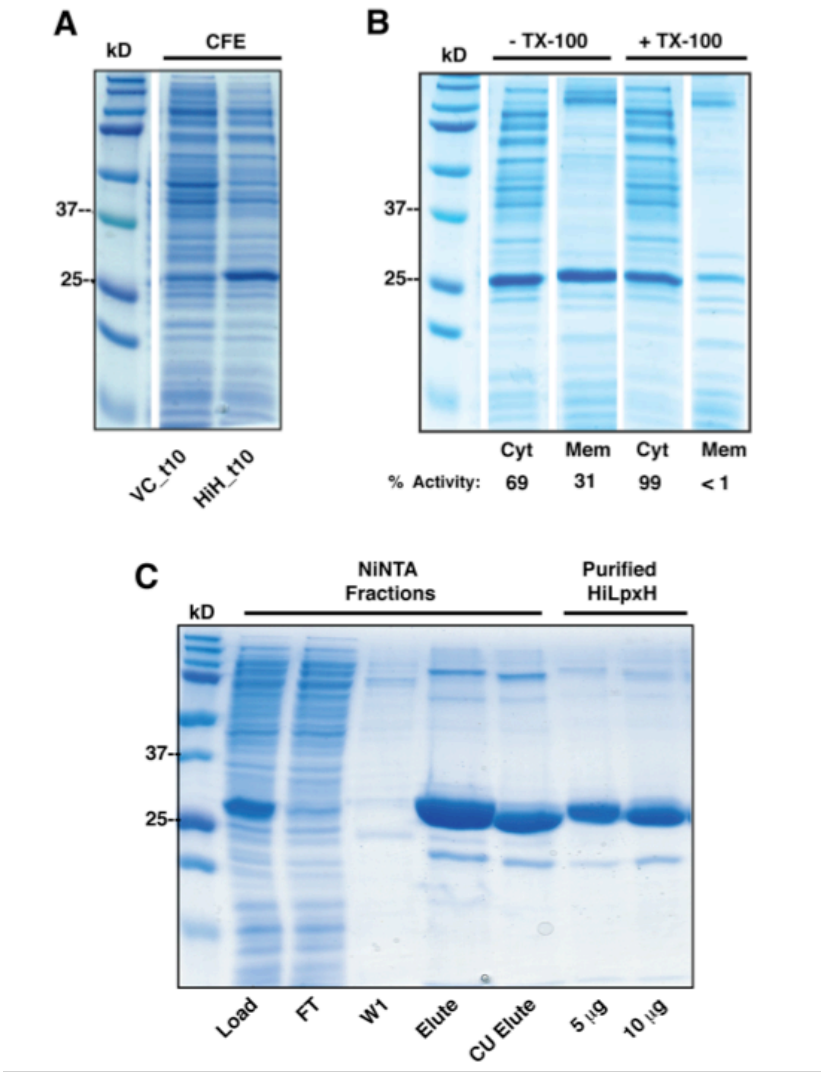

Figure 16: SDS-PAGE Analysis of Over-expression and Purification of HiLpxH

(A) Cell-free extract (CFE) of VC_t10 and HiH_t10 prepared as described in Experimental Procedures. The 27 kD band that is present in the HiH_t10 lane and not in the VC_t10 lane corresponds to over-expressed HiLpxH. (B) Analysis of fractions from HiLpxH purification outlined in Materials and Methods. Fractions from the Ni-NTA purification include the load denoting the solubilized cell-free extract from HiH10_t that was loaded onto the column, FT representing the flow through from the column, W1 signifying the 50 mM imidazole wash, and Elute indicating the tagged HiLpxH obtained from the 400 mM imidazole wash. The CU elute lane shows protein that flowed through the second clean-up Ni-NTA column after TEV-protease digestion. The purified HiLpxH fractions depict the final sample of purified HiLpxH that was used in radiographic assays and EPR experiments. The labels 5 μg and 10 μg indicate how much protein was loaded in each lane.

Table 4: Purification of HiLpxH from HiH_t10

Step	Protein (mg)	Volume (mL)	Units (mmol/min)	Specific Activity (mmol min^{-1} mg^{-1})	Fold Purification
NiNTA Load	1400	400	182	0.13	1
NiNTA Elute	210	140	273	1.3	10
Final Sample	112	16	874	7.8	60

2.2.2 HiLpxH Activity in Optimized Autoradio-graphic Assay.

As discussed above, LpxH activity can be monitored with a TLC-based assay that utilizes [β-^{32}P]-UDP-DAGn. Previously published assay conditions contained 25 mM HEPES pH 8.0, 100 μM UDP-DAGn, and 1,000 cmp/μL [β-^{32}P] UDP-DAGn (40). Based on the observations of increased stability of the *E. coli* ortholog in the presence of $MnCl_2$ and slight activation of the enzyme upon pre-incubation with the metal (40), we added 1 mM $MnCl_2$ to the assay dilution buffer as well as to the reaction. Additionally, we supplemented the reaction with 0.05 mg/mL BSA and 0.05% Triton X-100 to aid in protein stability and substrate solubility.

Our new assay conditions proved to enhance the *in vitro* catalysis of LpxH. When purified HiLpxH was assayed with these modifications, we were able to track conversion of [β-^{32}P]-UDP-DAGn to [^{32}P]-lipid X (Fig. 17A) and calculate an activity that

was 1000-fold higher than that calculated when HiLpxH was assayed under previously reported conditions (Fig. 17B). This increase in activity under optimized conditions was also observed when the cell-free extract of strains over-expressing HiLpxH (HiH CFE) and EcLpxH (EcH CFE) were tested for lipid X formation. The LpxH expression from both of these cell-free extract samples appeared equal by SDS-PAGE (data not shown) and corresponded to similar levels of activity under both conditions, indicating the activation was not ortholog-specific. Furthermore, activity in the optimized system is linear with both time (Fig. 17C) and protein concentration (Fig. 17D).

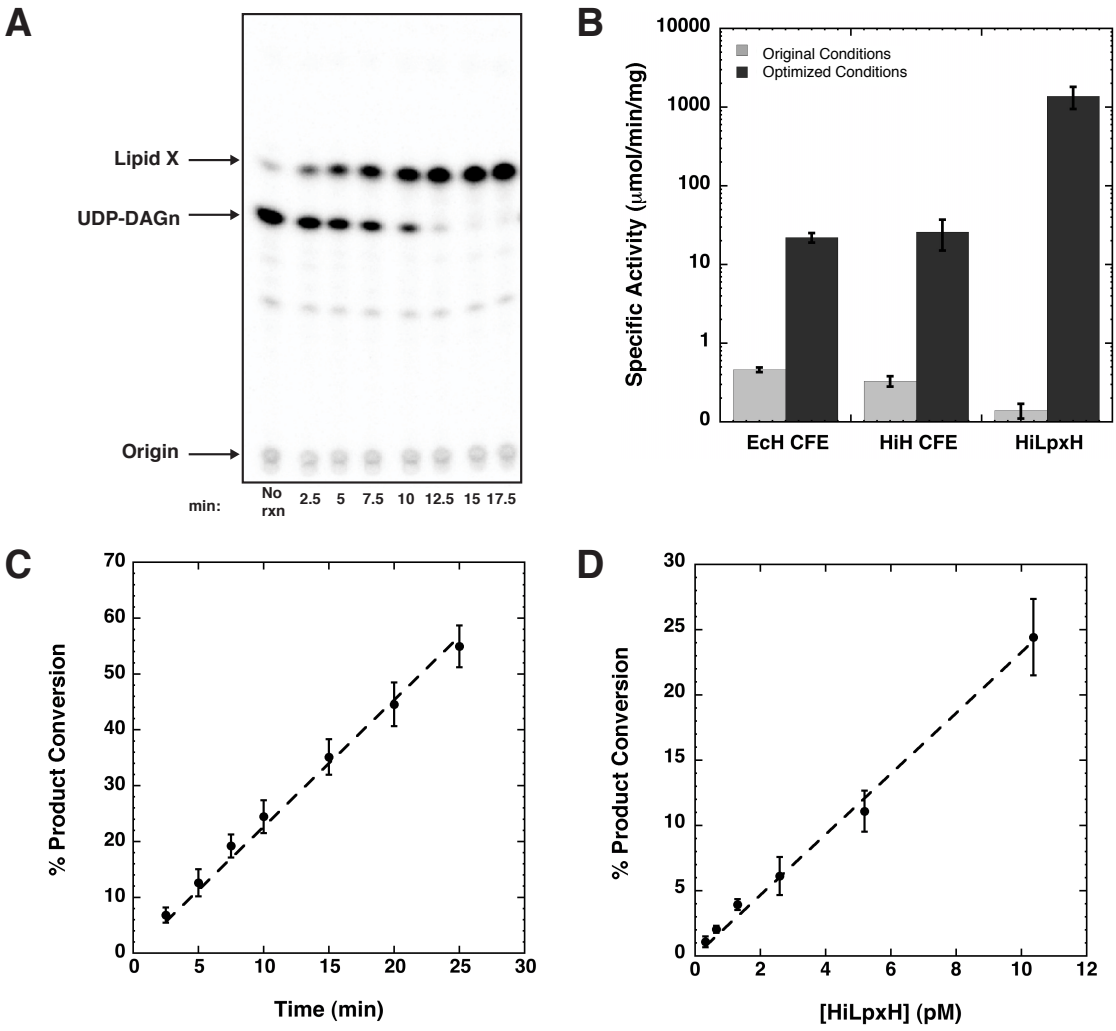

Figure 17: Assay for LpxH Activity

(A) Scan of phosphoscreen exposed to silca TLC plate from a representative HiLpxH assay using 10 pM enzyme. Product conversion is calculated by quantifying intensity of lipid X as a percentage of the total intensity of each lane and then subtracting the background conversion calculated from the no enzyme (no rxn) control. (B) Specific activity of various protein samples under original assay conditions compared to optimized assay conditions. Cell-free extract of samples over-producing EcLpxH (EcH CFE) and HiLpxH (HiH CFE) were prepared in parallel and exhibit similar levels of protein expression. (C) Percent of 100 μM UDP-DAGn converted to lipid X at specific time points under standard assay conditions with 10 pM HiLpxH. Data was fit to a linear curve using KaleidaGraph and showed an R^2 value of 0.998. (D) Percent of 100 μM UDP-DAGn converted to lipid X at various HiLpxH concentrations after 10 min under standard reaction conditions. KaleidaGraph was once again used to fit data to a linear curve with an R^2 value of 0.995. Plots generated in (C) and (D) are the result of the average of three independent data sets.

2.2.3 Apparent Kinetic Parameters, pH Rate Profile, and Detergent Dependence of HiLpxH.

While the enzymatic properties of EcLpxH had been reported previously (40), these observations were obscured by sample impurity, less-than-optimal assay conditions, and low enzymatic activity. Therefore, it is critical to revisit the characterization of LpxH using a highly purified protein sample and our newly optimized assay conditions. The specific activity of purified HiLpxH was determined at varied concentrations of UDP-DAGn to calculate the basic kinetic parameters of the enzyme (Fig. 18A). When this information was fit to a Michaelis-Menten model, it resulted in an apparent K_M of 79.4 ± 11.0 μM for the lipid substrate and an apparent V_{max} of 18.1 ± 0.9 mmol $min^{-1}mg^{-1}$,

The high specific activity of HiLpxH also enabled us to determine the pH dependence of LpxH catalysis. LpxH is most active at slightly alkaline pH values and exhibits a sharp decrease in its catalytic activity at low pH. It is important to note that such drop in LpxH activity at acidic pH is not due to enzyme instability as pre-incubation of HiLpxH at low pH does not alter the apparent enzyme activity at the standard condition of pH 8.0 (data not shown). These data were fit to a single lobed pH curve described by Eq. 1 with a pK_a=6.6 ± 0.4 (Fig. 18B).

Finally, in order to gain insight into how LpxH interacts with a hydrophobic surface, the activity of HiLpxH was assessed at a range of Triton X-100 concentrations from 0 to 18 mM. As shown in Fig. 18C, the enzyme is active without detergent and

demonstrates stimulation in hydrolysis as the detergent concentration nears the critical micelle concentration (0.19 mM). At detergent amounts above the critical micelle concentration, the protein initially shows a decrease in hydrolytic ability, after which activity appears to be unaffected by the detergent concentration in the assay. Such behavior is not indicative of surface dilution kinetics, suggesting that while the enzyme likely associates with the surface of the detergent-substrate micelles *in vitro* during catalysis, it is not directly imbedded in a detergent micelle.

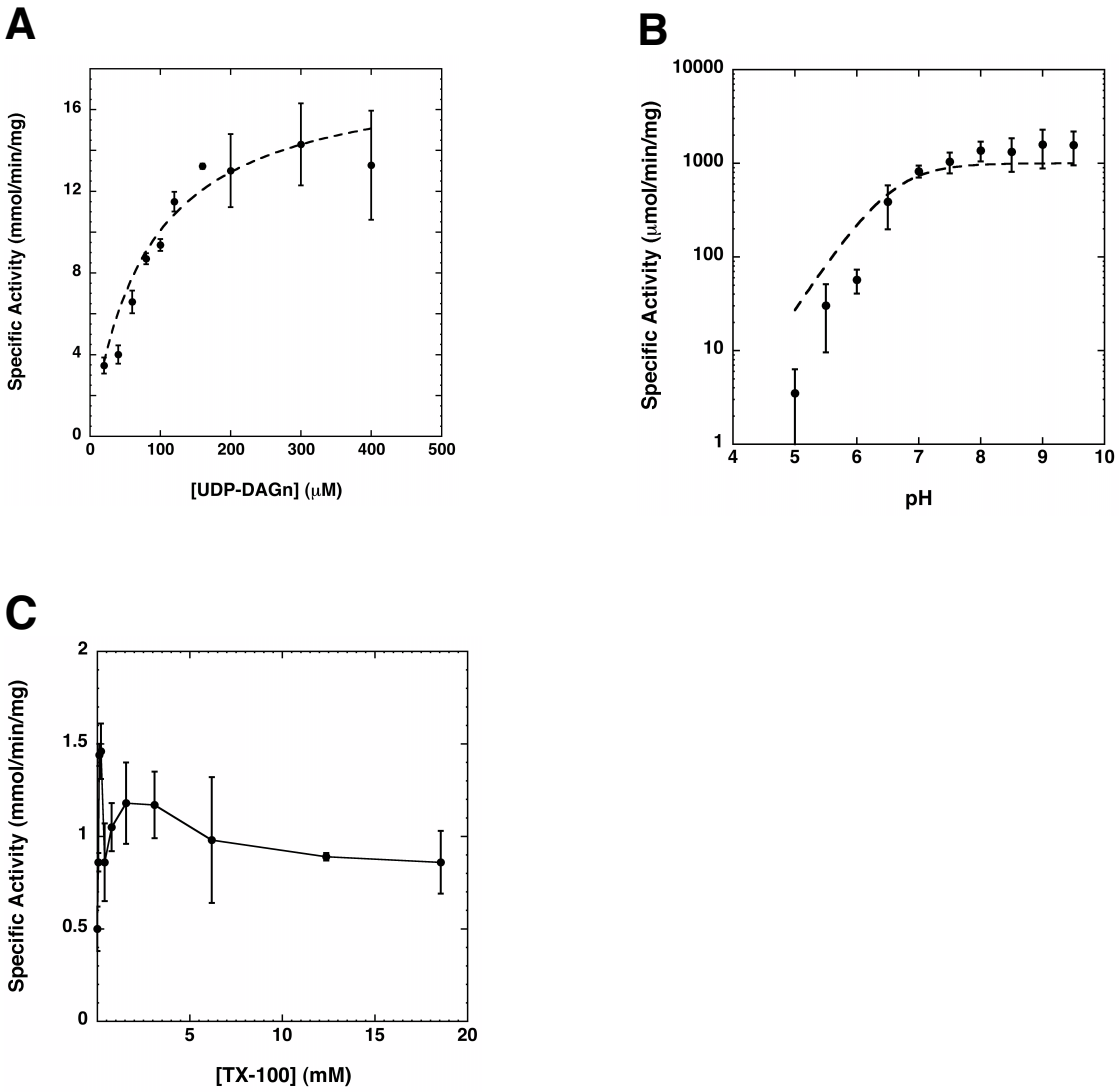

Figure 18: Kinetic Enzymatic Analysis of HiLpxH

(A) HiLpxH activity under standard conditions is dependent upon UDP-DAGn concentration. The apparent K_M was 79.4 ± 11.0 μM and the apparent V_{max} was 18.1 ± 0.9 mmol min^{-1} mg^{-1}, both calculated by fitting the data to KaleidaGraph. (B) Changes in pH alter the *in vitro* activity of HiLpxH. The enzyme shows exhibits a dramatic increase in activity as the pH of the reaction reaches 7, but very little change upon progressively more alkaline conditions. Data was fit to Eq. 1 using KaleidaGraph, yielding a pK_a of 6.6 ± 0.4. (C) Effect of Triton X-100 concentration on HiLpxH specific activity at 100 μM UDP-DAGn. Surface dilution kinetics are not apparent as activity does not appear to have a strong correlation with detergent amount and the enzyme displays detectable activity even at very low Triton X-100 concentrations. All plots shown were each generated from the average of three separate experiments

2.3 Discussion

The conversion of UDP-DAGn to lipid X by LpxH is an important step in lipid A biosynthesis (40,82). Previous studies of *E. coli* LpxH identified it as a peripheral membrane protein, but limited conclusions could be drawn from further studies due to sample purity (60%) and low enzymatic activity under assay conditions (40). The lack of an efficient purification scheme or robust method for *in vitro* assessment prevented further study of the protein, leaving the enzyme kinetic properties of LpxH catalysis a mystery.

In order to reveal the true characteristics of LpxH, we first sought to improve the purification method of the hydrolase. We cloned and purified *H. influenzae* ortholog of LpxH to near homogeneity. This ortholog also behaves as a peripheral membrane protein and thus we incorporated a detergent solubilization step to increase the protein yield. Interestingly, a dramatic increase in total active units (480%, Table 1) was observed in the final sample after removing the His-tag, suggesting that although the inclusion of a metal affinity tag facilitated protein purification, its presence inadvertently impaired the enzyme activity.

Second, we aimed to optimize LpxH assay conditions based on previously reported observations about the positive effect Mn^{2+} had on the behavior EcLpxH. Incorporation of $MnCl_2$ into the standard reaction conditions along with the addition of BSA and Triton X-100 yielded a 1000-fold enhancement of activity of purified HiLpxH

compared to that observed under original assay conditions. The enhancement was also seen in samples of cell-free extracts over-expressing HiLpxH and EcLpxH; moreover, the activities of these samples were similar to each other under each respective assay condition. These observations indicate enhanced activity under optimized assay conditions is not an ortholog-specific phenomenon. Later experiments including BSA and Triton X-100 but without $MnCl_2$ (see Chapter 3; "No metal" sample described in metal dependence assays) only stimulated activity 2-fold, implying the presence of the metal was the main contributor to the improved condition.

Armed with a more homogenous protein sample and a more dynamic method of catalytic evaluation, we elected to re-examine the kinetic parameters of LpxH. We found that HiLpxH has an apparent K_M of 79.4 μM, similar to that reported for *E. coli* ortholog, 61.7 μM (40). Remarkably, the apparent V_{max} of HiLpxH, 18.1 mmol min^{-1} mg^{-1}, is ~1000-fold greater than that reported for EcLpxH (40), which was determined in the absence of BSA, Triton X-100, and $MnCl_2$. It is likely that the presence of $MnCl_2$ is the primary reason for this drastic change in V_{max} (see above discussion), alluding to the important role of the metal ion in hydrolysis. In contrast, the comparable values of the apparent K_M determined both in the absence and presence of metal suggest the Mn^{2+} has little effect on the binding of the UDP-DAGn substrate.

The low enzymatic activity of the previous EcLpxH assay also affected the interpretation of the pH-rate profile, which showed only small variation of EcLpxH

activities within the same order of magnitude over the entire range of tested pH values (40). In contrast, the pH-rate profile of HiLpxH reveals a 1000-fold increase in activity over three pH units (from 5 to 7), and this level of activity is maintained under basic conditions. The mono-limbic shape of the pH-rate profile HiLpxH is similar to that reported for LpxI, a functional ortholog of LpxH which also hydrolyzes UDP-DAGn to lipid X (41). The ability of HiLpxH to recover activity after pre-incubation at low pH values indicates the reduction in LpxH hydrolytic ability is not due to a loss in overall enzyme stability and implies that a deprotonation event is necessary for catalysis.

Perhaps the most notable difference between EcLpxH and HiLpH was their activity in the presence of detergent. Although it was reported that EcLpxH demonstrated surface dilution kinetics, with the enzyme showing inactivation at high levels of detergent (40), HiLpxH retains a relatively consistent level of activity over a wide range of detergent concentrations well beyond the critical micelle concentration of detergent. Such a discrepancy most likely does not reflect an ortholog difference, as the sequence of HiLpxH and EcLpxH are highly similar. Rather, it is more probable that the low purity of the EcLpxH protein and unsatisfactory assay conditions falsely led to the observation of reduced enzymatic activity in a micellar system. Since HiLpxH does not obey surface dilution kinetics, it is likely this enzyme is free roaming in solution and scavenges its lipid-like substrate in a micellar environment to perform catalysis, much like the model suggested for LpxI (41) (Fig. 11). This similarity in membrane association

is consistent with the idea that LpxI and LpxH are functionally interchangeable within the lipid A pathway.

3. LpxH Utilizes a Mn^{2+} Cluster in for Lipid X Production

3.1 Introduction

In the proceeding chapter, we present in detail the purification and basic characterization of an ortholog of LpxH from *H. influenzae.* This work heavily relied on the use of an optimized *in vitro* assay that utilized Mn^{2+}. The incorporation of the cation into the assay conditions was based on a previous report that pre-incubation of a partially purified sample of the *E. coli* ortholog of LpxH with $MnCl_2$ enhanced activity 3 fold (40). Additionally, it was observed that the presence of $MnCl_2$ enriched UDP-DAGn hydrolase activity in the membrane fraction of cell-free extracts over-expressing EcLpxH. Investigators hypothesized that Mn^{2+} may play a role in maintaining enzyme structure, facilitating membrane association, or contributing to the formation of the active site of EcLpxH (40), however no definitive metal dependence of the protein was ever reported.

Along with elementary *in vitro* observations, bioinformatic analysis also provides evidence to support the hypothesis that LpxH uses metal ions for catalysis. Sequence alignment of LpxH orthologs reveal a DXH(X)$_{\sim 25}$GDXXDR(X)$_{\sim 25}$GNHD/E (where X is any residue; the final histidine is replaced with an arginine in LpxH orthologs) motif that is found in the calcineurin-like phosphoesterase (CLP) superfamily (Pfam00149). Besides calcineurin, enzymes of the CLP superfamily also include protein serine/threonine phosphatases (101), purple acid phosphatases (104), nucleotidases, sphingomyelin

phosphodiesterases (100), exonucleases, and cyclic nucleotide phosphodiesterases (103). These enzymes perform catalysis using an ordered shell of water molecules and two divalent or trivalent metal cofactors coordinated by conserved residues of the metallophosphoesterase motif (103,105) (Fig. 12). The two metals have been shown to form a cluster, separated by only a few angstroms. It has been postulated that the metal ions serve to bridge an oxide that performs a nucleophilic attack, to stabilize the formation of a phosphorane intermediate, and to coordinate a nucleophilic hydroxyl group to allow for deprotonation (105,106).

Despite this homology to a family of CLP enzymes, it was still unclear if LpxH utilized a metal cluster for hydrolysis. Compared to other enzymes of this family, LpxH hydrolyzes a unique substrate containing both lipid and nucleotide moieties and does so by breaking a pyrophosphate bond, a type of chemistry that to our knowledge has not been previously reported for CLP enzymes (103). In fact, the hydrolase reaction catalyzed by LpxH is more commonly carried out by enzymes in the Nudix family, which cleave the pyrophosphate bond of nucleoside diphosphates linked to another moiety (128). Also, the lack of biochemical analyses pertaining to the metal-dependence of LpxH further added to the mystery of whether the enzyme functions like other members of the CLP family.

In order to clarify the mechanism of LpxH hydrolysis, we used *in vitro* activity assessment and electron paramagnetic resonance (EPR) spectroscopy to study the metal

dependence of HiLpxH. We show that HiLpxH activity is stimulated over 600-fold by Mn^{2+}, a vast enhancement compared to any other metals tested. Our EPR studies reveal the presence of a Mn^{2+} cluster comprised to two binding sites with differing affinities. As these findings support the similarity of LpxH to other CLP enzymes, we proceeded with mutagenesis studies to assess the functional importance of the predicted Mn^{2+}-binding residues in the conserved metallophosphoesterase motif. Overall, these new observations highlight a strong mechanistic similarity of LpxH to members of the CLP family and allow for a prediction of LpxH's active site structure.

3.2 Materials and Methods

3.2.1 Chemicals and Reagents

Reagents for bacterial growth included yeast extract, tryptone, and Bacto agar, and were purchased from Difco (Detroit, MI). The 4-(2-hydroxyethyl)-1 piperazineethanesulfonic acid (HEPES), phosphate-buffered saline (PBS) components, HCl, salts, ampicillin, isopropyl-β-D-thiogalactoside (IPTG), fatty acid-free bovine serum albumin (BSA), ethylenediaminetetraacetic acid (EDTA), and dithiothreitol (DTT) were purchased from Sigma-Aldrich (St. Louis, MO). Methanol, chloroform, pyridine, and acetic acid were obtained from EMD Science (Gibbstown, NJ). Radioactive γ-^{32}Pi was purchased from PerkinElmer (Waltham, MA). The plasmids used in this study were purified using Qiagen Mini-Prep kits (Qiagen, Valencia, CA) according to the manufacturer's protocol. DNA fragments were purified using QIAquick Spin kits.

Sequencing was carried out by Eton Bioscience, Inc (Research Triangle Park, NC). Unless otherwise noted, protein concentration was determined either by BCA Assay or Bradford Assay (Thermo Scientific, Waltham, Massachusetts) depending on compatibility with buffer components. Both of these methods were carried out as described by the manufacturer.

3.2.2 Generation and Purification of Point Mutants

QuikChange (Stratagene) mutagenesis was used to make alanine point mutants of conserved residues within HiLpxH. The method was carried out as described by the manufacturer, with pHiHt10 (Table 2) serving as template DNA. Specific primers (Integrated DNA Technologies) (Table 5) were created for each desired alanine substitution, and sequencing with T7 forward and reverse primers was used to confirm the mutations. The mutated pHiHt10 vectors (Table 6) were transformed into chemically competent *E. coli* C41(DE3) to create respective expression strains (Table 7). These strains, along with wild-type HiH_t10, were grown under conditions described for HiLpxH purification in Chapter 2 except that the culture volume was 250 mL. Cells from each of the growths were centrifuged at 5,000 × *g*, and collected pellets were washed with 30 mL of cold PBS and then stored at -80 °C. For lysis, the frozen pellet from each mutant strain and the wild-type strain was thawed, resuspended in 8 mL of ice-cold 20 mM HEPES pH 8.0, and passed twice through a French pressure cell (SIM-AMINCO; Spectronic Instruments) at 18,000 psi. The debris from the resulting lysate was removed

by centrifugation at 10,000 × *g* and the subsequent supernatant was collected as cell-free extract and stored at -80 °C.

Purification of the protein from these growths was the same as HiLpxH, but adjusted to account for the smaller culture size. The cell-free extract was thawed, diluted, and solubilized as described for HiLpxH. Following the centrifugation step after detergent incubation, the supernatant was removed and diluted with the appropriate stocks to make a 20 mL solution of ~3 mg/mL protein, 20 mM HEPES pH 8.0, 200 mM NaCl, 20 mM imidazole, and 0.5% Triton X-100. This solution from each strain was then loaded by gravity onto separate columns of 1 mL Ni-NTA resin (Qiagen) that had been pre-equilibrated in 20 column volumes of the load buffer described above. Washing, detergent exchange, and elution were carried out as outlined for HiLpxH. Samples from each wash of the column were analyzed by SDS-PAGE to ensure proper fractionation. Following elution, the samples were each concentrated to 3 mL using 5 mL Amicon Ultra 10K molecular weight cutoff centrifuge concentrators (Millipore) and then dialyzed overnight against 1 L of 20 mM HEPES pH 8.0, 200 mM NaCl. Resulting protein solutions from each mutant and the wild-type sample were further concentrated to 500 μL and stored in -80 °C.

Table 5: Primers Used for Creation of HiLpxH Point Mutants

Name	Purpose	Primer sequence (5'-3' orientation)
H11A_F	To mutate HiLpxH H11 to alanine	TGAAACATAGCTATTTTATTTCTGATTTGG CTTTAAGCGAAACTCAGCCAGAATT
H11A_R	To mutate HiLpxH H11 to alanine	AATTCTGGCTGAGTTTCGCTTAAAGCCAAA TCAGAAATAAAATAGCTATGTTTCA
D42A_F	To mutate HiLpxH D42 to alanine	GAACGGCTTTACATTTTGGGTGCTCTTTTTG ATTTTTGGATTGGTG
D42A_R	To mutate HiLpxH D42 to alanine	CACCAATCCAAAAATCAAAAAGAGCACCC AAAATGTAAAGCCGTTC
R81A_F	To mutate HiLpxH R81 to alanine	GTTATTTTCAGCACGGCAACGCTGATTTCT TGATTGGTGAAC
R81A_R	To mutate HiLpxH R81 to alanine	GTTCACCAATCAAGAAATCAGCGTTGCCGT GCTGAAAATAAC
H115A_F	To mutate HiLpxH H115 to alanine	CAATTGATTACACTTTATGATAAAAAAATC TTACTTTGTGCTGGCGATACGCTTTGTATT
H115A_R	To mutate HiLpxH H115 to alanine	AATACAAAGCGTATCGCCAGCACAAAGTA AGATTTTTTTATCATAAAGTGTAATCAATT G
D117A_F	To mutate HiLpxH D117 to alanine	AAAATCTTACTTTGTCATGGCGCTACGCTT TGTATTGATGATGAG
D117A_R	To mutate HiLpxH D117 to alanine	CTCATCATCAATACAAAGCGTAGCGCCATG ACAAAGTAAGATTTT
D123A_F	To mutate HiLpxH D123 to alanine	CGATACGCTTTGTATTGATGCTGAGGCTTA CCAACAATTTC
D123A_R	To mutate HiLpxH D123 to alanine	GAAATTGTTGGTAAGCCTCAGCATCAATAC AAAGCGTATCG
H196A_F	To mutate HiLpxH H196 to alanine	GTAAATTTATTAATTCACGGAGCCACACAC CGTGAGGCGATTCA
H196A_R	To mutate HiLpxH H196 to alanine	TGAATCGCCTCACGGTGTGTGGCTCCGTGA ATTAATAAATTTAC

Table 6: Plasmids Harboring HiLpxH Point Mutants

Plasmid	Description	Source
pET21b	high-copy expression vector containing a T7 promoter, Amp^R	Novagen
p21t10	modified pET21b vector encoding C-terminal TEV-protease cleavage site followed by a His10 tag, Amp^R	this work
pHiHt10	p21t10 containing *H. influenzae lpxH*, Amp^R	this work
pKJB2	pET21a+ plasmid containing *E. coli lpxH*, Amp^R	(40)
pHiHt10	p21t10 containing *H. influenzae lpxH*, Amp^R	this work
pD9At10	p21t10 containing *mutatued H. influenzae lpxH* encoding for a D9A mutation, Amp^R	this work
pH11At10	p21t10 containing mutatued *H. influenzae lpxH* encoding for a H11A mutation, Amp^R	this work
pD42At10	p21t10 containing mutatued *H. influenzae lpxH* encoding for a D42A mutation, Amp^R	this work
pR81At10	p21t10 containing mutatued *H. influenzae lpxH* encoding for a R81A mutation, Amp^R	this work
pH115At10	p21t10 containing mutatued *H. influenzae lpxH* encoding for a H115A mutation, Amp^R	this work
pD117At10	p21t10 containing mutatued *H. influenzae lpxH* encoding for a D117A mutation, Amp^R	this work
pD123At10	p21t10 containing mutatued *H. influenzae lpxH* encoding for a D123A mutation, Amp^R	this work
pH196At10	p21t10 containing mutatued *H. influenzae lpxH* encoding for a D196A mutation, Amp^R	this work

Table 7: *E. coli* Strains Used for Expression of HiLpxH Point Mutants

Strain	Description	Source
DH5α	F^- *Δ(argF-lacZYA)U169 deoR phoA supE44 Φ80 Δ(lacZ)M15 gyrA96 relA1 endA1 thi-1 hsdR17 recA1* λ^-	Invitrogen
C41(DE3)	F^- *ompT hsdS*$_B$ (r_B^- m_B^-) *gal dcm* (DE3)	(125)
VC_t10	C41(DE3) harboring p21t10, Amp^R	this work
HiH_t10	C41(DE3) harboring pHiHt10, Amp^R	this work
D9A_t10	C41(DE3) harboring pD9At10, Amp^R	this work
H11A_t10	C41(DE3) harboring pH11At10, Amp^R	this work
D42A_t10	C41(DE3) harboring pD42At10, Amp^R	this work
R81A_t10	C41(DE3) harboring pR81At10, Amp^R	this work
H115A_t10	C41(DE3) harboring pH115At10, Amp^R	this work
D117A_t10	C41(DE3) harboring pD117At10, Amp^R	this work
D123A_t10	C41(DE3) harboring pD123A10, Amp^R	this work
H196_t10	C41(DE3) harboring pH196At10, Amp^R	this work

3.2.3 Metal Dependence of HiLpxH

To analyze the metal dependence of HiLpxH, a modified procedure for the optimized autoradiographic assay described in Chapter 2 was employed. First, a pure HiLpxH sample (obtained as outlined in Chapter 2) was diluted with standard reaction buffer that replaced 1 mM $MnCl_2$ with 2 mM EDTA, incubated on ice for 20 min, then

diluted again into standard reaction buffer with no $MnCl_2$, and incubated on ice for an additional 10 min. This EDTA-treated enzyme was next added to reaction mixtures in which 1 mM $MnCl_2$ was replaced by no di- or trivalent metal ion, 2 mM NaCl, or each of the following chloride salts at 1 mM: Ca^{2+}, Co^{2+}, Cu^{2+}, Fe^{3+}, Mg^{2+}, Mn^{2+}, Ni^{2+}, and Zn^{2+}. To ensure linear activity under each condition, the concentration of HiLpxH in the assays were varied from 35 to 178 nM.

Another form of the modified autoradiographic assay was used to assess HiLpxH dependence on $MnCl_2$ in which the protein was diluted in standard reaction buffer containing no $MnCl_2$ and then diluted into reactions in which the $MnCl_2$ concentration ranged from 0 to 5 mM. Protein concentration was 980 pM in the 0 mM assay condition and 10 pM in all others.

3.2.4 EPR Spectroscopy

X-band EPR spectra were recorded using Bruker Biospin (Billerica, MA) Bruker E-500 spectrometer equipped with super high Q cavity providing a conventional perpendicular EPR mode (*i.e.*, microwave magnetic field B_1 is perpendicular to the static magnetic field B_0). All room temperature spectra were recorded at the same experimental conditions: 10 G modulation amplitude at 100 kHz, 2 mW incident microwave power at 9.86 GHz frequency. For EPR measurements at cryogenic temperatures the spectrometer was outfitted with ESR 910 cryostat and ITC-4 temperature controller (Oxford Instruments, Concord, MA). Temperature at the sample

cavity was calibrated using a CernoxTM thin film sensor (Lake Shore Cryotronics Inc., Westerville, OH). Incident microwave power was kept at levels to avoid saturation and modulation amplitude was set to about 1/3 to 1/4 of the narrowest peak-to-peak line width.

3.2.5 Manganese Titration with EPR Detection at Room Temperature

To assess binding of Mn^{2+} to HiLpxH, 80 μL of a solution containing 100 μM purified HiLpxH (Chapter 2), 20 mM HEPES pH 8.0, and 200 mM NaCl was titrated in successive additions with 1 μL of 1.645 mM $MnCl_2$ stock containing the same buffer as the protein solution. After each addition of manganese stock, the sample was mixed and incubated for >5 min at room temperature. Subsequently, approximately 20 μL of the titrated solution was drawn into a quartz capillary with 0.70 mm i.d. and 0.87 mm o.d. (VitroCom, Mountain Lakes, NJ). One end of the capillary was sealed with Critoseal® (McCormick Scientific, St. Louis, MO) and inserted into a 3 mm i.d. quartz EPR tube (Wilmad-LabGlass, Vineland, NJ). The tube was then fixed inside the EPR resonator so that the section of the capillary containing the aqueous sample was covering the entire sensitivity region of the EPR resonator while the Critoseal® plug was located outside. After taking an EPR spectrum, the protein solution was recovered into the vial containing the rest of the sample and a new portion of $MnCl_2$ was added. The same quartz tube was used for all the protein containing samples. When changing the sample, solution was drawn in and out of the capillary twice to ensure complete replacement of

the previous sample. For a control calibration of EPR signal intensity *vs*. Mn^{2+} concentration, the same procedure was used except that a buffer-only solution was used.

After collection of spectra, the concentration of free Mn^{2+} ion present in solutions was evaluated by either least-squares fitting of the high field hyperfine component of the six-line Mn^{2+} EPR spectrum using EWVoigt program (129) or by measuring peak-to-peak intensity of that component as the peak line width did not change. Both measurements yielded identical results. The determined free Mn^{2+} concentration were analyzed based a two-site binding model (Eq. 2):

$$P + M \xrightarrow{K_{a1}} P_1M$$
$$P + M \xrightarrow{K_{a2}} P_2M$$
$$P_1 + M \xrightarrow{K_{a2}} PMM$$
$$P_2 + M \xrightarrow{K_{a1}} PMM$$

Equation 2: Two-Site Ligand Binding

P is the protein with only the first (P_1M), and the second (P_2M), or both metal binding sites occupied by metal ion *M*, and K_{a1} and K_{a2} are the corresponding association constants. All experimental spectra were corrected for a small background signal from the resonator that was recorded using a capillary containing only protein solution in buffer. Least-squares fitting of experimental data was accomplished using the Levenberg-Marquardt optimization and parameter uncertainties were determined by standard covariance matrix method using SigmaPlot (Systat Software, San Jose, CA).

3.2.6 Manganese Titration with EPR Detection at Cryogenic Temperatures

Low temperature EPR experiments were employed for further assessment of the Mn^{2+}-protein interaction and for the existence of a Mn^{2+} cluster. For these experiments, samples containing 20 mM HEPES pH 8.0, 200 mM NaCl, 10% (v/v) glycerol and 234 μM of HiLpxH were incubated with molar equivalents of $MnCl_2$ ranging from 0 to 2.0. After assembly, these samples were stored at -80 °C. Just before an EPR measurement, a sample was thawed and drawn into 3 mm i.d. precision quartz EPR tubes (Wilmad-LabGlass) and then frozen again by immersing the tube into liquid nitrogen before being placed in a pre-cooled EPR cryostat.

3.3 Results

3.3.2 Metal Dependence of HiLpxH

While it had been previously suggested that Mn^{2+} plays a role in the structure or catalysis of EcLpxH (40), the exact function of metal ions in LpxH remained to be elucidated. In order to determine how metal ions altered the capability of LpxH to hydrolyze UDP-DAGn, we used an autoradiographic TLC-based assay to monitor the *in vitro* activity of the enzyme in the presence of various metal salts. First, highly purified HiLpxH was incubated in standard reaction buffer in which the $MnCl_2$ was replaced with 2 mM EDTA to remove any co-purifying metal ions. The protein was then diluted into standard assay conditions containing 1 mM of the following chloride salts: Ca^{2+},

Co^{2+}, Cu^{2+}, Fe^{3+}, Mg^{2+}, Mn^{2+}, Ni^{2+}, and Zn^{2+}. Assay conditions where the di- or trivalent metal salt was replaced by 2 mM NaCl or no metal additive were also included as controls. Activity was monitored over time and the specific activity was calculated as previously outlined in Chapter 2. Results were compared to the activity of HiLpxH in the presence of no metal (Fig. 19A). The Mn^{2+} assay condition showed activity that was 670-fold greater than the condition with no metal. The Ni^{2+}, Co^{2+}, and Fe^{3+} conditions also enhanced activity; however, the increase (10-50 fold) was substantially lower than that seen when Mn^{2+} was present. The activity of the enzyme was negligible in NaCl, indicating that the ionic strength of the reaction was not responsible for any stimulation observed. The enzyme did show residual activity in the absence of metal, albeit only visible at enzyme concentrations 1000-fold greater than that usually used in the assay.

To further investigate Mn^{2+}-dependent stimulation, HiLpxH activity was determined using the autoradiographic assay containing a range of Mn^{2+} concentrations (Fig. 19B). Enzyme activity increased with Mn^{2+} concentrations up to 2.5 mM, a ~10^8-fold molar excess compared to the HiLpxH concentration in the assay. After this point, there seemed to be no further stimulation in product hydrolysis. This pattern was indicative of Michaelis-Menten saturation kinetics, suggesting the metal acts as a pseudo-substrate for HiLpxH. Consequently the data was fit to determine an apparent K_M of 487 ± 113 μM for Mn^{2+}. This term was designated the K_{Metal} for the enzyme.

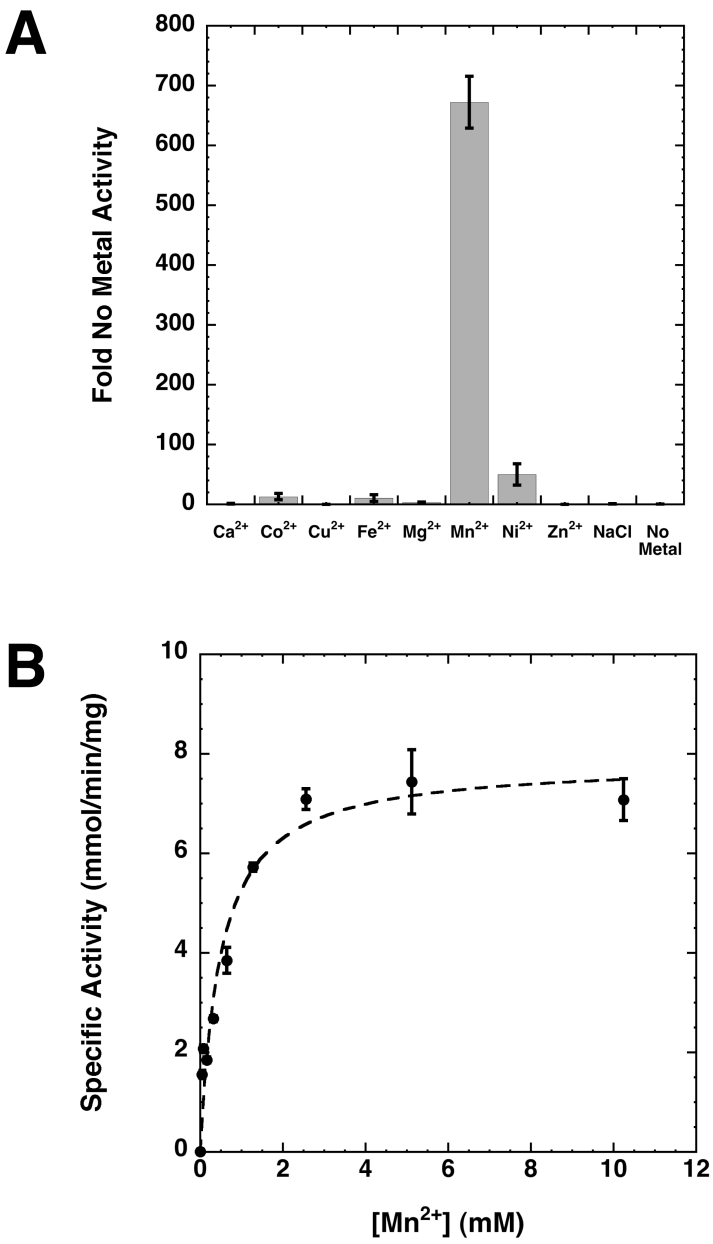

Figure 19: Metal Dependency of HiLpxH

(A) HiLpxH treated with EDTA was assayed under standard conditions supplemented with either metal, NaCl, or no metal. Resulting specific activity was calculated and compared to the specific activity of the no metal control. Data shown is the mean of three separate experiments. (B) UDP-DAGn hydrolysis activity of HiLpxH was determined as a function of $MnCl_2$ concentration in the assay. This data was fit to a Michaelis Menten model with KaleidaGraph to obtain a K_M of 487 ± 113 μM for Mn^{2+}.

3.3.2 Evidence for Two Mn^{2+} Binding Sites in HiLpxH

While *in vitro* assays showed stimulation of hydrolase activity in the presence of Mn^{2+}, we wished to further probe the interaction of Mn^{2+} with HiLpxH. To do so, we generated a Mn^{2+} titration curve using EPR spectroscopy, a technique that has been used to characterize the Mn^{2+} binding site in another CLP family enzyme, bacteriophage λ protein phosphatase (130). This approach relies on the fact that a Mn^{2+} ion coordinated to a protein binding site exhibits very broad EPR lines caused by large zero-field splitting effects, making it undetectable at room temperature, whereas free Mn^{2+} yields a distinct EPR signal under the same condition.

Representative room temperature EPR spectra from the titration of HiLpxH with manganese are shown in Fig. 6A. For samples with Mn^{2+}-to-protein ratio above 1:1, an EPR spectrum revealed a six-line hyperfine pattern (nuclear spin I=5/2) with a splitting of approximately 95 G positioned at g≈2.0 that is characteristic of free (hexaaqua) Mn^{2+} ion. The intensity of the spectrum varied, increasing concomitantly with the manganese-to-protein ratio (Fig. 6A). Spectra obtained from samples with Mn^{2+}-to-protein ratio of ≤1 demonstrated no detectable six-line component characteristic of the free Mn^{2+} ion, indicating that the free metal concentration was below the EPR detection limit (<1 μM) and that nearly all the Mn^{2+} ions in these samples are bound to the protein.

The spectra were further analyzed to assess the binding of the metal ion to LpxH. As the intensity of the six-line hyperfine component correlates to the amount of free

Mn^{2+} in the sample tube, the concentration of unassociated ion could be determined. This was accomplished by a double integration of the high field hyperfine component of the HiLpxH-$MnCl_2$ titration spectra and a calibration of the double-integrated intensity from a control titration containing only $MnCl_2$. Fig. 20B shows the intensity of EPR spectra of free hexaaqua Mn^{2+} ion as a function of total [Mn^{2+}] for samples containing either $MnCl_2$ in buffer (squares) or $MnCl_2$ and HiLpxH (circles). In all protein-containing samples, the intensity of Mn^{2+} EPR signal is less than that in the control samples without the protein. Above ~200 μM Mn^{2+}, which represents [Mn^{2+}]/[HiLpxH] ratios above 2, the slopes of both plots are approximately the same, indicating that concentration of protein-bound Mn^{2+} species plateaus and that each HiLpxH binds two Mn^{2+} ions.

Based on this observation, the titration curve in Fig. 6B was fit with a two-site binding model (Eq. 2). While the least-squares fit was of exceptionally high quality (R_{sqr}=0.998) for K_{a2}, yielding a value of 5.8±0.6×10^5 M^{-1} (or K_{d2}=1.7 μM), it was found to be insensitive to K_{a1} as long as K_{a1}>50 x 10^6 M^{-1} (or K_{d1} < 20 nM). Indeed, no free Mn^{2+} was detectable in EPR spectra when the metal-to-protein ratio is below 1, consistent with the notion that the binding affinity for the first metal is very tight, well below the detection limit of the EPR instrument (~ 1 μM).

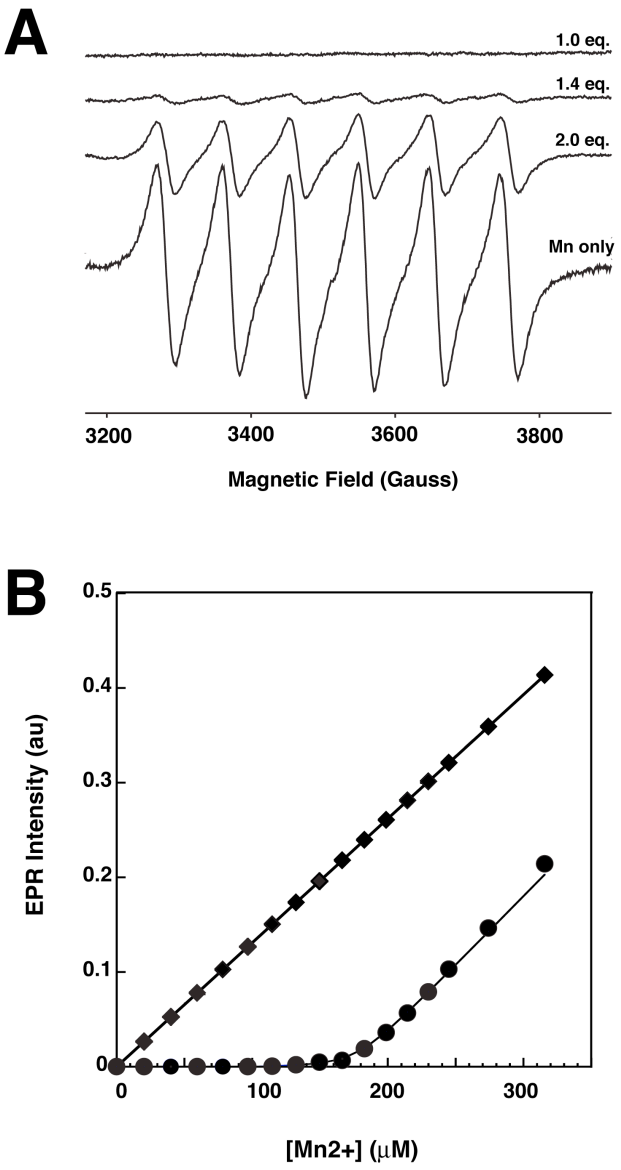

Figure 20: Room Temperature EPR Analysis of Mn^{2+} binding

(A) Representative room temperature CW X-band EPR spectra from samples containing 100 μM of HiLpxH and the appropriate concentration of $MnCl_2$ to yield: 1 equivalent of Mn2+, 1.4 equivalents of Mn^{2+}, and 2.0 equivalents of Mn^{2+}. For a comparison, an EPR spectrum from a control sample containing only buffer and MnCl2 at the same concentration as 0.6 Mn^{2+} equivalents. (B) Double integrated intensity of free (hexaaqua) Mn^{2+} EPR signal as a function of Mn^{2+} concentration for the room temperature titration experiment (circles) and a control titration experiment without the protein present (squares). Line represents least-squares fit using a two-site binding model.

3.3.3 Indication of Di-Mn^{2+} Cluster Formation in HiLpxH.

Observing that two metal ions seem to associate with HiLpxH and knowing that other members of the CLP family have been identified to contain metal centers, the possibility of such cluster formation in HiLpxH was investigated using cryogenic EPR spectroscopy. Fig. 21A shows representative experimental CW EPR spectra measured at 28 K from a buffered protein solution in absence of $MnCl_2$ (top) and from protein samples with varying Mn^{2+}-to-protein ratios. This temperature was chosen to achieve a measurable thermal population of several different spin states to yield a large number of potentially detectable transitions, some of which are expected to yield characteristic features to identify formation of an exchange-coupled Mn^{2+} cluster (131-135). It should be noted that the EPR spectrum of HiLpxH in absence of Mn^{2+} revealed small but easily observable feature at g=4.3 (Fig. 7A, marked by a dashed line) that was assigned to a low symmetry Fe^{3+} ion non-specifically bound to protein. The g=4.3 signal was used as an internal EPR intensity marker, as the protein concentration was kept constant in all samples.

The cryogenic experiments reveal that an increase in [Mn^{2+}]/[HiLpxH] ratio resulted in systematic changes in EPR spectra at this temperature indicated by the progressive appearance of new features upon further addition of $MnCl_2$ to the samples. Some of these features are attributed to Mn^{2+} ions bound to the protein while others likely arise from non-associated hexaaqua Mn^{2+}, as such features are also obtained from

a control experiment using a $MnCl_2$ solution supplemented with 10% (v/v) glycerol (Fig. 21A, "Mn only" spectrum). The control spectrum is easily identified by a sharp six-line hyperfine pattern at g=2.04 (Fig. 21A, marked with arrow) arising from electronic spin S=±1/2 transition that is split into six lines with a splitting of about 95 G by the Mn^{2+} nuclear spin I=5/2.

For a symmetric exchange-coupled pair of Mn^{2+} ions in an isotropic case, eleven hyperfine lines are expected by EPR, with hyperfine coupling constant of approximately half of that for a single Mn^{2+} ion (136). Such patterns are evident in the cryogenic EPR spectra of HiLpH and $MnCl_2$. Specifically, at g≈7.7 we observed a component with multiline pattern characterized by an effective hyperfine splitting of approximately 40.2 G. Such a pattern appears first in the spectrum from the HiLpxH sample containing 1.25 equivalents of Mn^{2+}. The intensity of this pattern increased with greater metal-to-protein ratios (Fig. 21B). The hyperfine splitting constants for binuclear Mn^{2+} complexes reported in the literature range from 40 to 47 G (133-135,137-143). Thus, the splitting of 40.2 G we observed for the HiLpxH/Mn^{2+} sample is consistent with the existence of binuclear manganese center in the protein.

In support of the spectral feature at g≈7.7, other spectral features similar to those detected for a binuclear $Mn_2[(OPPh_2)_2N]_4$ complex (144) were observed at g≈14 in HiLpxH samples with more than one Mn^{2+} equivalent (Fig. 7B). The signals at g≈3.1 and 2.48 (Fig. 21B) also can be attributed to a binuclear cluster (131), although they might

exhibit a substantial overlap with the signal originating from a singly-occupied HiLpxH Mn^{2+} site as well as the free Mn^{2+} signal. While none of these components show resolved hyperfine patterns with splitting characteristic of the binuclear Mn^{2+} center, such a loss in resolution is not uncommon for many binuclear Mn^{2+} complexes (131-135).

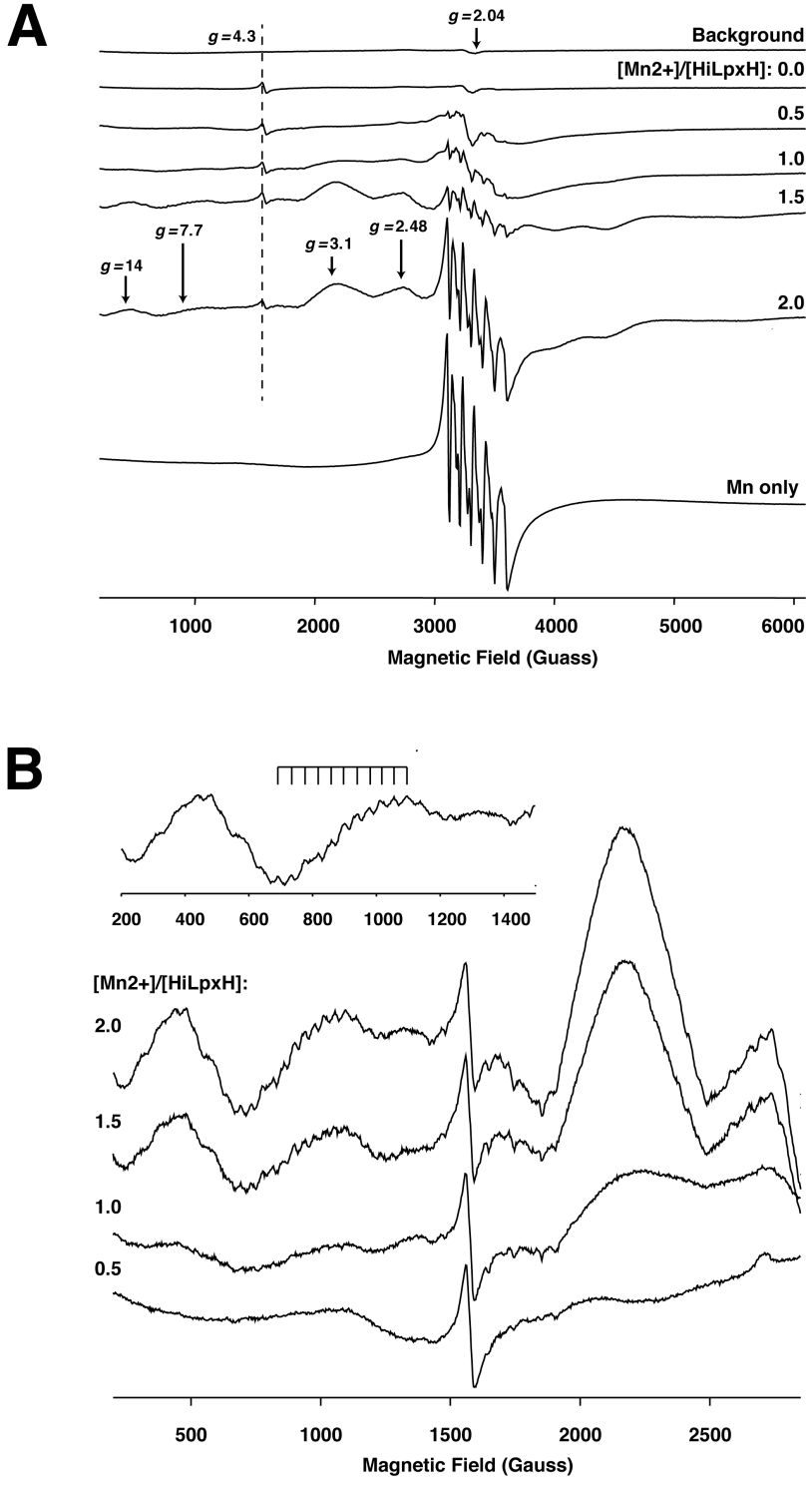

Figure 21: Cryogenic EPR Spectra of HiLpxH

(*Caption continued on next page*)

Figure 21: (A) Representative CW X-band EPR spectra measured at 28 K. From top to bottom are background signal from an EPR resonator outfitted with a low temperature quartz insert; signal from samples containing a range of [Mn2+] /[HiLpxH] ratios; and signal from a Mn^{2+} only solution. Position of the g=4.3 marker originating from a low symmetry Fe^{3+} ion non-specifically bound to the protein is shown by a dashed line. The areas of the spectra indicating the presence of a di- Mn^{2+} cluster. g=14, 7.7, 3.1, and 2.48, are denoted by arrows. (B) Spectra from (A) enhanced in the range 500 to 2500 G to highlight the increase in hyperfine splitting in g=7.7 at greater [Mn^{2+}] /[HiLpxH] ratios.

3.3.4 Point Mutagenesis of Conserved Residues

After establishing that LpxH possesses a binuclear Mn^{2+} metal cluster, we proceeded to examine the functional role of conserved residues in catalysis. Sequence alignment of LpxH orthologs reveals three areas of amino acid conservation (Fig. 22) that show homology to the motifs characteristic of the CLP family. The most conserved CLP family motif, DXH(X)$_{\sim 25}$GDXXDR(X)$_{\sim 25}$GN*H*D/E where X indicates any amino acid (the italicized histidine is not completely conserved in LpxH orthologs and is replaced by an arginine), is clustered at the N-terminal region of LpxH (Motif 1, green). The middle region of the protein contains a motif of a highly conserved histidine followed by an aspartate (Motif 2, cyan) that is less ubiquitous in the CLP family and not always detectable from sequence alignment (106). Lastly, at the C-terminus of LpxH there is a UUXGHXH motif (Motif 3, orange), with U representing any hydrophobic residue, which was first characterized in a sub-class of CLP enzymes that are involved in DNA repair and polymerization (102,145).

To assess the importance of these areas of conservation, we made the following alanine point mutants of amino acids (Fig. 22, underlined) from the motif in each region: D9A, H11A, D42A, R81A in Motif 1; H115A and D117A in the Motif 2; and H196A in Motif 3. These point mutants, along with a wild-type HiLpxH control, were expressed in *E. coli* with a C-terminal His_{10} tag and purified using Ni-NTA chromatography. The mutant proteins over-expressed at levels comparable to that of wild-type and the final purities of all protein forms were similar (data not shown). The isolated protein samples were analyzed for UDP-DAGn hydrolase activity using the radioactive assay and their resulting activities were compared to that of the wild-type control (Table 8). All of the point mutants showed a decrease in specific activity, however the residues of the motif in the N-terminal region displayed the most significant change. The D9A mutant exhibited a 20,000-fold inhibition of hydrolysis, 10-fold over any of the other mutants. The other mutants of the N-terminal region, as well as the H115A mutation in the middle region and the H196A mutation in the C-terminal region showed similar levels of hydrolysis inactivation. This is in contrast to the D117A mutant from the middle region that was only slightly impaired compared to wild-type.

Figure 22: Sequence Alignment of LpxH Orthologs

Motifs characteristic of the calcineurin-like phosphatases are boxed in color: green represents Motif 1, the most conserved residues across the family (DXHX$_{\sim 25}$GDXXDRX$_{\sim 25}$GNHD/E); cyan denotes a lesser conserved motif, Motif 2, not always clearly detectable through sequence alignment (usually a highly conserved His followed by Asp); and orange depicts Motif 3, an additional motif first identified in a subset of enzymes that are involved in DNA repair (UUXGHXH where U is a hydrophobic amino acid). Residues that were mutated to alanine are italicized and underlined. Alignment was generated using the ClustalW2 tool on the EBI website (http://www.ebi.ac.uk/Tools/msa/clustalw2/). LpxH orthologs listed include those from *H. influenzae* (HiLpxH), *E. coli* (EcLpxH), *Neisseria meningitidis* (NmLpxH), *Yersina pestis* (YpLpxH), Vibrio cholera (VcLpx), and *Francisella novidica* (FnLpxH). Sequences were obtained from the NCBI server.

Table 8: Activity of HiLpxH Point Mutants Compared to Wild Type HiLpxH

Conserved Region	Mutation	Specific Activity (μmol/min/mg)	Fold decrease compared to Wt
	Wt	6900 ± 700	1
Motif 1	D9A	0.03 ± 0.004	200000
	H11A	0.41 ± 0.02	20000
	D42A	0.09 ± 0.01	80000
	R81A	0.93 ± 0.04	7000
Motif 2	H115A	0.57 ± 0.008	12000
	D117A	3020 ± 90	2
Motif 3	H196A	1.4 ± 1	5000

3.4 Discussion

LpxH catalyzes the fourth step of the lipid A biosynthetic pathway, which involves the hydrolysis of UDP-DAGn to lipid X. Previous biochemical understandings of LpxH were based on studies with the ortholog from *E. coli.* This work suggested that a metal cofactor, specifically Mn^{2+}, might be important for protein stability or membrane association. Furthermore, LpxH is classified by sequence to belong to the calcineurin-like phosphoesterase (CLP) family that employs two clustered metal ions for catalysis. Despite these initial biochemical and bioinformatic hints that LpxH utilizes a metallic cofactor, its metal dependency was never reported.

One reason for the deficiency of information about the metal cofactors in LpxH was the inability to obtain a pure sample of the protein. We developed of a new scheme of LpxH purification, employing the ortholog from *H. influenzae* (HiLpxH) as described

in Chapter 2. This method results in a 95% homogenous sample of the hydrolase, thus allowing use to carry out detailed analysis of the role of metal ions in LpxH function.

3.4.1 Mn^{2+} Facilitates LpxH-Mediated Hydrolysis of UDP-DAGn

Since the identity of the active site metals can vary greatly across the CLP family (103), we assayed HiLpxH for UDP-DAGn hydrolysis in the presence of different metal ions to determine which metal might be the most physiologically relevant. We noted a significant increase in HiLpxH activity in the presence of Mn^{2+} that was >10-fold higher than the activation displayed by any other metal, making Mn^{2+} the most likely candidate for HiLpxH's cofactor. The calculated K_{Metal} of the enzyme for Mn^{2+} was 487 μM. While CLPs have been shown to contain two different metals in their binuclear active sites, those containing Mn^{2+} usually have this ion occupying both sites (103).

3.4.2 LpxH Contains a Mn^{2+} Cluster for Catalysis

We took advantage of the paramagnetic properties of Mn^{2+} to probe the binding of the metal to the HiLpxH. Using EPR at room temperature, we were able to monitor the change in signal intensity of the canonical six-line Mn^{2+} signature when HiLpxH was present with the ion in solution. Comparing this data to a standard curve of Mn^{2+} alone in solution, it is evident that two tight-binding Mn^{2+} ions are interacting with the protein, as the free Mn^{2+} signal generated from HiLpxH samples containing greater than 2 molar equivalents of Mn^{2+} increases at a similar slope as the standard curve. Fitting the titration data with a two-site binding model revealed two binding sites: the first site binds the

metal ion very tightly, having an extremely low K_d (< 20 nM), while the second site has a tight, but detectable K_d value of 1.7 μM. Varying affinity for metal ions at each site is common for CLP enzymes, as binding at one site can be as much as 100-times stronger than that at the second site (103,106).

Cryogenic EPR experiments allowed for further dissection of the interaction of Mn^{2+} with HiLpxH. The data from spectra of HiLpxH incubated with varying molar equivalents of Mn^{2+} show evidence of strong spin exchange coupling. Such coupling of the Mn^{2+} electronic spins has also been seen in a di-manganese cluster bridged by oxygen atoms, as studied by Hayden and Hendrich (142), making it likely that the two metal binding sites in HiLpxH are in close proximity and form a cluster. Similar conclusions about the existence of a di-nuclear cluster based on observations of spin coupling have been made in other CLP enzymes (103,130).

Cluster formation is beneficial for the catalysis of reactions, as the proximity of the metal ions in an active site allows for a symmetric delocalization of charge that is not possible with only one metal (107). This delocalized distribution over two metals permits them to act like a unit in stabilizing transition states of concerted mechanisms that facilitate the concurrent anionic ligand addition and anionic ligand dissociation. In the case of hydrolases, this stabilization of the transition state lowers the activation barrier for both nucleophilic attack by the activated water and phosphoester bond cleavage. Additionally, it has been reported that having two close Mn^{2+} ions in an active

site decreases the strength of bridging-ligand field and potential increases the Lewis acidity of the metals, allowing them to have a higher affinity for ligands like H_2O and facilitating the formation of a hydroxide anion that performs the nucleophilic attack in a hydrolysis reaction (107).

Intriguingly, while both our enzymatic assay and the EPR measurements establish LpxH as a metalloenzyme, the two techniques yielded very different affinities for Mn^{2+} binding. Fitting of metal-dependent enzymatic stimulation yield an apparent K_{Metal} of ~0.5 mM, whereas the EPR measurements reveals two binding sites with binding affinities in the low nM and μM ranges respectively. This discrepancy may be due to the presence of UDP-DAGn in the enzymatic assay, as divalent ions such as Mn^{2+} have been shown to coordinate the phosphate group of nucleotides. Since UDP-DAGn contains such a moiety, it is possible that Mn^{2+}-UDP-DAGn interaction promotes LpxH catalytic activity, thus generating a high K_{Metal}. In some CLP enzymes, such an interaction of metal ions with substrates has been proposed to be part of the catalytic sequence in that a low-affinity metal ion binds to the enzyme complexed with the phosphoryl group of the substrate (106).

An alternative, and perhaps more likely, explanation for the disparity in metal affinity calculations described above may be the existence of three Mn^{2+} binding site in LpxH: two sites in the binuclear cluster revealed in the EPR studies with affinities in the low nM and μM ranges, and another weak-binding Mn^{2+} that facilitates the catalysis, but

only binds LpxH in the presence of the substrate UDP-DAGn, yielding an apparent K_{Metal} in the high μM to sub-mM range. Supporting this notion, members of the protein phosphate M (PPM) family have been shown to contain a third Mn^{2+} cofactor in proximity of the di-metal cluster found in their active sites (146). This third metal has been shown to have significantly weaker affinity (high μM to sub-mM) than the ions in metal cluster (146) and has been suggested to directly take part in catalysis (147) or have a regulatory role important in substrate recognition (148).

3.4.3 Functional Importance of Conserved Residues Define LpxH as a CLP

The presence of a Mn^{2+}-cluster is a feature LpxH shares with the CLP family, however the type of chemistry performed by the lipid A biosynthetic enzyme is not canonically displayed by this group of proteins. Rather, the hydrolase reaction catalyzed by LpxH is more commonly carried out by enzymes in the Nudix family, which cleave the pyrophosphate bond of nucleoside diphosphates linked to another moiety (128). While these enzymes also use metals and activated water molecules in catalysis, they have a characteristic sequence motif ("Nudix box") of $GX_5EX_7REUXEEXGU$, with glutamate residues in the conserved motif positioning the cofactors. The metal cofactors in Nudix enzymes are almost always Mg^{2+} (128), making them much less diverse that those of the CLP family.

In the CLP family, metal chelation is achieved by use of the residues in the Asp-rich metallophosphoesterase motif, highlighted in Fig. 23A (103,106). The functional

groups of these amino acids directly serve as ligands to the ions and perform secondary coordination of waters and amino acids that in turn coordinate the metals, as observed in the structure of bacteriophage λ protein phosphatase (Fig. 23B). The two metal cofactors are often bridged by a carboxylate group-containing residue (D49, Fig. 23B); such a configuration is a common structural motif in binuclear enzymes (103,107).

The investigated alanine point mutants of conserved residues in the HiLxpH metallophosphoesterase motifs showed a significant decrease in activity, supporting the similarity of the protein to the CLP family despite the unique substrate it prefers. In particular, mutants D9A, H11A, and D42A showed the largest decrease in activity. These residues in HiLpxH are likely to participate in metal coordination, similar to corresponding residues in other CLP enzymes (149-151) (seen with the positions of D20, H22, and D49 in the structure of bacteriophage λ protein phosphatase in Fig. 23B), and their mutations impair hydrolysis by abrogating metal binding. The diminished activity of H115A and H196A can also be explained by a cofactor-coordination function, as the counterparts of these residues in other CLP enzymes serve as ligands to the metal ions (H139 and H186 Fig. 23B) (106,150,152). The D117A mutation only had a slight effect on HiLpxH activity suggesting it has a negligible role in catalysis. Support for this hypothesis comes in the position of D117's corresponding residue in bacteriophage λ protein phosphatase, which lies distant from the enzyme's binuclear site.

Taken together, the mutagenesis data from HiLpxH support an active site structure similar to that found in other CLP enzymes, with the residues of the conserved CLP motif in HiLpxH coordinating a high affinity binuclear Mn^{2+} site (Fig. 23C). This strongly suggests that despite the fact LpxH cleaves the pyrophosphate bond of a substrate containing a nucleoside di-phosphate linked to a lipid moiety, it is a unique member of the CLP family rather than the Nudix family (103).

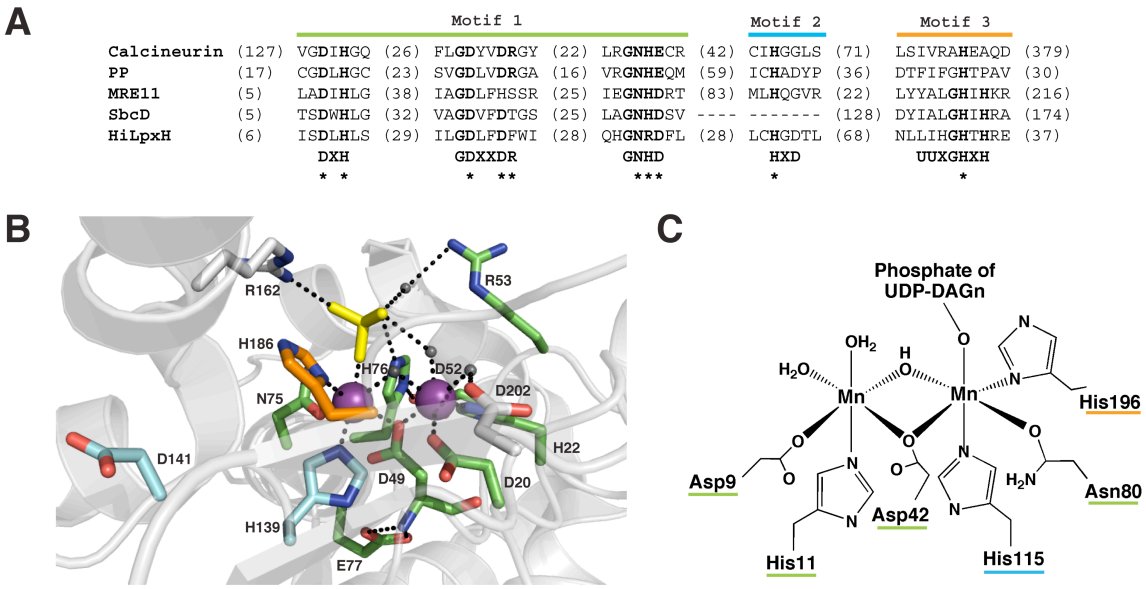

Figure 23: Proposed Structure of HiLpxH Active Site

A) Alignment of conserved CLP motifs in various family members. The most conserved portion of the motif is labeled Motif 1. Motif 2 and 3 indicate portions of the motif less ubiquitous throughout the family. (B) Active site of bacteriophage λ protein phosphatase modified from PDB 1G5B (150). Residues marked in green, cyan, and orange correspond to those that are part of Motif 1, 2, and 3 respectively and their location in the motifs are denoted by * in (A). Residues marked in gray are not part of the CLP motif but have roles in active site coordination. Mn^{2+} ions are represented by purple spheres, water molecules are indicated by dark gray spheres, and the SO_4 substrate mimic is shown in yellow. Black dashed lines indicate possible modes of coordination as suggested by intramolecular distances. (C) Proposed Mn^{2+} coordination of HiLpxH based on similarity to the enzymes of the CLP family.

.

4. Identification of LpxG, the UDP-2,3-diacylglucosamine Hydrolase in *Chlamydia trachomatis*

4.1 Introduction

Thus far, lipid A biosynthesis has been discussed from the focal point of LpxH, the enzyme that catalyzes the conversion of UDP-DAGn to lipid X through hydrolysis (40,82). While there is clear biochemical and genetic evidence that LpxH is responsible for this step of lipid A biosynthesis, it is not conserved in all Gram-negative bacteria (81); LpxH orthologs are primarily found in β, γ, and ε proteobacteria, but missing from many other organisms that make lipid A. This lack of conservation is not seen in the other early steps of lipid A biosynthesis, as orthologs for LpxA, LpxC, LpxD, LpxB, and LpxK are highly conserved (81).

The conservation of the enzymes both proceeding and following LpxH, as well as the similar backbone structure of the final lipid A molecule, led to the assumption that the enzymatic process of hydrolyzing UDP-DAGn to lipid X still occurs in in bacteria lacking LpxH, but it is carried out by a different protein (41). Bioinformatic analysis of several Gram-negative bacteria lacking LpxH, specifically those of the α-proteobacteria family, revealed a gene of unknown function that seemed to cluster with other lipid A biosynthetic enzymes. An ortholog of this gene from *Caulibactor crescentus* termed *lpxI,* was shown to encode for a hydrolase that was capable of converting UDP-DAGn into lipid X. Furthermore, expression of *lpxI* complemented a deletion of *E. coli*

lpxH. It was thus concluded that LpxI was responsible for the fourth step of the lipid A pathway in bacteria containing corresponding orthologs (41).

While the discovery of LpxI completed part of the puzzle of proteins responsible for UDP-DAGn hydrolysis, missing pieces still remain. Nearly all proteobacteria seem to contain either LpxH or LpxI, however the Chlamydiae phylum lacks orthologs of either protein (41,81). Of specific interest is one of the most characterized pathogens of this phylum, *C. trachomatis*. These bacteria display a fairly similar lipid A structure to that of *E. coli:* Both lipid A species have a disaccharide backbone composed of two diacylglucosamine molecules joined by a linked β 1′-6 linkage (153) (Fig. 14). There is slight difference in the acylation pattern compared to *E. coli*, with *C. trachomatis* lipid A lacking a sixth acyl chain as well as hydroxylated fatty acids at the 3 and 3′ positions (153). Despite this small variance, and the lack of a known UDP-DAGn hydrolase, *C. trachomatis* contains homologs for seven of the first eight lipid A biosynthetic enzymes found in *E. coli.* This strongly suggests the biosynthetic pathway proceeds through the same set of intermediates as found in *E. coli* and that an unidentified protein is performing the function of UPD-DAGn hydrolysis.

To investigate the existence of a UDP-DAGn hydrolase in *C. trachomatis*, we pursued biochemical and genetic studies of the bacteria. *C. trachomatis* is an obligate intracellular pathogen that is the leading cause of infectious blindness and sexually transmitted bacterial infections worldwide. It, along with the rest of Chlamydiae, has a

biphasic life-cycle that consists of an reticulate body (RB) and elementary body (EB) state (Fig. 12) (109). In the beginning stages of infection, *C. trachomatis* in metabolically inactive EB state attaches to the host epithelial cell. The bacteria are then internalized into the host and differentiate into the RB state. At this stage, the RBs form a membrane-bound inclusion and replicate. Midway through the infectious cycle, some of the RBs begin to change back into EBs. These newly formed EBs are released through extrusion or cell lysis, allowing them to initiate a new round of infection.

The bi-phasic, intracellular life cycle of *C. trachomatis* presents challenges to the identification of gene functions in the bacteria (109). Specifically, studies identifying LpxH in *E. coli* employed the Kohara library, which allowed for screening of infected strains for enhanced UDP-DAGn hydrolase activity (40). Such a strategy is not conducive in *C. trachomatis,* as it is not susceptible to phage infection. Furthermore, any strategy of functional identification involving a read-out of increase in UDP-DAGn hydrolase activity would be cantankerous--*C. trachomatis* must be cultured intracellularly, thus bacterial lysate activity would be diluted in the presence of the host's cellular milieu. While separation of *C. trachomatis* and host cell is possible, it would not be efficient in the context of a whole genome functional screen. A method for controlled gene expression in *C. trachomatis* has been recently described (120), however as accumulation of lipid X is not predicted have an easily discernable phenotype for *C. trachomatis*, this strategy would not be efficient. Other strategies involving targeted

genetic manipulation including gene deletions are not possible, as this technology has not been developed in *C. trachomatis* (109).

The lack of tools available for the genetic and biochemical manipulation of *C. trachomatis* makes it advantageous to use heterologous expression systems to screen for gene functionality. Thus, we developed genetic complementation screen for identifying the unknown UDP-DAGn hydrolase in *C. trachomatis.* By utilizing an *E. coli* strain engineered to have temperature-controlled expression of *lpxH,* we were able to assess a *C. trachomatis* open reading frame (ORF) library for functional complements of *lpxH.* As *lpxH* is essential, positive hits were easily detected by viability at high temperatures. Our screen identifies a candidate ORF, Ct461, that is conserved in other *Chlamydia* species and exhibits UDP-DAGn hydrolase activity both *in vivo* and *in vitro* (further discussed in Chapter 5). We conclude that Ct461 encodes for LpxG, a unique UDP-DAGn hydrolase. Overall, this study reveals yet another enzyme capable of the production of lipid X, helping to complete the landscape of the fourth step of lipid A biosynthesis. Additionally, it serves as a model for functional analysis of unknown genes in *C. trachomatis.*

4.2 Materials and Methods

4.2.1 Chemicals and Reagents

The 4-(2-hydroxyethyl)-1 piperazineethanesulfonic acid (HEPES), phosphate-buffered saline (PBS) components, HCl, salts, ampicillin, isopropyl-β-D-thiogalactoside (IPTG), fatty acid-free bovine serum albumin (BSA), Triton X-100 (TX-100) ethylenediaminetetraacetic acid (EDTA), and dithiothreitol (DTT) were purchased from Sigma-Aldrich (St. Louis, MO). Methanol, chloroform, pyridine, and acetic acid were obtained from EMD Science (Gibbstown, NJ). Radioactive γ-^{32}Pi was purchased from PerkinElmer (Waltham, MA). Unless otherwise noted, protein concentration was determined either by BCA Assay or Bradford Assay (Thermo Scientific, Waltham, Massachusetts) depending on compatibility with buffer components. Both of these methods were carried out as described by the manufacturer.

4.2.2 Bacterial Strains and Growth Conditions

The bacterial strains used in this study are listed in Table 9. Chemically competent cells were prepared using an established protocol. All P1 *vir* lysate preparation and infections were carried out according to the procedure outlined in Current Protocols in Molecular Biology (154) and any alterations have been denoted. Growth medium for liquid culture was Luria broth (LB), containing 5 g/L yeast extract, 10 g/L tryptone, and 10 g/L NaCl. LB supplemented with 7.5 g/L of bacto agar was used for solid phase growth. All media components were purchased from Difco (Detroit, MI).

Antibiotics were used at the following concentrations: 100 μg/mL ampicillin (Amp), 50 μg/mL kanamycin (Kan), 25 μg/mL chloramphenicol (Cam).

Table 9: Strains Used in the Discovery of LpxG

Strain	Description	Source or Reference
DH5α	*E. coli,* F⁻ Δ*(argF-lacZYA)U169 deoR phoA supE44 Φ80 Δ(lacZ)M15 gyrA96 relA1 endA1 thi-1 hsdR17 recA1λ⁻*	Invitrogen
C41	*E. coli,* F− ompThsdsB(rB−mB−) gal dcm (DE3) Δ(srl-recA)306::Tn10	(125)
C41_CtLib	C41, pDEST_Ctlib	This work
C41Ec	C41, pKJB2	This work
C41ΔHCtG	C41 ΔlpxH::kan, pKJB2	This work
BL21(DE3)	*E. coli,* F⁻ ompT gal dcm lon $hsdS_B(r_B^- m_B^-)$ λ(DE3 [lacI lacUV5-T7 gene 1 ind1 sam7 nin5])	Invitrogen
HY0	BL21(DE3), pKJB5	This work
HY1	BL21(DE3) *ΔlpxH::kan,* pKJB5	This work
HY1_Lib	BL21(DE3) *ΔlpxH::kan,* pKJB5, pDEST17_CtLib	This work
HY1_EcH	BL21(DE3) *ΔlpxH::kan,* pKJB5, pKJB2	This work
HY1_VC	BL21(DE3) *ΔlpxH::kan,* pKJB5, pHSC	This work
HY1_461Lib	BL21(DE3) *ΔlpxH::kan,* pKJB5, pDEST_461	This work
HY1_461	BL21(DE3) *ΔlpxH::kan,* pKJB5, p461	This work
HY1_733Lib	BL21(DE3) *ΔlpxH::kan,* pKJB5, pDEST_733	This work
HY1_733	BL21(DE3) *ΔlpxH::kan,* pKJB5, p733	This work
HY2_VC	BL21(DE3) *ΔlpxH::kan,* pMAK705, pKJB2	This work
CtG_t10	C41 harboring p461T	This work
VC_t10	C41 harboring pET21t10	This work
D125A_t10	C41 harboring pD125AT	This work
W3110A	*E. coli,* F- aroA::Tn10 msbA+ , TetR	(155)
W3110AΔHEc	W3110A *lpxH::kan* harboring pBAD33Ec	(41)
W3110AΔHCc	W3110A *lpxH::kan* harboring pBAD33Cc	(41)
W3110ACtG	W3110A, pBAD33461	This work
W3110A733	W3110A, pBAD33733	This work
W3110AΔHCtG	W3110A *lpxH::kan* harboring pBAD33461	This work

4.2.3 DNA Amplification and Analysis

All primers used in this study, listed in Table 10, were synthesized by Integrated DNA Technologies (Coralville, IA). PCR reactions employing the KOD method were carried out using a Mastercycler Gradient Thermocycler (Eppendorf, Hamburg, Germany) with the reagents and protocol of the KOD Hot Start Kit (EMD Chemicals, Gibbstown, NJ), however reactions were additionally supplemented with 3% (w/v) dimethyl sulfoxide and 1 M betaine unless otherwise noted. PCR reactions utilizing the TAQ method also used the Mastercycler Gradient Thermocycler (Eppendorf, Hamburg, Germany), but for these samples, reactions were performed with the reagents and protocol of Apex 2.0X Taq RED Master Mix kit (Genesee Scientific, San Diego, CA). PCR products were visually analyzed using 1% (w/v) agarose gels ran at 85 V in TAE buffer with HyperLadder 1 kb (Bioline, Taunton, MA) as a sizing reference. DNA fragments were purified either from agarose gel or directly from reactions using QIAquick Spin kits. The plasmids used in this study, listed in Table 11, were purified using Qiagen Mini-Prep kits (Qiagen, Valencia, CA) according to the manufacturer's protocol.

Table 10: Primers Used in the Discovery of LpxG

Name	Purpose	Primer sequence (5'-3')
T7_For	To sequence segments of DNA cloned into T7 vectors	TAATACGACTCACTATAGGG
T7_Rev	To sequence segments of DNA cloned into T7 vectors	CTAGTTATTGCTCAGCGGTG
5002_For	To amplify the region of the *E. coli* genome surrounding *lpxH;* complementary to DNA 500 bp upstream of *lpxH*	GCCAGTAACGCCGCGTTT
5002_Rev	To amplify the region of the *E. coli* genome surrounding *lpxH;* complementary to DNA 500 bp donstream of *lpxH*	CACCAATCAAACGGAACAGGATGC
p21	To amplify the *kan* cassette	CCAGGATCTTGCCATCCTATGGA
Ct461_For	To amplify Ct461 from *C. trachomatis* ORFeome library; incorporates truncated codons from N-terminal region; confers 5' *Nde1* site	GCGCGCCATATGTTCGTTTCTGTGGGT ATTACTGCATCTTTAACAACTATCTTA GCAGCACCTGTTTTGACATGGGTTTG GGCCAATCACT
CT461_Rev	To amplify Ct461 from *C. trachomatis* ORFeome library; confers 5' *SalI* site	CGC GCG GTCGAC CTA AGG TTC ATA GAG GCA CCT CAT TAA AC
CT461thru_ Rev	To amplify Ct461 from *C. trachomatis* ORFeome library; eliminates stop codon; confers 5' *SalI* site	GCGCGCGTCGACAGGTTCATAGAGGC ACCTCATTAA AC
Ct733_For	To amplify Ct733 from *C. trachomatis* ORFeome library; incorporates truncated codons from N-terminal region; confers 5' *Nde1* site	GCGCGCCATATGTTAATAAACTTTAC CTTTCGCAACTGTCTTTTGTTCCTTGT CACACTGTCTAGTGTCCCTGTTTTCTC AGCACCTCAACCTCGCG
Ct733_Rev	To amplify Ct733 from *C. trachomatis* ORFeome library; confers 5' *SalI* site	GCGCGCGTCGACCTATAAATGGATAC TAACGGTTCCATTTAAGTGA
D59A_For	To mutate CtLpxG D59 to alanine	CGCATTGTACAGATTTCGGCTTTACAC CTAAACCACTCG
D59A_Rev	To mutate CtLpxG D59 to alanine	CGAGTGGTTTAGGTGTAAAGCCGAAA TCTGTACAATGCG

Table 11: Plasmids Used in the Discovery of LpxG

Plasmid	Description	Source or Reference
pMAK705	Temperature sensitive replicon; Cam^R	(156)
pKJB5	pMAK705 *E. coli lpxH;* Cam^R	(82)
pDONR221	Gateway® entry vector; Kan^R	Invitrogen
pDONR_CtLib	pDONR221 harboring Ct ORFeome library*;* Kan^R	This work
pDONR_461	pDONR221 harboring Ct461 lacking the codons for the N-terminal transmembrane region of the protein product; Kan^R	This work
pDONR_733	pDONR221 harboring Ct733 lacking the codons for the N-terminal transmembrane region of the protein product; Kan^R	This work
pDEST17	Gateway® destination vector compatible with T7 expression; encodes for N-terminal HIs6 fusion; contains ribosome binding site and ATG start codon upstream His-tag; Amp^R	Invitrogen
pDEST_CtLib	pDEST17 containing *C. trachomatis* ORFeome library; Amp^R	This work
pDEST_461	pDEST17 containing Ct461 lacking the codons for the N-terminal transmembrane region of the protein product; Amp^R	This work
pDEST_733	pDEST17 containing Ct733 lacking the codons for the N-terminal transmembrane region of the protein product; Amp^R	This work
pET21a, b	High-copy expression vector containing a T7 promoter; Amp^R	Invitrogen
pET21t10	Modified pET21b with TEV-protease cleavage and His_{10} tag 3' of *XhoI* site; Amp^R	(157)
pHSC	Modified pET21b with TEV-protease cleavage site and His10 tag 3' of HindII siteI; Amp^R	Dr. Hak Suk Chung
p461	pHSC harboring C. trachomatis ORF 461; Amp^R	This work
p733	pHSC harboring C. trachomatis ORF 733; Amp^R	This work
pKJB2	$pET21a^+$ plasmid containing *E. coli lpxH;* Amp^R	(40)
pBAD33	Arabinose inducible vector; Cam^R	Invitrogen
pBAD33Ec	pBAD33 harboring *E. coli lpxH*; Cam^R	(41)
pBAD33Cc	pBAD33 harboring *C. crescentus lpxI*; Cam^R	(41)
pBAD33461	pBAD33 harboring *C. trachomatis* ORF 461; Cam^R	This work
pBAD33733	pBAD33 harboring *C. trachomatis* ORF 733; Cam^R	This work
p461T	pHSC harboring C. trachomatis ORF 461 lacking stop codon to generate C-terminal His10 tag cleavable by TEV-protease; Amp^R	This work
pGD59AT	p461T with D125A mutation; Amp^R	This work

4.2.4 *C. trachomatis* Cell Culture

*C. trachomatis (*serovar LGV biovar L2 434/Bu*)* was grown in HeLa cells (CCL-2; ATCC), cultivated in a T175 flask at 37°C. The infected culture was incubated for 30 h and inclusion and EB formation was confirmed via microscope. For harvesting, media was removed from the culture and cells were washed twice with 5 mL of PBS. Next, a 5 mL aliquot of PBS was added to the culture and a cell scraper was used to disrupt the adhered cells. This sample was collected in a falcon tube and centrifuged at 3,500 × g. After removal of the supernatant, the pelleted cells were resuspended in 750 μL of a buffer containing 20 mM HEPES pH 8.0 and 1.0 % w/v Triton X-100 (TX-100) and then lysed by sonication. Remaining debris was removed with centrifugation at 10,000 × g. The resulting supernatant, termed "HeLa + Ct," was aliquotted and stored at -80°C. The same procedure was carried out using an identical HeLa culture that was not infected with *C. trachomatis,* with final samples being designated "HeLa".

4.2.5 *C. Trachomatis* Lysate Activity

To test for UDP-DAGn hydrolase activity in *C. trachomatis*, samples of HeLa + Ct were tested for lipid X formation using two slightly modified versions of the autoradiographic assay described below. The first revised condition left out the non-radioactive form of the substrate (100 μM UDP-DAGn) of the reaction in order to increase assay sensitivity. DDM was also omitted due to the high amount of detergent already present in the lysate samples. The second condition was identical to the first

except 1 mM EDTA was used in place of 1 mM $MnCl_2$. Both reactions contained 20 mM HEPES pH 8.0, 0.5% (w/v) BSA, and 1,000 cpm/μL [β-^{32}P] UDP-DAGn. Thawed HeLa + Ct and HeLa samples were assayed in parallel under these two conditions, with final concentrations of protein and TX-100 in all assays being 1.5 mg/mL and 0.33% w/v, respectively.

4.2.6 Generation of C41ΔHEc

A P1 *vir* lysate was prepared from W3110AΔHEc employing the top agar method and used to infect E. coli C41 harboring pKJB2 (C41EcH). After incubation with the phage and subsequent outgrowth, cells were plated on LB-agar containing Kan, Amp, and 5 mM sodium citrate and grown for 18 h at 37°C. Resulting colonies were re-purified twice on the aforementioned LB plates to remove any remaining phage. Colony PCR utilizing the KOD method with primers 5002_For and 5002_Rev were used to amplify the region upstream and downstream of lpxH in these bacteria; oligonucleotide products were sequenced to determine the presence of the *kan* cassette. This strain was designated C41ΔHEc.

4.2.7 Construction of pDEST *C. trachomatis* Genomic Library

Each clone from a *C. trachomatis* ORFeome library harbored in *E. coli* (158) was inoculated into an individual well of a microtiter plates containing 200 uL of LB supplemented with Kan. Resulting cultures (~1000) were incubated for 18 h at 37°C, shaking at 220 rpm. Next, several representative library pools were generated from

combining 100 uL samples of ~44 clones. These pools were then centrifuged and mini-prepped to obtain library plasmids. Each pool yielded ~10 μg of DNA. Approximately 1.5 μg of DNA from each pool was combined to yield "pDONR_Ctlib."

Gateway technology was employed to transfer the ORF inserts in pDONR_CtLIb into pDEST17 to generate pDEST_CtLib. Three separate Gateway® LR Clonase® (Invitrogen, Carlsbad, CA) reactions were carried out according to specifications from the manufacturer except reaction incubation was 24 h at 25°C. The number of reactions was chosen to ensure 10-fold coverage of the ORFeome contained in the pDONR vector sample. Transformations of 1 μL aliquots from each reaction into chemically competent C41(DE3) were repeated until all three reactions had been consumed (~26 total transformations). Each resulting cell sample was grown in 1 mL of LB for 1 h at 37°C and plated on LB-agar supplemented with Amp. (Specifically, each transformation was spread on two LB-agar plates: the first plate contained only 100 μL of the transformation while the second contained the remaining 900 uL). After growth at 37°C for 18 h, >20,000 resulting colonies (ensuring 20,000-fold coverage) were collected and pooled into a 250 mL culture of LB containing Amp. The pool of bacteria was grown for 2 h at 37°C, after which 1 mL samples were taken for glycerol-stock storage. The final cell sample containing pDEST_CtLib was termed C41_CtLib.

4.2.8 Generation of Screening Strain HY1

To generate a temperature-controlled *lpxH* expression strain, pKJB5 was first transformed into chemically competent BL21(DE3) cells, yielding strain HY0. Next, HY0 was infected with a P1 *vir* lysate prepared from C41ΔHEc using the top-agar method. The C41ΔHEc strain was chosen to produce the viral material, as it was more similar to the background of the recipient HY0 than W3110AΔHEc, thus increasing the efficiency of the infection. After incubation with the C41ΔHEc lysate, HY0 cells were outgrown for 7 h at 30°C. This temperature was chosen due to the temperature sensitive replicon in pKJB5. Cells were then spread on LB-agar containing Kan, Cam, and 5 mM sodium citrate. Resulting colonies, termed strain HY1, were re-purified twice on plates similar to those on which they were initially grown. To confirm *kan* insertion, two colony PCR experiments utilizing the KOD protocol were carried out on 4 HY1 colonies (HY1 col 1 through HY1 col 4) and results were compared to those from BL21(DE3) and W3110AΔHEc via agarose gel. The first experiment employed primers 5002_For and 5002_Rev to amplify the area of the genome surrounding *kan* insert. The second also used 5002_For, but additionally contained p21 to ensure that a product was only generated if *kan* was present. As a final verification, the products from the first experiment were sequenced to ensure the HY1 clones contained *kan* in the context of *lpxH.*

4.2.9 Confirmation of Temperature-Sensitive Phenotype for HY1

HY1 col 1 through HY col 4 were used to inoculate four separate 5 mL LB cultures supplemented with Kan and Cam. Cultures were incubated at 30°C for 20 h, shaking at 220 rpms, then measured for their OD_{600}. The equivalent of ~10^9 cells were taken from each culture and resuspended in 1 mL LB to generate a sample with OD_{600} of 1. Eight serial dilutions of every sample were made in LB, each decreasing cell concentration 10-fold. A 3 μL aliquot from each of the resulting dilutions, ranging from 10^1 to 10^8 fold decrease in cell concentration from the original sample, was spotted on an LB-agar plate supplemented with Kan and then incubated at 30°C. This spotting was repeated a second and third time on identical plates that were incubated at 37°C and 44°C, respectively. After 24 h, plates from all three temperatures were compared for growth.

4.2.10 Complementation Screen

To screen the *C. trachomatis* ORFeome for *lpxH* complementation, first a sample of C41_CtLib outgrowth was mini-prepped to obtain an aliquot of pDEST_CtLib. Next, 300 ng of pDEST_CtLib was transformed into chemically competent HY1 cells to generate HY1_CtLib. After outgrowth in 1.7 mL of LB for 3 h at 30°C, three 500 μL aliquots of HY1_CtLib were plated on separate LB-agar plates supplemented with Amp and then incubated at either 30°C, 37°C, or 44°C. This was repeated with three 50 μL aliquots of the same outgrowth, resulting in two HY1_CtLib samples for each

temperature (500 μL and 50 μL platings). In parallel, HY1 was also transformed with equal amounts of pKJB2 and pET16b to generate HY1_EcH and HY1_VC, respectively. These cells were outgrown and plated in 500 μL and 50 μL amounts at 30°C, 37°C, and 44°C as described for HY1_CtLib. Plates were assessed for growth after 24 h and final colony number of each of the 18 plates was recorded after 48 h.

To efficiently analyze complementation screen results, colony PCR was performed on a representative sample of HY1_CtLib colonies surviving at high temperatures. This sample was comprised of all colonies (85 total) present on the plates containing 50 μL of HY1_CtLib outgrowth after incubation at 37°C and 44°C. PCR was carried out using the TAQ method with T7_for and T7_rev primers to amplify the ORF insert of the pDEST_CtLib plasmid harbored by each colony. The size of each resulting oligonucleotide product was analyzed using gel electrophoresis. Identical PCR reactions were also carried out for three surviving HY1_VC colonies (two from 37°C, one from 44°C) to serve as a control. Finally, a selection of PCR products (41 total) reflecting the distribution of ORF lengths were purified and sequenced using T7_for and T7_rev primers.

4.2.11 Independent Confirmation of Screen Hits from Library Plasmids

The ORF appearing at the highest frequency in the analyzed HY1_CtLib colonies, Ct461, was tested independently for *lpxH* complementation. To do so, the *E. coli* strain harboring Ct461 in pDONR221 (pDONR_461) from the *C. trachomatis* ORFeome library

(158) was used to inoculate 5 mL of LB supplemented with Kan. This culture was grown for 18 h at 37°C, shaking at 220 rpm, and then mini-prepped to obtain plasmid DNA. Resulting pDONR_461 was mixed with pDEST17 in a Gateway® LR Clonase® (Invitrogen) reaction following the manufacturer's protocol. Plasmid product was transformed into chemically competent DH5α cells, outgrown for 1 h at 37°C in LB, and plated on LB-agar plates containing Amp. After 18 h of incubation at 37°C, a resulting colony was used to inoculate 5 mL of LB supplemented with Amp. This culture was grown for 18 h at 37°C, shaking at 220 rpm, and then mini-prepped to obtain the plasmid pDEST_461. The same procedure was repeated for the ORF appearing at the second highest frequency, Ct733, to obtain pDEST_733. Sequencing with T7_for and T7_rev primers was used to confirm successful insertion of the desired ORF into pDEST17 vectors.

Plasmids pDEST_461, pDEST_733, and pKJB2 were transformed into chemically competent HY1 cells to generate HY1_461Lib, HY1_733Lib, and HY1_EcH, respectively. After outgrowth at 30°C in 1 mL of LB, three 250 μL aliquots of each cell sample was plated on LB-agar supplemented with Amp. Each plate from each strain was incubated at a different temperature (30°C, 37°C, or 44°C) for 24 h and then assessed for growth.

4.2.12 Cloning of *C. trachomatis* Genes

Amplification of Ct461 from pDEST_461 was accomplished using the KOD method of PCR with primers Ct461_For and Ct461_Rev. These primers incorporated

codons for the N-terminal region of the protein that were truncated from the gene during construction of the original pDONR library (158). They also added *Nde1* and *SalI* restriction sites to the 5′ and 3′ ends of the gene. PCR products were purified using gel extraction.

To generate an expression vector with a C-terminal His_{10} tag that was cleavable by Tobacco Etch Virus (TEV) protease, additional nucleotides were added to pET21b (Novagen/EMD Chemicals) to encode for the 7 amino acids of the protease site (ENLYFQG) (124) and the 4 additional histidine residues needed to elongate the affinity tag. This was accomplished using QuikChange (Stratagene, La Jolla, CA) mutagenesis with primers designed to insert the additional nucleotides 3′ to the *Hin*dIII restriction site in pET21b. The reaction was carried out using the manufacturer's protocol with an additional supplement of 3% (w/v) dimethyl sulfoxide. Following nucleotide insertion, the resulting plasmid, pHSC, was confirmed by sequencing and transformed into DH5α for storage.

Insertion of amplified Ct461 into pHSC was accomplished by digestion of both the PCR fragment and the vector with *Nde*1 and *Sal*I (New England Biolabs) under conditions described by the manufacturer. After treatment of pHSC with antarctic phosphatase (New England Biolabs) under conditions described by the manufacturer, digested Ct461 was inserted into the plasmid with T4 ligase (Invitrogen) as directed by the manufacturer. The ligation product, p461, was transformed into chemically

competent DH5α *E. coli* for storage. Sequencing with T7_for and T7_rev primers confirmed the appropriate insertion of Ct461into pHSC.

The same cloning procedure was carried out substituting Ct461_Rev with Ct461thru_Rev. This primer generated a form of Ct461 lacking a stop codon upstream of the *SalI* site, therefore ligation into pHSC created a construct encoding for a His_{10} tag cleavable by TEV-protease at the C-terminus of the protein. This plasmid was termed p461t and transformation into C41(DE3) to yield CtG_t10.

Amplification of Ct733 was also accomplished using the KOD method of PCR with primers Ct733_For and Ct733_Rev. Like the corresponding Ct461 primers, these oligonucleotides incorporated truncated N-terminal codons as well as *Nde1* and *SalI* restriction sites. Following the aforementioned method of digestion and ligation into pHSC, the resulting plasmid product was designated p733 and transformed into DH5α *E. coli* for storage.

4.2.13 Assessment of HY1 Temperature Complementation

4.2.13.1 Agar Plates

To test the ability of full length Ct461 and Ct733 to complement *lpxH* in *E. coli*, p461 and p733 was transformed into chemically competent HY1 to yield HY1_461 and HY1_733, respectively. Successful transformants were selected for survival at 30°C on LB-agar supplemented with Kan, Amp, and Cam. After 24 h, a resulting colony of each strain was re-purified under the same conditions.

Single colonies from HY1_461, HY1_733, HY1_EcH, and HY1_VC grown at 30°C for 48 h on LB-agar containing Amp and Cam were dissolved in 8 μL of LB. A 2 μL aliquot of each colony sample was spotted onto the same LB-agar plate containing Amp and Kan. These spots were spread over a section of the plate, after which the plate was placed at 30°C. A duplicate plate was generated from the same colony resuspensions and placed at 44°C. Following 48 h incubation, plates were assessed for growth.

4.2.13.2 Growth Curve in Liquid Media

To create an additional positive control for temperature-sensitive growth, chemically competent BL21(DE3) was transformed with pKJB2 and pMAK705 and plated at 30°C on LB-agar supplemented with Amp and Cam. A resulting colony was repurified under the same conditions and then subjected to infection with P1 *vir* lysate prepared from C41ΔHEc. After incubation with the phage, cells were outgrown at 30°C to retain the pMAK705 plasmid, and then plated at the same temperature on LB-agar containing Amp, Cam, Kan, and 5 mM sodium citrate. Resulting colonies were re-purified twice under the same conditions. This procedure resulted in the creation of strain HY2_VC.

For the growth curve, single colonies of HY1_461, HY1_733, HY2_VC, and HY1_VC were used to inoculate 5 mL of LB media supplemented with Amp and Cam. Resulting cultures were grown at 30°C, 220 rpms for 20 h and then diluted to a OD_{600} of 0.05 in 50 mL of LB containing Amp and Cam. Incubation at 30°C, 220 rpms continued

until cultures reached mid-log phase. At this time, cells from each strain were pelleted with centrifugation at 3,500 × *g*, resuspended in LB lacking antibiotic, and diluted to a OD_{600} of 0.01 in 25 mL of pre-warmed LB containing Amp. These cultures were then grown at 44°C, 220 rpm using a water bath shaker. The OD_{600} of each strain was recorded every 30 min. When cultures reached an OD_{600} of ~0.3, they were back-diluted 10-fold into fresh pre-warmed LB supplemented with Amp. Accumulated growth, as measured by OD_{600}, was plotted over time using a log scale.

4.2.14 Generation and Characterization of W3110AΔHCtG

For ligation of Ct461 into pBAD33, p461 was digested with *XbaI* and *SalI* (New England Biolabs) according to the manufacturer's protocol. Digestion with *XbaI* allowed for retention of the ribosome binding site upstream of the Ct461 start codon. The desired product was isolated from the parent plasmid by gel electrophoresis and subsequent extraction of the band corresponding to ~1200 bp. A sample of pBAD33 was also digested with *XbaI* and *SalI*, gel purified, and then treated with antarctic phosphatase (New England Biolabs) under recommended conditions. T4 ligase (Invitrogen) was employed to insert the Ct461 fragment into pBAD33 with reaction conditions as outlined by the manufacturer. The ligation product, pBAD33_461, was transformed into chemically competent DH5α. Sequencing with Ct461_For and Ct461_Rev confirmed the plasmid construction. Ct733 was also ligated into pBAD33

using the aforementioned procedure, substituting p733 for p461. The resulting construct, pBAD33_733, was confirmed using Ct733_For and Ct733_Rev.

Plasmids pBAD33_461 and pBAD33_733 were transformed into chemically competent W3110A to yield W3110ACtG and W3110A733, respectively. A P1 *vir* lysate, prepared from W3110AΔHEc using the top-agar method, was employed to transduce the *kan* cassette into W3110ACtG. After phage incubation, cells were outgrown at 37°C for 3 h and then plated on LB agar containing Cam, Kan, 0.02% (v/v) arabinose, and 5 mM sodium citrate. Resulting colonies were repurified twice under the same conditions; the subsequent strain was denoted W3110AΔHCtG. To confirm *kan* insertion, colony PCR employing the TAQ protocol was carried out with primers 5002_For and p21. Results were compared to those from W3110A and W3110AΔHEc via agarose gel. Additionally, the region upstream and downstream of the *kan* insertion was amplified using the KOD colony PCR method with primers 5002_For and 5002_Rev, and products were sequenced to verify the identity of the antibiotic cassette. A similar infection using W3110A733 as a host strain was attempted, but did not generate any surviving transductants. For growth comparison, single colonies of W3110AΔHEc and W3110AΔHCtG were dissolved in 8 uL of LB, and then 2 μL aliquots from each strain were spotted on LB-agar plates supplemented with Cam, Kan, and 0.02% arabinose or just Cam and Kan. Spots were spread over a portion of the plate to evenly distribute bacteria and then incubated at 37°C for 24 h.

4.2.15 Ct461 Expression

Preparation of Ct461 cell free extract (Ct461 CFE) began with inoculating an overnight culture of LB with a single colony of CtG_t10. This overnight culture was subsequently used to inoculate 250 mL of LB supplemented with ampicillin to an OD_{600} of 0.02. Cultures were incubated at 30 °C with aeration at 220 rpm until they reached OD_{600} of 0.7-0.8, then induced for expression by the addition of 1 mM IPTG and grown for an additional 4 to 5 h until the OD_{600} reached ~4. Cells from the growths were pelleted by centrifugation at 5,000 × *g*, washed with 35 mL of cold PBS, and then stored at -80 °C. For lysis, the frozen pellet was thawed, resuspended in 25 mL of ice-cold 20 mM HEPES pH 8.0, and passed twice through a French pressure cell (SIM-AMINCO; Spectronic Instruments) at 18,000 psi. The debris from the resulting lysate was removed by centrifugation at 10,000 × *g* and the subsequent supernatant was collected as cell-free extract (CFE) and stored at -80 °C. The same protocol was carried out to obtain VC CFE and D59A CFE, except VC_t10 and D59A_t10 were used for culture inoculation, respectively.

4.2.16 UDP-DAGn Hydrolase Activity Assay in Cell-Free Extracts

Autoradiographic assays for hydrolase activity were similar to that previously described (40,157), but with slight modification. Reactions mixtures were a final volume of 12.5 μL in 0.6 mL polypropylene tubes and contained 20 mM HEPES pH 8.0, 0.5% (w/v) BSA, 0.035% (w/v) DDM, 1 mM $MnCl_2$, 100 μM UDP-DAGn (prepared as

previously described (127)), 1,000 cpm/μL [β-^{32}P] UDP-DAGn, and protein or lysate sample. All reaction components besides the protein sample were mixed to a volume of 10 μL and equilibrated at 30 °C for 10 min, after which 2.5 μL of protein was added to start the reaction. Final protein concentrations in the assays ranged from 0.05 mg/mL to 1.0 mg/mL and were adjusted as necessary to maintain linear activity within the time frame being tested. If required, samples were diluted in a buffer identical to the assay mixture but lacking any lipid substrate or DDM before addition to the reaction. HiLpxH was obtained as described in Chapter 2. Aliquots of 1.5 μL were taken from the reactions at various time intervals and spotted onto 20 cm × 20 cm glass-backed silica gel thin layer chromatography (TLC) plates (EMD Chemicals, Darmstadt, Germany). These plates were developed in a 25:15:4:2 chloroform: methanol: water: acetic acid tank system, dried, exposed to phosphoscreens, scanned, and quantified as previously described (40,157).

4.2.17 Generation of Ct461 point mutant D59A

QuikChange (Stratagene) mutagenesis was used to make alanine point mutants of a conserved aspartate within Ct461. The method was carried out as described above, with p461t serving as template DNA. Primers D59A_For and D59A_Rev were employed to generate the desired alanine substitution and sequencing with T7_For and T7_Rev primers was used to confirm the mutations. The mutated p461t vector, pGD59AT, was

transformed into chemically competent *E. coli* C41(DE3) to create expression strains D59A_t10. Mutant cell free extract (D59A CFE) was obtained as described above.

4.3 Results

4.3.1 UDP-DAGn Hydrolase Activity is Present in *C. trachomatis* Lysates

It is well established that *C. trachomatis* produces lipid A (153), however there are no orthologs for the known enzymes capable of catalyzing the fourth step of the molecule's biosynthetic pathway, the hydrolysis of UDP-DAGn to form lipid X (81,159). In order to confirm the presence of this activity despite the absence of a protein currently known to encode this function, we assessed *C. trachomatis* lysates for lipid X formation. HeLa cells were infected with *C. trachomatis* EBs and incubated for 30 h, allowing the *C. trachomatis* to transition to the RB state, form inclusions, multiply, and transition back into the EB state. After this time, the bacteria and host cells were harvested and lysed to obtain a lysate sample termed "HeLa + Ct". A culture of uninfected HeLa cells was also grown and lysed in parallel to serve as a control lysate ("HeLa"). These samples were then analyzed for UDP-DAGn activity using an autogradiographic assay.

Over the time course tested, HeLa + Ct lysate showed linear production of lipid X (Fig. 24). This formation was not seen when HeLa lysate was assayed under the same conditions. Furthermore, replacement of $MnCl_2$ with EDTA in the *in vitro* system corresponded to decrease in activity and loss of linear product formation, indicating observed hydrolysis was metal dependent (Fig. 24). Such dependence is a characteristic

of the other known UDP-DAGn hydrolases, LpxH (157) and LpxI (159). Overall, the *in vitro* autoradiographic data led to the conclusion that *C. trachomatis* indeed contains an enzyme that is capable of hydrolyzing UDP-DAGn.

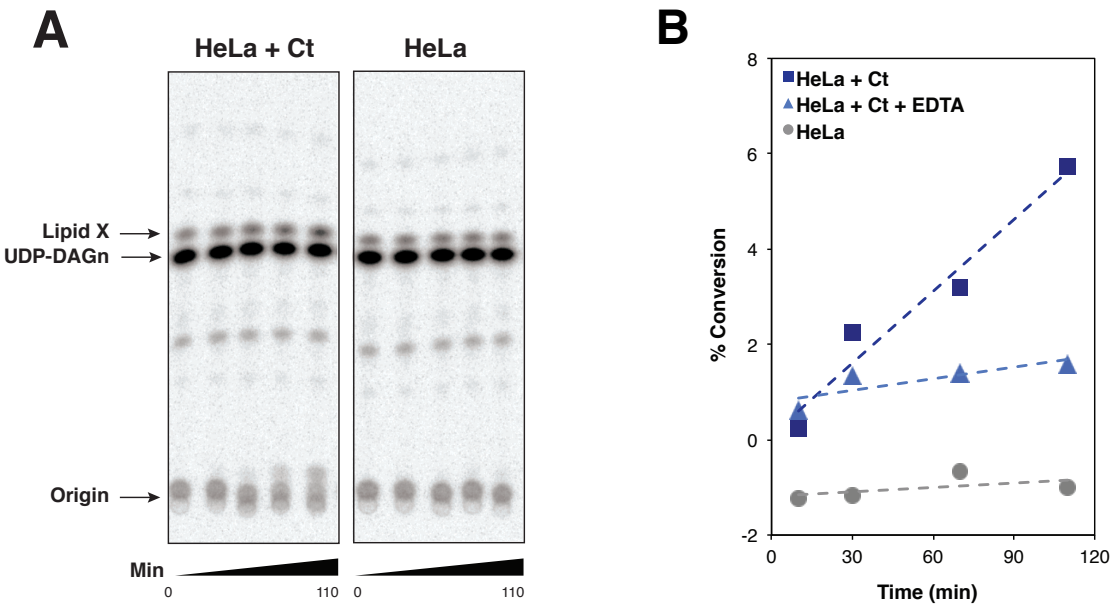

Figure 24: UDP-DAGn Hydrolase Activity in *C. trachomatis* Lysates

(A) Scan of phosphoscreen exposed to silca TLC plate from UDP-DAGn hydrolase assay of *C. trachomatis* lysates in the presence of Mn^{2+}. "HeLa + Ct" denotes presence of bacteria while "HeLa" represents lysate of host cell alone. Bands corresponding substrate (UDP-DAGn) and product (Lipid X) are denoted. (B) Percent of UDP-DAGn converted to lipid X by *C. trachomatis* lysates at specific time points under assay conditions with Mn^{2+} (HeLa + Ct) and with EDTA (HeLa + Ct + EDTA). Also depicted is activity of host HeLa lysates absent of bacteria (HeLa). Equal amount of protein was utilized in all assay conditions. Data was fit to a linear curve and showed an R^2 value of 0.954, 0.701, and 0.319 for HeLa + Ct, HeLa + Ct + EDTA, and HeLa samples, respectively . Product conversion was calculated by quantifying intensity of lipid X as a percentage of the total intensity of each lane and then subtracting the background conversion calculated from a no enzyme control.

4.3.2 Genetic Complementation Screen for UDP-DAGn Hydrolase Identification

4. 3. 2. 1 Screen Design

To identify the gene that encoded for the observed production of lipid X, we designed a complementation screen. The enzyme LpxH is well established to catalyze the hydrolysis of UDP-DAGn for the biosynthetic process of lipid. As *lpxH* is essential in

E. coli, we sought to find a *C. trachomatis* gene capable of permitting survival of an *lpxH* knockout. Overall, this strategy relied on the creation of *C. trachomatis* genetic library that could be expressed in *E. coli* and the construction of a strain in which the expression of *lpxH* was disrupted.

To construct the library, we utilized a collection of *E. coli* clones harboring each *C. trachomatis* ORF (CtORF) in pDONR221 (158). The plasmids from each of these clones were purified, pooled, and then transferred to pDEST17 using Gateway® technology. This vector contains a T7 promoter region and ribosome binding site 5′ to the ORF-insert, allowing for expression of the *C. trachomatis* DNA in DE3-strains of *E. coli.* The product of the Gateway® reaction was transformed into C41(DE3) *E. coli* and plated on ampicillin, as resistance to the antibiotic implied presence of a CtORF-containing pDEST17 vector. To ensure ample coverage of the 1,000-clone library, 20,000 ampicillin resistant colonies were used to obtain the final *C. trachomatis* pDEST library pool.

The essentiality of *lpxH* meant that any disruption of the gene had to be complemented in order for the bacteria to maintain viability. This complementation would need to be controllable to permit survival as a read-out for the *C. trachomatis* library screen. We chose temperature to regulate *lpxH* expression, as this method had been previously reported to permit tight control of the gene (82). The plasmid pKJB5, a temperature-sensitive construct containing *E. coli lpxH,* was transformed into BL21(DE3). This background strain was chosen to permit eventual T7 expression of library DNA. P1

vir transduction was used to replace the chromosomal copy of *lpxH* with *kan* in this strain, thus creating HY1.

Analysis of HY1 was necessary to confirm the appropriate genotype and phenotype. Through PCR, the strain was verified to lack a genomic copy of the UDP-DAGn hydrolase. Amplification of the 500 base pairs flanking the replaced *lpxH* in the HY1 chromosome yields a larger product than that generated from a wild-type BL21(DE3) strain (Fig. 25A). This increase in size, which corresponds to the presence of *kan* in that region, is also seen in the previously characterized deletion strain W3110AΔHEc (159). PCR with primers specific to *kan* creates an oligonucleotide product in HY1 and W3110ΔHEc and not BL21(DE3) (Fig. 25A). HY1 colonies were tested for a temperature-sensitive phenotype by dilution plating of identical cultures at 30°C, 37°C, and 44°C. Cells maintain viability at low temperature due to expression of *lpxH* from pKJB5; however, an increase in temperature halts replication of pKJB5, preventing the growth of HY1 colonies (Fig. 25B).

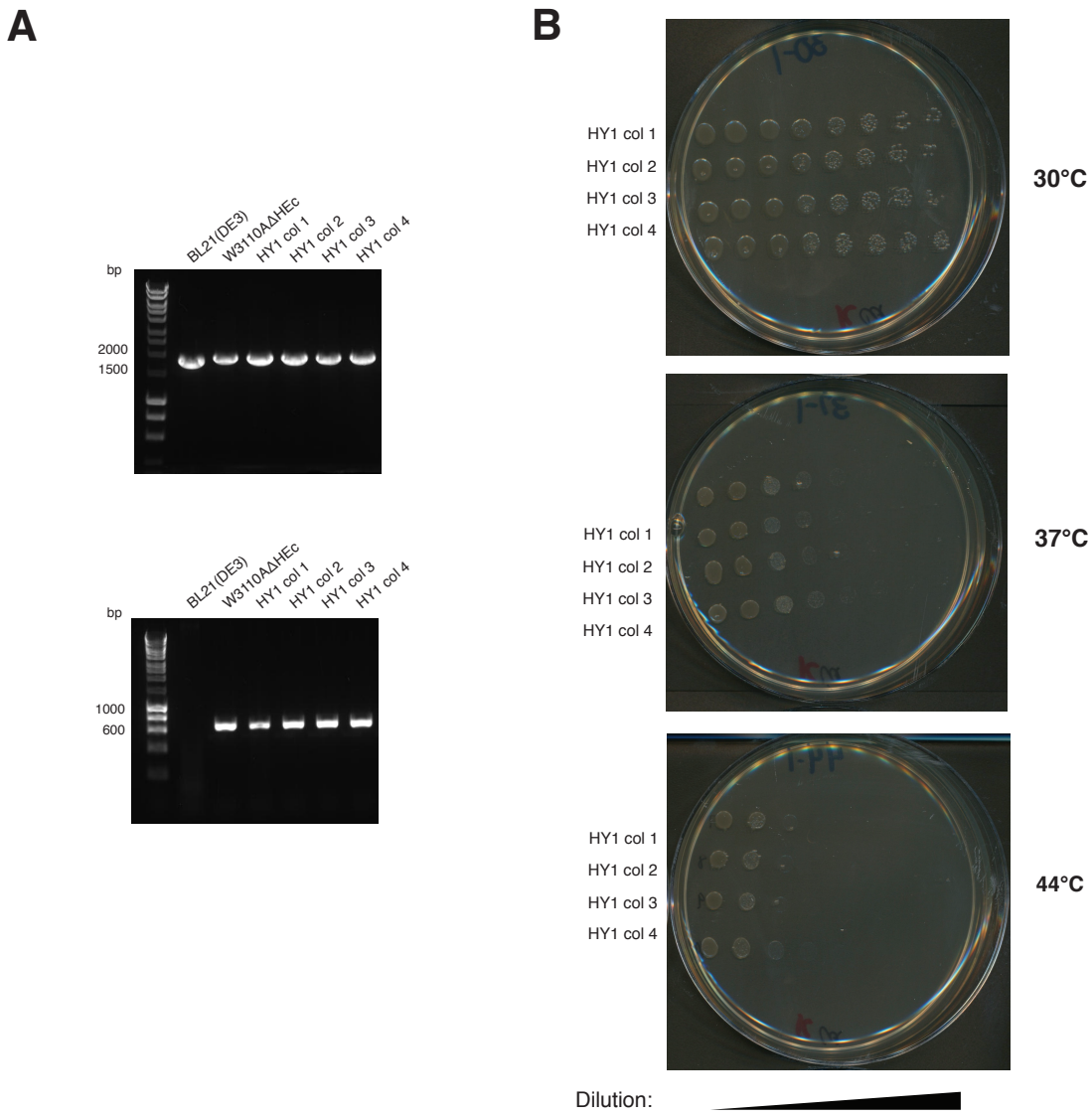

Figure 25: Confirmation of Genotype and Phenotype of HY1

(A) The top panel depicts colony PCR results from amplification of genome 500 bp upstream and downstream of *lpxH* with 5002_For and 5002_Rev of indicated *E. coli* strains. For wild-type strain BL21(DE3), product size reflects to presence of *lpxH,* as confirmed by sequence analysis. A shift if band size is observed for W3110AΔHEc, correlating to the replacement of *lpxH* with the larger *kan.* Tested colonies of HY1 (col 1 through col 4) all yield bands matching the size of W3110AΔHEc, signifying *lpxH:kan.* Identical results are displayed in the bottom panel, albeit internal kanamycin primer p21 replacing 5002_Rev. In this case, the 600 bp product is only generated if *kan* is present in the context of *lpxH.* (B) Temperature dilution plating of four representative HY1 colonies. Equal amounts of tested colonies were serially diluted and subsequently plated at 30°C, 37°C, and 44°C. Dilution begins at 10^1 fold and increases by 10-fold from left to right, ending in 10^8.

4.3.2.2 Screen Implementation

Using HY1 and our generated *C. trachomatis* pDEST library, we implemented the complementation screen. HY1 was transformed with pDEST_CtLib to generate HY1_Lib. Two different amounts of HY1_Lib were plated and incubated as a set at either 37°C or 44°C. While optimal deactivation of pKJB5 occurs at 44°C (82), 37°C was included to ensure successful expression of protein from the library plasmids. The two cell amounts distributed on the paired plates differed by 10-fold (500 μL of transformation versus 50 μL) to facilitate accurate counts of resulting colonies. To ensure adequate coverage of the library, another set of HY1_Lib plates was incubated at 30°C. As the low temperature would permit survival of all bacteria harboring a pDEST plasmid regardless of complementation ability, the number of plasmids screened could be directly determined from the number of resulting colonies at 30°C. This two dilutions-three temperatures plating procedure was repeated with HY1 transformed with pKJB2 (HY1_Ec) and pHSC (HY1_VC) to serve as additional controls.

Screen results can be seen in Fig. 26. For all strains tested, incubation of the more concentrated plating sample at 30°C yielded a lawn that, based on the number of bacteria appearing on the more dilute plating sample, was estimated to contain ~25,000 colonies. As the library contained ~1000 clones (158), this number ensured 20,000-fold coverage of the *C. trachomatis* ORFeome. A lawn also appeared at 44°C for HY1_Ec plates (data not shown), confirming that the presence of *lpxH* on pKJB2 rendered the

bacteria insensitive to temperature shift. A clear dependence on growth temperature was observed for HY1_Lib and HY1_VC; there was marked decrease in colony number on the more dilute plates at 37°C for both strains and even further reduction in surviving bacteria at 44°C (Fig 26A). This was also observed for samples in which a higher number of bacteria were originally plated (data not shown).

As HY1_VC's only functional copy of the essential gene *lpxH* in is harbored in a temperature sensitive plasmid, it was assumed that residual survival at high temperatures was due to mutations in the plasmid that rendered it heat resistant. HY1_Lib was also susceptible to these mutations; however there was a noticeable increase in the number of viable colonies for HY1_Lib over HY1_VC for both plating amounts, especially at 44°C (34 versus 9, respectively for the more dilute platings (Fig. 26B). Furthermore, the HY1_Lib colonies were non-uniform in size and appeared at different rates compared to those of HY1_VC. Together this suggested that UDP-DAGn hydrolase complementation by *C. trachomatis* DNA was in fact occurring in HY1_Lib.

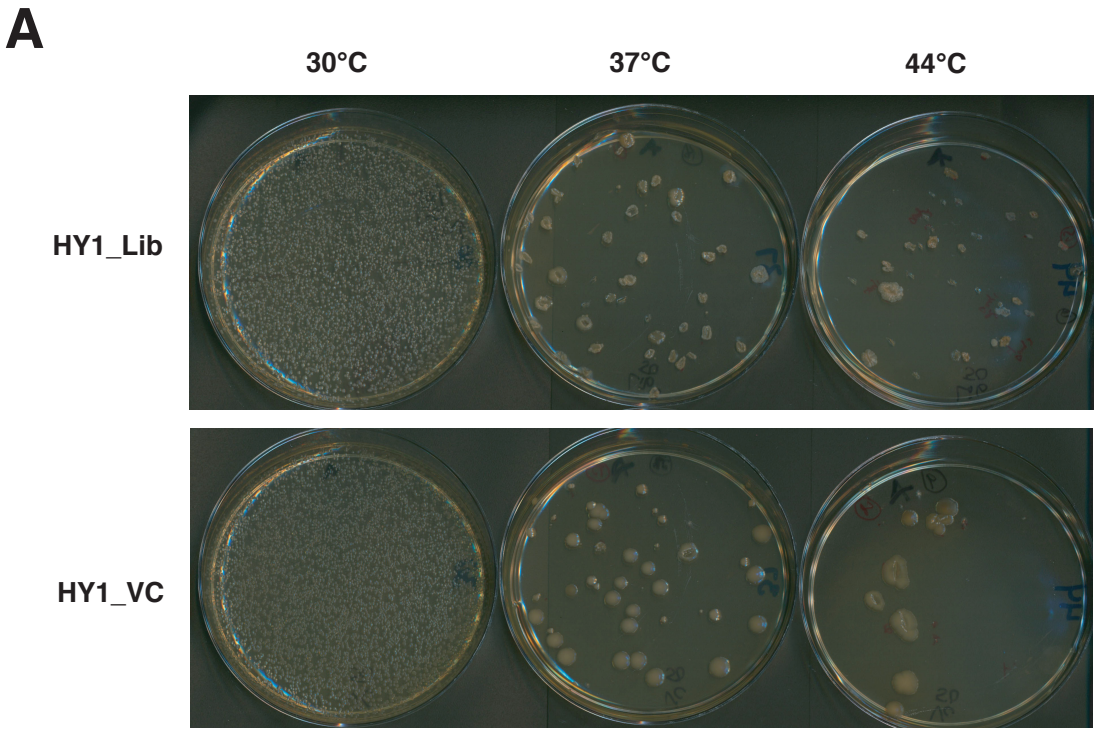

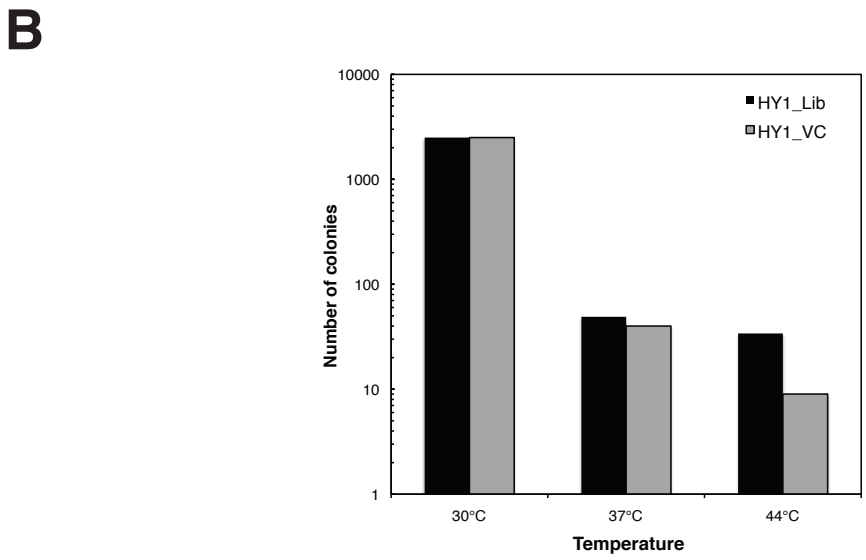

Figure 26: Enhanced Temperature Complementation of HY1_Lib

(A) LB agar plates from growth of 50 μL of HY1_Lib and HY1_VC transformations at three tested temperatures. Plates were supplemented with ampicillin for selection. (B) Quantification of colonies appearing on plates in (A). Increase in colony number is observed for HY1_Lib over HY1_VC at 37°C and further distinction in survival is evident at 44°C.

4.3.3 Assessment of Screen Results by PCR

To differentiate specific *lpxH* complementation in temperature-resistant colonies of HY1_Lib over non-specific background, we analyzed the CtORFs harbored in the host bacteria: Presumably, actual complementation could only be carried out by a specific ORF, and thus clones harboring this ORF should appear at a higher frequency compared to clones in which survival was mediated by a mutation in the temperature sensitive plasmid. A sample of HY1_Lib colonies surviving at 37°C and 44°C were subjected to colony PCR with T7 primers aimed to amplify the region of the pDEST plasmid containing *C. trachomatis* DNA. This sample was comprised of all 85 colonies appearing on plates containing the 10-fold more dilute sample of bacteria (colonies seen in Fig. 26A). The sizes of resulting products were assessed via agarose gel electrophoresis, thus allowing for an efficient way to determine the distribution of ORF lengths found in screen hits. Nearly 40% of the colonies tested contained an ~1100 bp insert (Fig. 27A, green arrow), 4-fold higher than the occurrence of any other sized band (Fig. 27B). The high frequency of this insert suggested it specifically conferred viability to *lpxH* deletion strains, therefore making it the most likely candidate for encoding the UDP-DAGn hydrolase. Sequencing of 14 of the 1100 bp PCR products revealed the insert corresponded to *C. trachomatis* ORF 461 (Ct461).

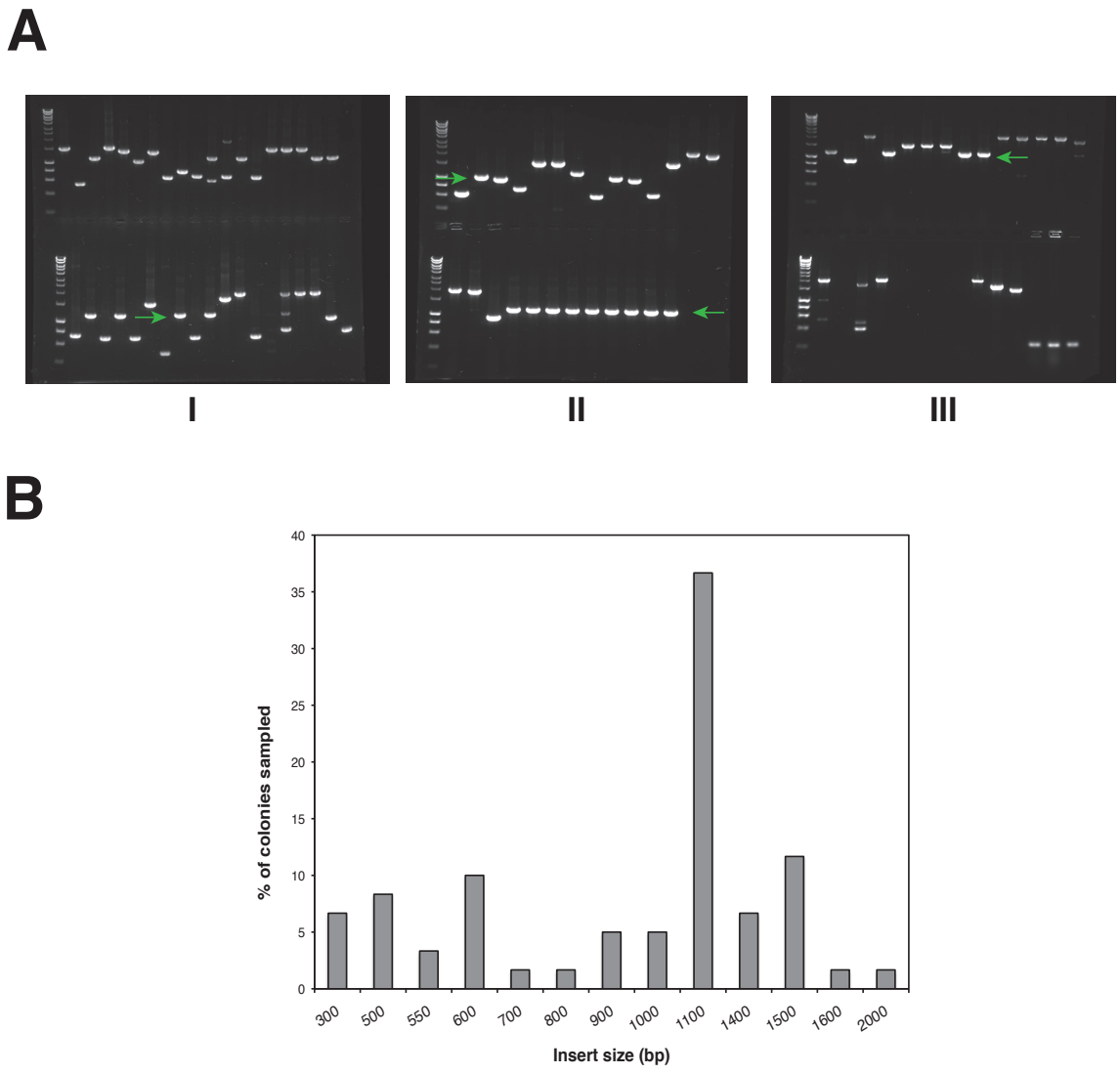

Figure 27: Colony PCR Analysis of Complementation Screen

(A) PCR results from amplification of 88 temperature-resistant HY1_Lib colonies with T7_For and T7_Rev. All reactions were performed in parallel with results being analyzed on three separate 1% agarose gels (I, II, and III). The first lane in each row of each gel contains HyperLadder 1 kb (Bioline, Taunton, MA). Green arrows point to bands designated as 1100 bp in size. (B) Occurrence of various band sizes shown in (A). All bands were estimated for size based on their position compared to the ladder and to each other. The total number appearing at each individual size was divided by the entire sum of bands analyzed to determine % of occurrence in the colonies sampled.

4.3.4 Temperature Complementation Verification Identifies Candidate UDP-DAGn Hydrolase Gene

As a final verification of the specificity of the ability of Ct461 to complement *lpxH,* the gene was independently assessed for temperature rescue of HY1. The appropriate *E. coli* clone from the *C. trachmatis* ORFeome library was used to obtain pDONR_461, which was then used to generate pDEST_461. This plasmid was transformed into the screening strain to yield HY1_461Lib. In a plating procedure similar to that carried out for the library screen, HY1_461Lib exhibited robust survival at both 30°C and 44°C (Fig. 28). In parallel, the ORF appearing at the second highest frequency in the screen, Ct733 (~1500 bp PCR product), was also tested for complementary in the same way with strain HY1_733Lib. This strain was not able to efficiently survive at the higher temperature (Fig. 28) indicating its appearance in library results was likely due to mutations in the temperature sensitive plasmid and not ORF function. Thus, it was concluded that the ORF appearing at the highest frequency in the library screen is able to complement *lpxH* function in *E. coli.*

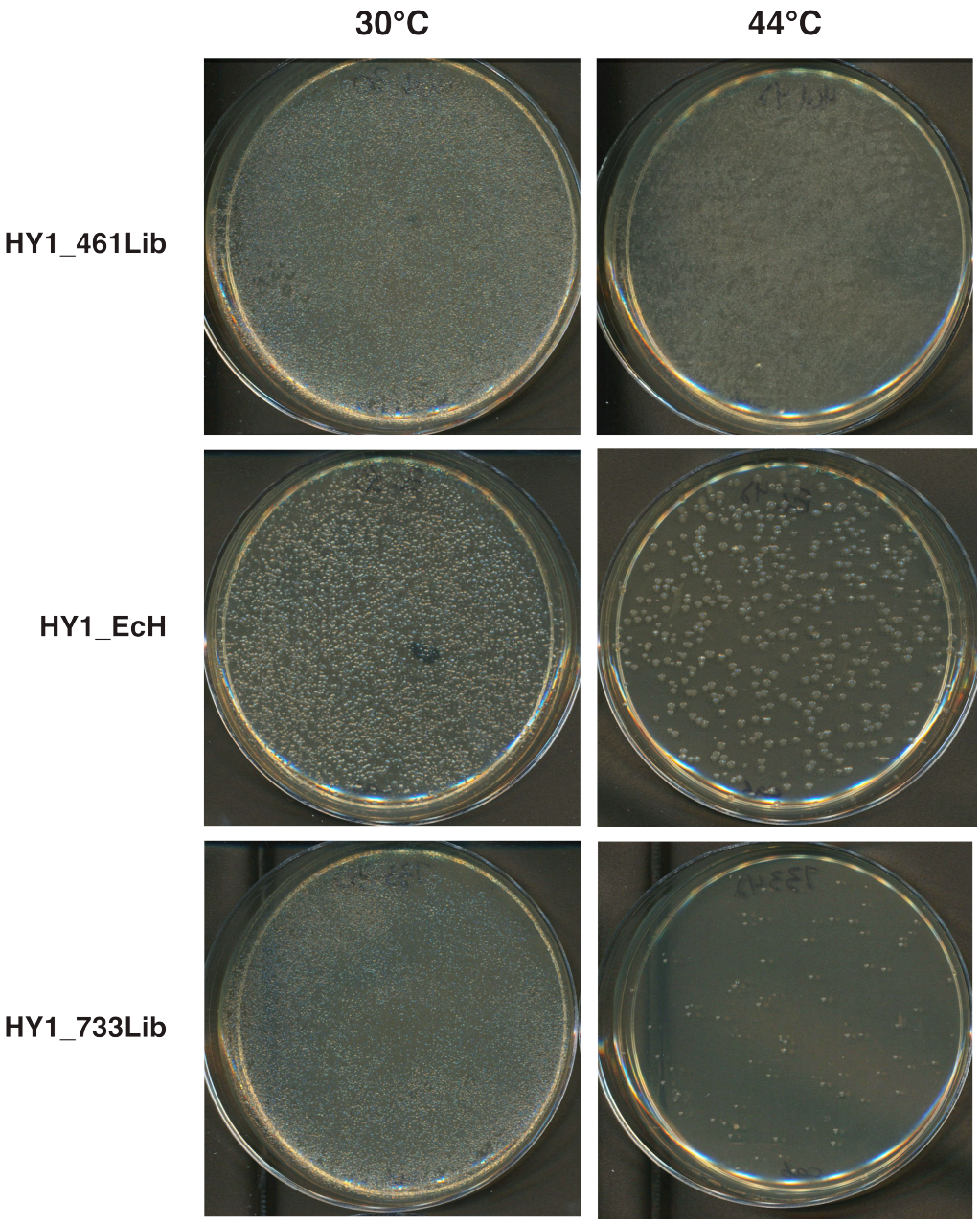

Figure 28: Confirmation of HY1 Complementation of Screen Hits

LB agar plates of HY1 transformed with individual plasmids from the pDEST library and grown at 30°C and 44°C. The two strains depicted, HY1_461Lib and HY1_733Lib, represent individual transformation of library pDEST plasmids occurring the first and second most frequently, respectively, in analysis of temperature resistant HY1_Lib. Identical plating of HY1_EcH is also shown at 30°C and 44°C as a control. Equal amounts of bacteria were plated at each condition for each strain, as determined by OD_{600}. The agar media was supplemented with ampicillin for selection.

4.3.5 Ct461 Displays *In Vivo* UDP-DAGn Hydrolase Function in HY1

Analysis revealed Ct461 encodes for a 37 kD uncharacterized metallophosphoesterase. The full-length protein product of the ORF is predicted to have an N-terminal transmembrane helix, however this region was truncated from the ORF during construction of the pDONR library (158). These trimmed codons were added back to the N-terminal region of Ct461 and the full-length gene, harbored in p461, was used for subsequent assessment. It was also noted that Ct733 was shortened at the N-terminal region during the generation of the library due to the presence of a similar predicted transmembrane domain (158); the complete version of the gene was constructed in p733. While Ct733 was not suspected to be capable of UDP-DAGn hydrolase activity, it was used as a control in further experiments to test the specificity of Ct461 function.

To confirm the ability of full-length Ct461 to perform UDP-DAGn hydrolase activity in *E. coli*, p461 was transformed into HY1, creating HY1_461. This strain was assessed for temperature sensitivity on LB-agar. It displayed survival at both 30°C and 44°C, similar to HY1_Ec, and was healthier in growth at 44°C compared to HY1_VC (Fig. 29A). HY1_733, HY1 transformed with p733, displayed a phenotype similar to HY1_VC (Fig. 29A).

As a more definitive assessment of the capability of Ct461 to rescue *lpxH* deficiency, growth of HY1_461 at 44°C was monitored in liquid media and compared to

control strains. Parallel cultures of HY1_461, HY1_VC, HY1_733, and HY2_VC were inoculated at 30°C and allowed to reach mid-log phase. After dilution to the same OD_{600}, the cells were shifted to 44°C. Linear growth, as tracked by accumulated OD_{600}, was observed for all four strains until 300 min, after which HY1_VC and HY1_733 lose viability (Fig. 29B). Presumably, this arrest in survival correlates to the loss of the temperature-sensitive *lpxH* plasmid, as these strains no longer contain a complement for the chromosomal absence of the gene. HY2_VC and HY1_461, however, do not plateau in growth (Fig. 29B) as presence of temperature insensitive plasmids (pKJB5 and p461, respectively) are able to complement the deletion of the lipid A biosynthetic enzyme at 44°C.

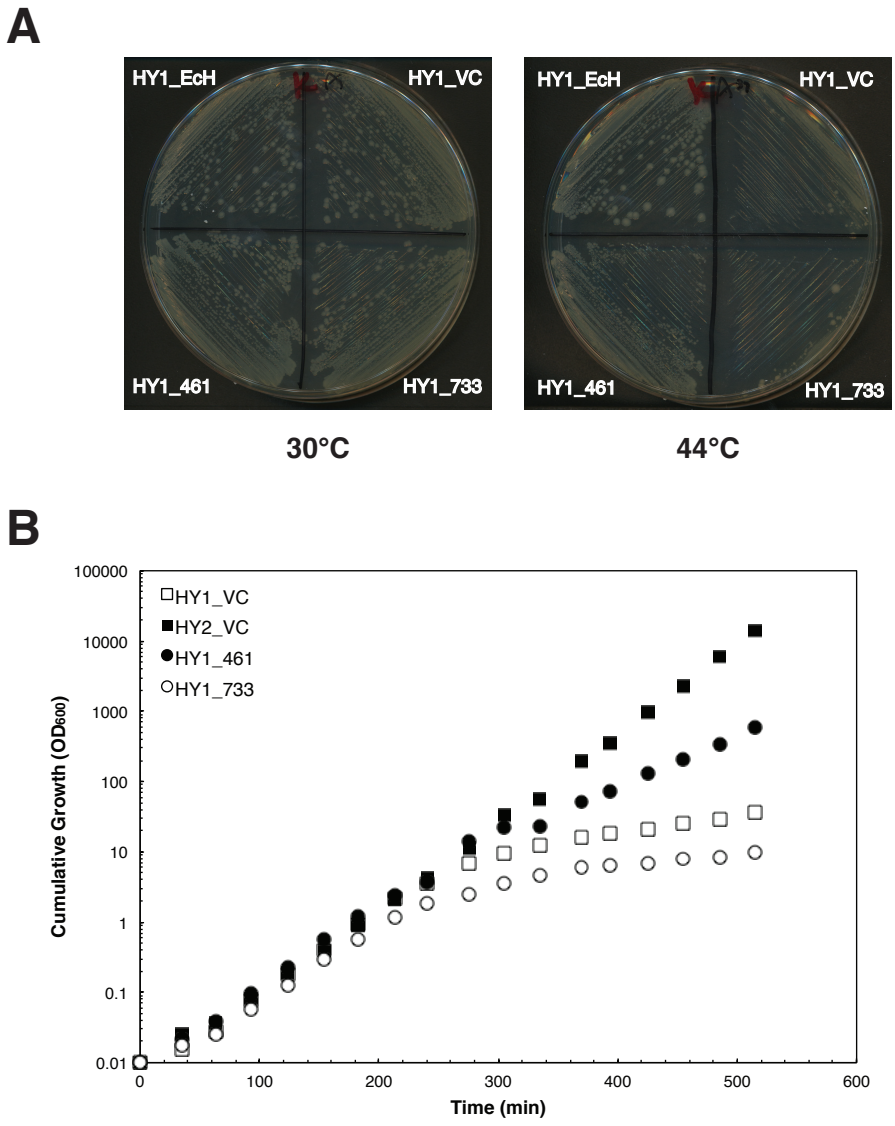

Figure 29: Ct461 Rescues HY1 at 44°C

(A) LB agar plates depicting growth of each HY1_VC, HY1_461, HY1_733, and HY1_EcH at 30°C and 44°C. Equal amounts of bacteria were streaked onto solid media supplemented with Amp and Kan for each respective HY1 strain at each temperature. (B) Growth curve of HY1_VC, HY2_VC, HY1_461, and HY1_733 in liquid media at 44°C. Cultures of each strain were grown to mid-log phase in LB supplemented with ampicillin and chloramphenicol at 30°C and then back-diluted to OD_{600} 0.01 into pre-warmed LB supplemented with ampicillin. To maintain log-phase growth, cultures were back-diluted 10-fold upon reaching OD_{600} 0.3-0.4. Cumulative growth was determined from OD_{600} measurements taken at designated time intervals and plotted on a logarithmic scale.

4.3.6 Ct461 Rescues *lpxH::kan* Viral Transduction in W3110A

Temperature-independent verification of Ct461's functional properties was also completed using P1 *vir* transduction. Full length Ct461 was ligated into pBAD33 and then transformed into W3110A, generating W3110A461. Transduction of *lpxH::kan* into the strain yielded W3110AΔHCtG. Colony PCR of W3110AΔHCtG with an internal *kan* primer and a primer specific to the region of the chromosome upstream of *lpxH* generated a product that was of equal size to that seen for W3110ΔHEc , a previously created *lpxH::kan* strain (Fig. 30A). In contrast, identical PCR analysis of wild-type W3110A yielded no oligonucleotide. W3110AΔHCtG was viable on LB-agar, and showed enhanced growth when supplemented with arabinose, which induced production of Ct461 from the pBAD plasmid (Fig. 30B). This *lpxH::kan* transduction procedure proved unsuccessful when Ct461 was replaced with Ct733.

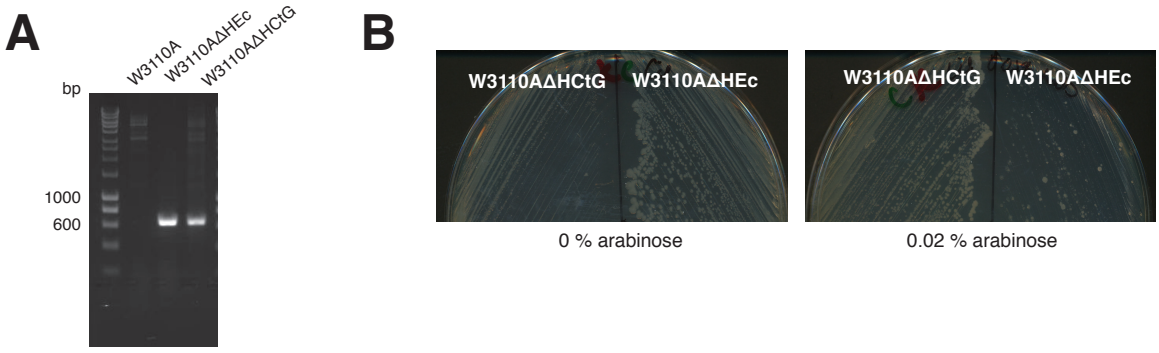

Figure 30: Ct461 Complements *lpxH::kan* in W3110A *E. coli*

(A) Colony PCR results of various W3110A strains employing 5002_For and p21 primers. Based on the sequence of indicated primers, products are only generated if tested strain harbors a lpxH::kan genotype, as indicated by the band around 600 bp for the previously characterized W3110AΔHEc. W3110AΔHCtG displays a similar result, while wild-type W3110A lacks any such oligonucleotide artifact. (B) Survival of W3110AΔHCtG and W3110AΔHEc at 37°C after streaking on LB agar supplemented with ampicillin and chloramphenicol. In the right panel, growth medium has been additionally supplemented with 0.02 % (w/v) arabinose to stimulate expression of the pBAD33-derived plasmid harbored by both W3110AΔHCtG and W3110AΔHEc.

4.3.7 Expression of Ct461 Corresponds to Enhanced Lipid X Production *In Vitro*

After establishing the ability of Ct461 to function as a UDP-DAGn hydrolase *in vivo*, we sought to assess the *in vitro* activity of the ORF. Ct461 was cloned into an expression vector, which generated a C-terminal His-tag on the protein product. This vector, p461t, was transformed into C41(DE3) to produce CtG_t10. Cell free extracts (CFE) were prepared from CtG_H10 grown in the presence of IPTG (denoted Ct461 CFE) and then tested for lipid X production using an autoradiographic TLC-based assay. Over the tested time course, Ct461 CFE produced more product than equal amounts of

CFE prepared from vector control strain VC_t10 (Fig. 31A). This corresponded a specific activity of 47.0 nmol/mg/mL for Ct461 CFE versus 0.9 nmol/mg/mL for VC CFE (Fig. 31B). Futhermore, the species generated in Ct461 reactions migrated the same as that created by HiLpxH (157), confirming its identity as lipid X.

To ensure the observed hydrolysis was unambiguously due to the enzymatic activity, an alanine point mutation was constructed in a highly conserved aspartate residue, D59, of Ct461. Based on Ct461's homology to calcineurin-like phosphoesterases, this residue is hypothesized to play an important role in protein catalysis (see Chapter 5 for further discussion). CFE samples from C41(DE3) cells expressing this mutant protein (D59A CFE) displayed similar levels of UDP-DAGn hydrolysis as that seen for VC_t10 samples, with a specific activity of 1.3 nmol/mg/mL (Fig. 31).

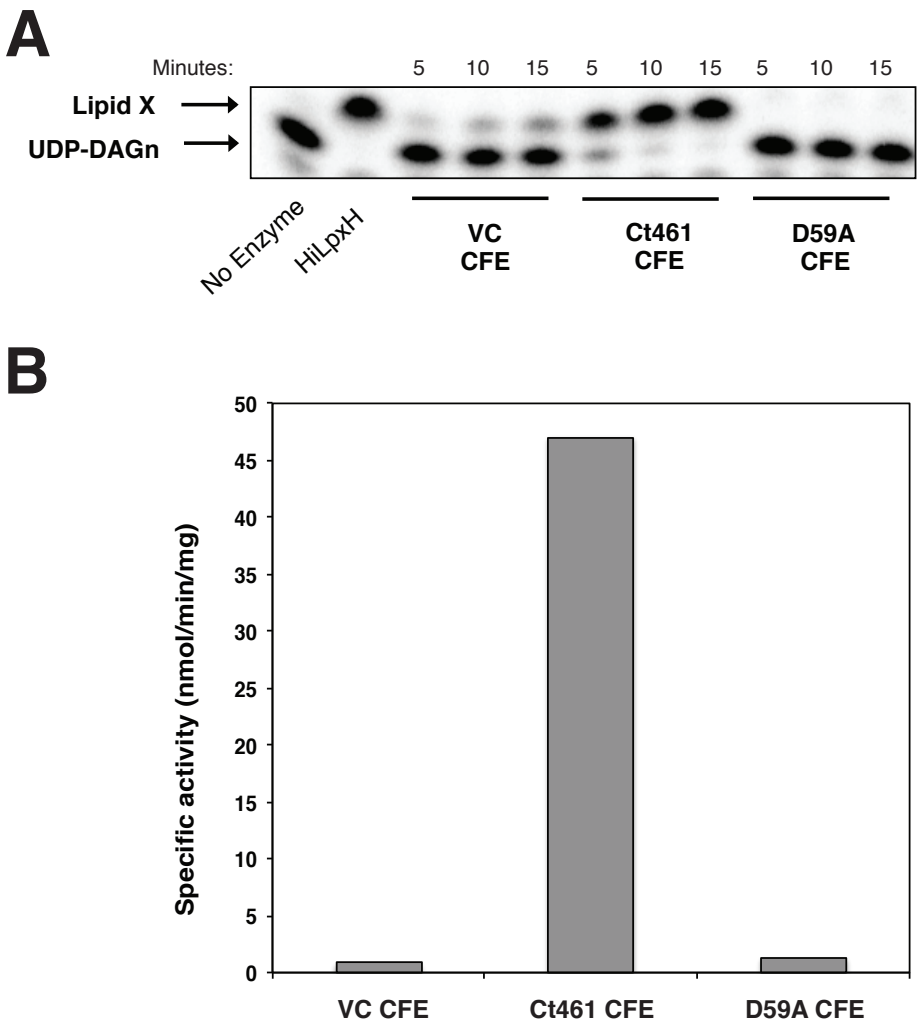

Figure 31: Expression of Ct461 Enhances UDP-DAGn Hydrolysis *In vitro*

(A) Scan of phosphoscreen exposed to a silca TLC plate from an assay of cell-free extracts (CFE) prepared from VC_t10 (VC CFE), CtG_t10 (Ct461 CFE), and D59A_t10. Protein concentration in each reaction was ~1 mg/mL. Reactions lacking protein sample (No enzyme) and containing purified LpxH (HiLpxH) were included as negative and positive controls, respectively. Bands corresponding to UDP-DAGn substrate and lipid X product are denoted. (B) Comparison of the specific UDP-DAGn hydrolase activity for the samples described in (A). Values determined for individual samples are 0.9 nmol/mg/mL, 47.0 nmol/mg/mL, and 1.3 nmol/mg/mL for VC CFE, Ct461 CFE, and D59A CFE, respectively, and were calculated from autoradiographic assay data as previously described.

4.4 Discussion

Lipid A is a crucial part of the outer membrane of numerous Gram-negative bacteria (6,7). For many bacteria, its biosynthesis is necessary for survival, making the enzymes of the lipid A metabolic pathway potential antibiotic targets (6,7). In other bacteria, lipid A is not essential, but nonetheless plays an imperative role in the development of the organism. For example, in the pathogen *C. trachomatis,* inhibition of lipid A synthesis by targeting LpxC correlates with inability of the bacteria to differentiate from the RB state back into the infectious EB state (20). While the generation of the saccharolipid is of obvious importance, the pathway of lipid A biosynthesis in *C. trachomatis* was not completely understood. Lipid A of *C. trachomatis* is very similar to that *E. coli* (153), and unsurprisingly, the two bacteria share orthologs for nearly all of the biosynthetic enzymes. The once missing piece was an enzyme capable of the fourth step, UDP-DAGn hydrolysis. Thus we sought to identify the gene responsible for this function in *C. trachomatis* through implementation of a complementation screen in *E. coli.*

4.4.1 UDP-DAGn Hydrolase Activity in *C. trachomatis* Lysates Confirms Existence of Functionality

Despite the lack of a UDP-DAGn hydrolase homolog, *C. trachomatis* was hypothesized to contain an enzyme capable of the production of lipid X. Using a slightly modified version of our previously described autoradiographic assay (157), we were able to demonstrate linear, metal-dependent UDP-DAGn hydrolase activity in

lysates of HeLa cells infected with *C. trachomatis;* this activity was not present in lysates of HeLa cells alone. While lipid X production was evident, it was at a very low level. This may be due to only a small amount of *C. trachomatis* protein being present in the assayed sample compared to HeLa protein, as samples were prepared directly from infected cultures. Furthermore, it is possible that not all of the *C. trachomatis* in the sample were expressing protein capable of UDP-DAGn hydrolase activity. Specifically, as cultures were harvested 30 h post infection when RBs were asynchronously differentiating back into EBs (109), bacteria of both stages were present in the sample. Since LpxC inhibitors did not alter replication of RBs and EBs are not capable of duplication (20), the lipid A biosynthetic pathway may only be active in *C. trachomatis* when RBs are transitioning to EBs, effectively limiting the possibility of seeing UDP-DAGn hydrolase in our sample.

Overall, while detecting UDP-DAGn hydrolase activity in *C. trachomatis* lysates indicates *in vitro* evidence of functionality, it also highlights the limitations with studying this functionality in *C. trachomatis* directly. Activity is very low, making it difficult to assess any significant changes in lipid X production due to over-expression of certain genes. Moreover, over-expression of such genes would be tedious, as this technology has only been recently developed in *C. trachomatis* and is still not well understood (120).

4.4.2 Novelty of UDP-DAGn Hydrolase Identification Method is Advantageous for Functional Screening of *C. trachomatis* Genes

Having *in vitro* evidence of lipid X production in *C. trachomatis,* it was especially pertinent to search for a *C. trachomatis* gene encoding for UDP-DAGn hydrolase function. Limitations of genetic tools in *C. trachomatis* made it necessary to employ heterologous expression in *E. coli.* As UDP-DAGn hydrolysis is essential in *E. coli,* functionality of *C. trachomatis* genes could be easily assessed through their ability to rescue viability of an *lpxH* mutant. This strategy relied on generation of HY1, a conditional-lethal Δ*lpxH* strain with a temperature-controlled rescuing copy of *lpxH.* It was additionally necessary to create a library of *C. trachomatis* DNA. With use of Gateway® technology, we engineered an existing ORFeome library (158) for controlled expression in *E. coli.* Together, HY1 and the pDEST-library were effectively used to identify a *C. trachomatis* ORF capable of UDP-DAGn hydrolysis.

The overall strategy of employing *E. coli* to screen for functionality of *C. trachomatis* genes has been previously reported for identifying enzymes involved in meso-diaminopeimelic acid (m-DAP) synthesis (115), which is important for peptidoglycan assembly and lysine production. Like with lipid A, the m-DAP pathway was well characterized in *E. coli,* but orthologous genes for some enzymatic steps were missing was missing in Chlamydiales. Investigators generated a *C. trachomatis* genetic library through restriction digestion of genomic DNA to test for complementation of an *E. coli* m-DAP auxotroph, and were able to identify a candidate ORF that was confirmed

to play a unique role in m-DAP biosynthesis through subsequent biochemical experiments. Additionally, this strategy has been employed for identification of S-adenosylmethionine (SAM) transporters in *C. trachomatis* (116). Once again, *C. trachomatis* lacked genes homologous to previously characterized transporters despite showing evidence of SAM-dependent methylation reactions. As this transport functionality, encoded by *metK,* is essential in *E. coli,* a conditional-lethal Δ*metK* strain had to be created for complementation screening. Investigators used an *ara*-promoter to facilitate tight control of the rescuing copy of *metK,* thus allowing for hits to be identified by plating on glucose.

While generally similar to the aforementioned methods, the UDP-DAGn hydrolase screening method has novel aspects. First, the UDP-DAGn hydrolase screen employed a temperature-sensitive replicon to control the conditional-lethal Δ*lpxH* strain instead of an *ara* promoter (115). Use of an *ara*-promoter was investigated, however complete shut-down of *lpxH* expression was not achievable, as colonies were still capable of survival even when fucose was present in the media. This problem of leaky expression of essential genes from the *ara* was also described for the SAM transport experiments and was eventually circumvented by mutation of the *metK* start codon (115). Our alternative use of temperature as a regulator provided a straightforward method for controlling gene expression that did not rely on additional agents being supplemented to the media.

Second, the pDEST-library provided for a thorough, expression-optimized screen of the *C. trachomatis* ORFeome that would not be possible with a library created by restriction digestion of genomic DNA. The UDP-DAGn hydrolase screen library contained a clone of every individual ORF in *C. trachomatis,* whereas the aforementioned library screens utilized a pUC18-harbored library created by restriction digestion (115,116), meaning some library plasmids contained partial ORFs. Isolating each ORF separately prevents the possibility of false negatives due to partial gene products. Additionally, the pDEST-library was harbored in a plasmid containing a ribosome-binding site specific for expression in *E. coli.* This is an advantage over restriction-created libraries in which expression is contingent on the native promoter of the DNA sequence, which may not be read efficiently in *E. coli.* Finally, expression of the pDEST-library was controllable, as T7-dependent expression could be upregulated through addition of IPTG or left at low levels in the absence of inducer. Such control was not an option with the pUC-based library previously described (115,116).

A third unique aspect of the UDP-DAGn hydrolase screen was the method used to validate hits. The temperature-controlled replicon, while more efficient than use of the *ara* promoter, still allowed survival of HY1 at low frequency. As it was necessary to screen 20,000 colonies to ensure adequate coverage of the library, even this slight background was visible. Thus, it was necessary to discern which surviving HY1_Lib colonies were actual hits with specific UDP-DAGn hydrolase complementation and

which simply had residual temperature resistance. PCR with T7 primers provided an effective and time-efficient method for assessing *C. trachomatis* ORFs harbored viable colonies; it allowed for determination of the variety of ORFs present, making it possible eliminate those occurring at a low frequency.

It should be noted that a more direct approach at the library screen was attempted using P1 transduction. In this scheme, C41(DE3) harboring pDEST_CtLib would be infected with P1 phage carrying *lpxH::kan*. Resulting colonies capable of growth on kanamycin would be assumed to have an *lpxH* deletion, and their ability to survive could be attributed to the presence of a CtORF library plasmid capable of LpxH function. Unfortunately this strategy proved to be ineffective. A small population of C41(DE3) library transformants were noted to be kanamycin resistant, presumably due to the presence of unreacted pDONR_CtLib in the Gateway® reaction product. This contaminating resistance made it impossible to use kanamycin to screen for *lpxH* knock-outs, as described for the P1 strategy. Substitution of a restriction-enzyme generated library would have circumvent the issues caused by the incompleteness of the Gateway® reaction. However, as discussed above, there were many advantages to employing the pDEST library with each individual ORF under controllable expression. Thus we chose to employ the temperature-controlled strategy that accommodated for use of the optimized library.

4.4.3 Classification of Ct461 as UDP-DAGn Hydrolase is Supported by *In Vivo* and *In Vitro* Evidence

With use of HY1 and the pDEST-harbored library, we identified Ct461 as a likely candidate for the *C. trachomatis* UDP-DAGn hydrolase. The significant enrichment of the 1100 bp insert corresponding to Ct461 in temperature resistant HY1_Lib colonies indicates its specific complementation of *lpxH.* Sequencing of other PCR-amplified inserts of various sizes revealed a range of ORFs, most of which correspond to hypothetical proteins (Table 13). While some appear multiple times, their frequency is much less than seen for Ct461. Moreover, even the ORF insert occurring at the second highest frequency, Ct733, was not able to complement HY1 temperature sensitivity independently. Together, this suggests that the low-frequency ORFs identified in the screen were capable of survival due to mutations in the temperature sensitive replicon of the pKJB5 plasmid and not complementation events. Those occurring multiple times are most likely clones of the same surviving HY_lib colony and do not reveal independent occurrence of survival.

Besides the high frequency occurrence of Ct461 in the library screen, it shows other evidence of UDP-DAGn hydrolase function. When tested independently for temperature rescue of HY1, the ORF-harboring strain displayed robust survival both on plates and in liquid culture. This complementation was not temperature dependent, as the presence of the gene allowed for generation of an *lpxH* knock-out in *E. coli* W3110 using P1 *vir* transduction. The phenotype of complementation of *lpxH* in *E. coli* was also

observed with *lpxI,* thus corroborating it as a metric by which to discern UDP-DAGn hydrolase activity. Complementation has also proved effective in discerning non-specific hydrolases from biologically relevant ones, as Cdh, a protein shown to hydrolyze UDP-DAGn *in vitro,* cannot complement *lpxH in vivo* (40,82,89,91,92). Furthermore, as discussed above, the function of other *C. trachomatis* genes have been characterized by their ability to rescue mutants of orthologous *E. coli* genes. Currently, there is no method for gene knock-outs available in *C. trachomatis,* making complementation tests in a heterologous system one of the only available methods for determining gene function.

Use of the established assay for UDP-DAGn hydrolase activity provided for a method by which to assess the function of Ct461 *in vitro.* *E. coli* induced for over-expression of Ct461 clearly indicate an enhancement in lipid X production. This increase is not as significant as that seen when LpxH or LpxI is over-expressed, however the difference can be attributed to inefficient expression of Ct461, as protein production is not visible by SDS-PAGE (data not shown). The enriched *in vitro* activity is not detected when Ct461 with a mutation in a likely catalytic residue is over-expressed, providing further evidence that increased *in vitro* lipid X production observed in the cell-free extract can be credited to Ct461 activity.

Table 12: Sequencing Results of *C. trachomatis* UDP-DAGn Hydrolase Screen

Band Size (bp)	ORF	Encoded protein	# Occurrences	% Frequency
550	848	Hypothetical protein	1	2
600	814	Pututive membrane protein	1	2
600	255	Hypothetical protein	1	2
900	611	Hypothetical protein	1	2
900	383	Hypothetical protein	1	2
900	130	ABC amino acid transporter ATPase, GlnQ	1	2
1000	720	NifU	1	2
1000	583	Gp6D	2	5
1100	851	Methionine aminopeptidase	1	2
1100	461	Metallophosphoesterase	16	39
1100	406	Hypothetical protein	1	2
1100	451	Phophatidate cytidylyltransferase	1	2
1400	776	8-amino-7-oxonanoate synthetase, BioF	1	2
1500	733	Membrane protein	9	22
1500	132	Hypothetical protein	2	5
1600	197	Oligopeptide binding protein, oppA_3	1	2
		Total sequenced:	41	

4.4.4 Ct461 is a Unique Membrane-Associated CLP enzyme

Sequence analysis revealed Ct461 encodes for a 37 kD uncharacterized metallophosphoesterase. The protein is categorized to be part of the calcineurin-like phosphoesterase (CLP) superfamily (Pfam00149), which utilizes divalent cations for hydrolysis of phosphoester bonds (103,105). The observation of EDTA-inhibition of lipid X production in *C. trachomatis* lysates supports the classification of the bacteria's UDP-DAGn hydrolase as a metalloenzyme. The sequence of Ct461 has no similarity to that of LpxI orthologs (Table 13). The classification of Ct461 as a CLP places it in the same superfamily as LpxH, however Ct461 contains the more common "GNHD" family motif in contrast to the LpxH-specific "GNRD" sequence. Besides the common CLP family motif, Ct461 and LpxH show very limited sequence identity (Table 13) (see Chapter 5 for additional discussion).

Table 13: Alignment Statistics of Ct461 vs. LpxH and LpxI

Name	% Query Coverage	E-value	% Identity (Clustal W)
Ct461	100	0	100
LpxH	21	0.8	11
LpxI	2	3.5	9

Homologs of Ct461 are found across other *Chlamydia* species (see Chapter 5). Alignment reveals the clear presence of the CLP motif: DXH(X)$_{\sim 25}$GDXXDR(X)$_{\sim 25}$GNHD/E (where X is any residue). The residues of this motif have been shown to be the main contributors to catalysis in CLP enzymes, playing important roles in metal and water coordination (103,106). Studies of other enzymes of this type indicate the first aspartate residue of the motif coordinates one of the metal cofactors (150), thus mutations in this residue severely inhibit activity (103,106). As discussed above, a mutation in the corresponding aspartate in Ct461 (D59), nearly abolished observed activity in cell lysates. Not only does this mutation provide evidence that detected hydrolase activity can be attributed to Ct461, but it also suggests that Ct461 is performing catalysis in a way similar to other CLP enzymes.

Hydropathy analysis of Ct461 predicts an N-terminal transmembrane domain. During construction of the pDONR *C. trachomatis* library from which our pDEST library was generated, this region of the ORF was truncated to circumvent any issues with expression (158). Interestingly, even with the missing transmembrane portion, pDEST_461 was capable of *lpxH* complementation. It is likely the truncated Ct461 was still able to produce lipid X, as the residues comprising the CLP motif are not predicted to be part of this domain. Furthermore, as EcLpxH has no predicted transmembrane structure, a non-membrane bound Ct461 was still able to interact with the other proteins in the *E. coli* lipid A biosynthetic pathway. It should be noted that full-length Ct461 was

also able to complement *lpxH,* indicating that the *E. coli* pathway could also accommodate for full membrane association at the fourth step. This highlights the flexible and modular nature of lipid A biosynthesis.

4.4.5 Conclusion

With evidence from *in vivo* complementation and *in vitro* lipid X production, we conclude that Ct461 encodes for a specific UDP-DAGn hydrolase in *C. trachomatis.* This protein, which will be henceforth referred to as LpxG, completes the puzzle of lipid A biosynthesis in *C. trachomatis* and arms us with information to make more definitive conclusions about the role the molecule plays in the physiology of this bacteria. Further biochemical and genetic characterization of LpxH is described in the following chapter.

While the discovery of LpxG is an important result of our work, an equally important outcome was the development of a strategy to screen for functionality of uncharacterized *C. trachomatis* genes using *E. coli.* The lack of genetic tools in *C. trachomatis* paired with its distant evolutionary relationship to well-characterized organisms like *E. coli* have left many mysteries surrounding the functional identification of genes in the organism. Despite their phylogenetic differences, the molecular structures of the products of metabolic pathways in *E. coli* and *C. trachomatis* are similar, making it possible to use the former as a heterologous expression system of the latter (115,116,160).

Our screening strategy that involves a genomic library with each ORF on a separate plasmid and is optimized for controlled expression in *E. coli* could prove an efficient method for further characterization of *C. trachomatis* genes. Use of this library also allows for simple assessment of hit ORFs through visualization of T7-amplified PCR products. Finally, for investigations of functions which are essential in *E. coli*, temperature controlled conditional-lethal strains could be utilized for straightforward modulation of gene expression. Together, these attributes of the UDP-DAGn hydrolase screen make it an advantageous method for further application in the characterization of *C. trachomatis* gene products of unknown function.

5. Initial Biochemical Characterization of LpxG, a Third UDP-2,3-Diacylglucosamine Hydrolase

5.1 Introduction

The identity of the lipid A molecule residing in the outer leaflet of the outer membrane can differ greatly among Gram-negative bacteria due to the presence of species-specific modification enzymes that make changes to the structure of lipid A after it is synthesized (6,20). This results in an outer membrane optimized for the bacteria's niche environment (6,29). Despite the variation in the modification enzymes across Gram-negative bacteria, the proteins responsible for constructing nascent lipid A are highly conserved. Specifically, orthologs for LpxA, LpxC, LpxD, and LpxB, which catalyze the first, second, third, and fifth steps of the pathway, respectively, are in nearly all Gram-negative bacteria known to produce lipid A (81).

The conservation of aforementioned steps is reflected in the preserved disaccharide structure of the lipid A. LpxA (95,161), LpxC (38,162), and LpxD (39) work in sequence to transform the initial UDP N-acetylglucosamine into a di-acylated sugar nucleotide, UDP-2,3-diacylglucosamine (UDP-DAGn). This molecule serves as one substrate for glycosyl transferase, LpxB (90,127). The second substrate for LpxB, 2,3-diacylglucosamine 1-phosphate (lipid X), is formed from the hydrolysis of the pyrophosphate bond in UDP-DAGn. The joining of lipid X and UDP-DAGn forms disaccharide 2'3'-diacylglucosamine-(1'6)-2,3-diacylglucosamine 1-phosphate (also

known as disaccharide monophosphate, or DSMP), thus yielding the structure for the canonical conjugated carbohydrate backbone of lipid A (6).

Based on the current understanding of LpxB mechanism, the only way for production of a disaccharide linkage is through use of a lipid X substrate (90,127). No known LpxB ortholog is thought to be capable of joining UDP-DAGn molecules. Therefore, the hydrolysis of UDP-DAGn to form lipid X is an important chemical step in the lipid A pathway. Interestingly, the enzyme that catalyzes this hydrolysis is not conserved throughout Gram-negative bacteria (6,81). Some bacteria, namely the β, γ, and ε subsets of proteobacteria, utilize LpxH for the formation of lipid X (40). Other bacteria, such as α proteobacteria, have LpxI orthologs that are responsible for hydrolyzing UDP-DAGn (41). Finally, some bacteria known to produce lipid A contain neither LpxH nor LpxI, suggesting the possibility for a third protein capable of producing lipid X (see Chapter 4).

Due to their shared enzymatic ability, LpxH and LpxI can be classified as functional orthologs (41). *LpxI* can complement a knock-out of *lpxH* in *E. coli*, indicating that the LpxI can work synergistically with lipid A biosynthetic enzymes from an LpxH-containing species (41). Furthermore, both enzymes have been shown to co-purify with their product, lipid X (96) (Young and Raetz; unpublished data), suggesting a similar mechanism of delayed product release. In the *in vitro* environment, LpxH and LpxI

show similar pH rate profiles (41,157) and neither appear to obey surface dilution kinetics (discussed further in Chapter 2).

While similarities between LpxH and LpxI exist, there are also many differences. The two proteins have no shared sequence homology: LpxH belongs to a well-characterized family of calcineurin-like phosphoesterase (CLP) enzymes (40,157) while LpxI display unique motifs that are not found in other protein families (41). LpxH catalyzes hydrolysis through the addition of a water molecule on the α-phosphate of UDP-DAGn (40) while LpxI attacks the β-phosphate (41). Both enzymes are thought to have some interaction with the inner membrane, however LpxI appears to be much less hydrophobic than LpxH based on cell lysate fractionation (41,157). Finally, while both enzymes are activated by metal ions, LpxH shows a very strong dependence on Mn^{2+} for catalysis (157) whereas LpxI prefers Mg^{2+} and is activated by a lesser extent (41).

We have recently identified a third enzyme capable of UDP-DAGn hydrolysis in *C. trachomatis,* LpxG (see Chapter 4). LpxG expression can complement a knock-out of *lpxH* in *E. coli* and corresponds with an increase in UDP-DAGn hydrolysis activity as determined by autoradiographic assay, thus classifying LpxG as a functional ortholog of LpxH and LpxI. In order to better understand how the enzymatic properties of this newly identified protein compare to its operative counterparts, we carried out initial purification and biochemical characterization of *C. trachomatis* LpxG (CtLpxG). We report the use of mass spectrometry to assess the enzyme's mechanism of hydrolytic

attack. Based its homology to CLP metalloenzymes, we investigated the metal dependence of CtLpxG and found Mn^{2+} stimulates enzyme activity 35-fold. Additionally, we provide initial evidence that CtLpxG behaves like a CLP enzyme, as a point mutation in the conserved metallophosphoesterase motif abrogates activity. Finally, we compare the ability of CtLpxG, EcLpxH, and CcLpxI to perform UDP-DAGn hydrolysis *in vivo* with heterologous expression in an *lpxH* knock-out of *E. coli*. Overall, this work provides a foundation for more detailed enzymatic characterization of LpxG and allows for initial comparison of the new hydrolase to its known functional orthologs, LpxH and LpxI. Continued work aimed at fully understanding the enzymatic and evolutionary relationships among LpxG, LpxH, and LpxI would provide important insight into the variation of the lipid A pathway. Additionally, these three enzymes could serve as a model system for the study of functional orthologs.

5.2 Materials and Methods

5.2.1 Chemicals and Reagents

The 4-(2-hydroxyethyl)-1 piperazineethanesulfonic acid (HEPES), phosphate-buffered saline (PBS) components, HCl, salts, ampicillin, isopropyl-β-D-thiogalactoside (IPTG), fatty acid-free bovine serum albumin (BSA), Triton X-100 (TX-100) ethylenediaminetetraacetic acid (EDTA), and dithiothreitol (DTT) were purchased from Sigma-Aldrich (St. Louis, MO). Methanol, chloroform, pyridine, and acetic acid were obtained from EMD Science (Gibbstown, NJ). Radioactive γ-^{32}Pi was purchased from

PerkinElmer (Waltham, MA). Unless otherwise noted, protein concentration was determined either by BCA Assay or Bradford Assay (Thermo Scientific, Waltham, Massachusetts) depending on compatibility with buffer components. Both of these methods were carried out as described by the manufacturer.

5.2.1 Bacterial Strains and Growth Conditions

The bacterial strains used in this study are listed in Table 14. Growth medium for liquid culture was Luria broth (LB), containing 5 g/L yeast extract, 10 g/L tryptone, and 10 g/L NaCl. LB supplemented with 7.5 g/L of bacto agar was used for solid phase growth. All media components were purchased from Difco (Detroit, MI). Antibiotics were used at the following concentrations: 100 μg/mL ampicillin (Amp), 50 μg/mL kanamycin (Kan), 25 μg/mL chloramphenicol (Cam).

Table 14: Strains Used in the Characterization of LpxG

Strain	Description	Source or Reference
C41	*E. coli*, F− ompThsdsB(rB−mB−) gal dcm (DE3) Δ(srl-recA)306::Tn10	(125)
CtG_t10	C41 harboring p461T	Chap. 4
D125A_t10	C41 harboring pD125AT	Chap. 4
W3110A	*E. coli*, F- aroA::Tn10 msbA+ , TetR	(155)
W3110AΔHEc	W3110A *lpxH::kan* harboring pBAD33Ec	(41)
W3110AΔHCc	W3110A *lpxH::kan* harboring pBAD33Cc	(41)
W3110AΔHCtG	W3110A *lpxH::kan* harboring pBAD33461	Chap. 4

5.2.2 CtLpxG Expression and Purification

A typical prep of CtLpxG began with inoculating an overnight culture of LB with a single colony of CtG_t10 (created as described in Chapter 4). This overnight culture was subsequently used to inoculate 250 mL of LB supplemented with ampicillin to an OD_{600} of 0.02. Cultures were incubated at 30 °C with aeration at 220 rpm until they reached OD_{600} of 0.7-0.8, then induced for expression by the addition of 1 mM IPTG and grown for an additional 4 to 5 h until they OD_{600} reached ~4. Cells from the growths were pelleted by centrifugation at 5,000 × *g*, washed with 35 mL of cold PBS, and then stored at -80 °C. For lysis, the frozen pellet was thawed, resuspended in 25 mL of ice-cold 20 mM HEPES pH 8.0, and passed twice through a French pressure cell (SIM-AMINCO; Spectronic Instruments) at 18,000 psi. The debris from the resulting lysate was removed by centrifugation at 10,000 × *g* and the subsequent supernatant was collected as cell-free extract (CFE) and stored at -80 °C.

Cell-free extract was thawed and diluted to 5 mg/mL with 20 mM HEPES pH 8.0. A stock solution of 20% (w/v) n-dodecyl-β-D-maltoside (DDM, Avanti Polar Lipids, Alabaster, AL), was used to bring the cell-free extract to a final detergent concentration of 1% (w/v). Additional stock solutions were added to the sample to obtain NaCl and glycerol concentrations of 300 mM and 10% (v/v), respectively. All subsequent steps were carried out at 4 °C. The resulting solution was then mixed by inversion for 1 h and then subjected to ultracentrifugation at 100,000 × *g* for 45 min. The supernatant was

removed and diluted with the appropriate stocks to make a 25 mL solution of ~5 mg/mL protein, 20 mM HEPES pH 8.0, 300 mM NaCl, 10% glycerol, and 20 mM imidazole. This solution was loaded by gravity onto a packed column of 1 mL of Ni-NTA resin (Qiagen) that had been pre-equilibrated in 20 column volumes of load buffer (20 mM HEPES pH 8.0, 300 mM NaCl, 10% glycerol, 20 mM imidazole, 0.01% DDM). The loaded column was next washed with an additional 10 column volumes of load buffer followed by a 20 column volume wash with load buffer supplemented with 30 mM imidazole (final imidazole concentration of 50 mM). Elution of the protein was accomplished by five separate 1 column volume washes with a solution of 20 mM HEPES pH 8.0, 300 mM NaCl, 10% glycerol, 0.01% DDM, and 300 mM imidazole. Each wash was collected in a separate tube. Elution fractions were subjected to SDS-PAGE analysis and the two containing the majority of the protein (usually second and third elutions) were pooled to obtain a final sample of CtLpxG, referred to below as LpxG. This sample ranged in concentration from 0.15-0.5 mg/mL and was kept in a buffer of 20 mM HEPES pH 8.0, 300 mM NaCl, 10% glycerol, 0.01% DDM, and 300 mM imidazole.

Expression and purification of CtLpxG mutant D59A were carried out according to the same procedure described above, except D59A_t10 (created as described in Chapter 4) was used in place of CtG_10. Resulting purified protein was termed D59A.

5.2.3 CtLpxG Activity Analysis

. Autoradiographic assays for hydrolase activity were similar to that previously described in Chapter 2, but with slight modification. Reactions mixtures were a final volume of 12.5 μL in 0.6 mL polypropylene tubes and contained 20 mM HEPES pH 8.0, 0.5% (w/v) BSA, 0.035% (w/v) DDM, 1 mM $MnCl_2$, 100 μM UDP-DAGn (prepared as previously described (127), 1,000 cpm/μL [β-^{32}P] UDP-DAGn, and protein sample. All reaction components besides the enzyme were mixed to a volume of 10 μL and equilibrated at 30 °C for 10 min, after which 2.5 μL of enzyme was added to start the reaction. If necessary, enzyme samples were diluted in a buffer identical to the assay mixture but lacking any lipid substrate or DDM before addition to reaction mixtures. Aliquots of 1.5 μL were taken from the reactions at various time intervals and spotted onto 20 cm × 20 cm glass-backed silica gel thin layer chromatography (TLC) plates (EMD Chemicals, Darmstadt, Germany). These plates were developed in a 25:15:4:2 chloroform: methanol: water: acetic acid tank system, dried, exposed to phosphoscreens, scanned, and quantified as previously described in Chapter 2.

5.2.4 Metal Dependence of CtLpxG

To analyze the metal dependence of CtLpxG, a modified autoradiographic assay described aboce was employed. First, a concentrated stock of EDTA was added to a sample of LpxG to obtain a final chelator concentration of 50 μM EDTA; the protein was then incubated on ice for 30 min. Next the sample was diluted 10-fold into various

reaction mixtures similar to those described above except that 1 mM $MnCl_2$ was replaced by no di- or trivalent metal ion, 2 mM NaCl, or each of the following chloride salts at 1 mM: Ca^{2+}, Co^{2+}, Cu^{2+}, Fe^{3+}, Mg^{2+}, Mn^{2+}, Ni^{2+}, and Zn^{2+}. Conditions in which the replacing component was 2 mM NaCl or 1 mM EDTA were also included as controls.

5.2.5 Mass Spectrometry Analysis of LpxG Reaction

The products of an LpxG reaction were analyzed by mass spectrometry, employing a similar method as used for analysis of LpxI (41). Briefly, 50 μL reaction mixtures consisting of 100 μM UDP-DAGn, 1 mM $MnCl_2$, 20 mM HEPES (pH 8.0), and 0.06 mg/mL of LpxG were prepared in the presence of either 100% $H_2{}^{16}O$ or an $H_2{}^{18}O/H_2{}^{16}O$ mixture (70:30, v/v) (Sigma-Aldrich, St. Louis MO). After incubation for 2 h at 30°C, the reactions were quenched by conversion to a 1.9 mL single-phase, acidic Bligh-Dyer system (126). A 10 μL aliquot of this material was analyzed by reverse-phase liquid chromatography and mass spectrometry (LC/MS) using a Shimadzu LC system (comprising a solvent degasser, two LC-10A pumps, and a SCL-10A system controller) coupled to a TripleTOF 5600 quadrupole time-of-flight tandem mass spectrometer (AB SCIEX, Framingham, MA). MS instrumental settings for negative ion ESI and MS/MS analysis of lipid species were as follows: ion spray voltage (IS) = -4500 V; current gas (CUR) = 20 psi (pressure); gas-1 (GS1) = 20 psi; declustering potential (DP) = -55 V; and focusing potential (FP) = -150 V. The MS/MS analysis used nitrogen as the collision gas. Data analysis was performed using the Analyst TF1.5 Software. LC was operated at a

flow rate of 200 μl/min with a linear gradient as follows: 100% of mobile phase A was held isocratically for 2 min, and then linearly increased to 100% mobile phase B over 14 min, and held at 100% B for 4 min. Mobile phase A consisted of methanol/acetonitrile/aqueous 1 mM ammonium acetate (60/20/20, v/v/v). Mobile phase B consisted of 100% ethanol containing 1 mM ammonium acetate. A Zorbax SB-C8 reversed-phase column (5 μm, 2.1 × 50 mm) was obtained from Agilent.

5.2.6 Qualitative Comparison of UDP-DAGn Hydrolase Complementation

To qualitatively assess the ability of Ct461 to complement an *lpxH* deletion in *E. coli* compared to the other known UDP-DAGn hydrolases, single colonies of W3110AΔHEc (41), W3110AΔHCc (41), and W3110AΔHCtG (see Chapter 4) were dissolved in 8 uL of LB. From this sample, 2 μL aliquots were taken from each strain and spotted on LB-agar plates supplemented with Cam, Kan, and 0.02% arabinose or Cam and Kan. Spots were spread over a portion of the plate to evenly distribute bacteria. Following incubation at 37°C for 24 h, plates were compared for growth.

5.3 Results

5.3.1 Purification of CtLpxG

In order to further characterize LpxG, a tagged construct of the protein was purified using NiNTA chromatography. Ct*lpxG* was cloned into a pET21 vector that encoded for a TEV-protease-cleavable histidine tag at the C-terminus of the protein. This construct was transformed into C41(DE3) to generate CtG_H10. Cell free extracts

(CFE) from CtG_H10 grown in the presence of IPTG were incubated with 1% DDM to solubilize over-expressed CtLpxG from the membrane. After centrifugation to remove any insoluble components, the resulting supernatant was loaded onto a NiNTA column ("Load" Fig. 32A). An initial low imidazole wash was used to remove non-specific species from the resin ("Wash" Fig. 32A) and subsequent elution with accomplished with high imidazole ("Elute" Fig. 32A). As evident by SDS-PAGE analysis, this sample was primarily comprised of a 37 kD species, which corresponds to the molecular weight of CtLpxG. The resulting LpxG sample (pool of Elute 2 and 3, Fig. 32A), was assayed for UDP-DAGn hydrolysis and showed time-dependent formation lipid X. UDP-DAGn hydrolysis ("LpxG" Fig. 33).

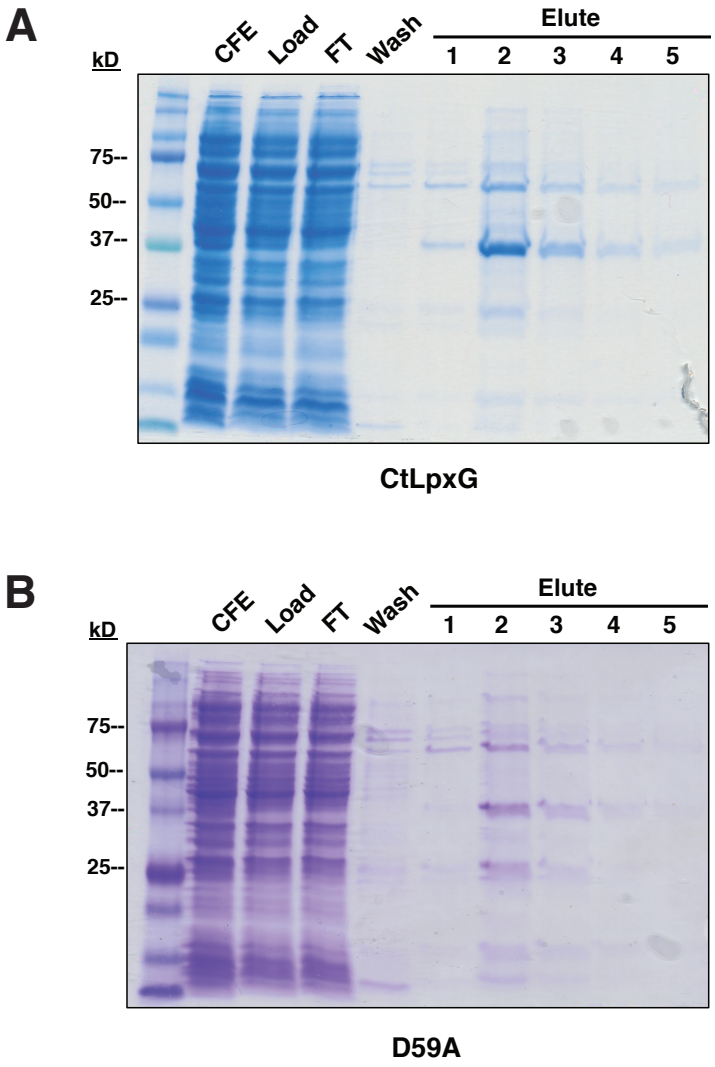

Figure 32: Gel Purification of LpxG

(A) SDS-PAGE analysis of samples from purification of CtLpxG as outlined in Materials and Methods. Fractions include cell-free extract (CFE) of CtG_t10; CFE after detergent solubilization, which was loaded onto the NiNTA colum (Load); flow through of the column load (FT); wash with 50 mM imidazole (Wash); and elution with 300 mM imidazole (Elute), which was carried out in five separate 1 mL fractions and labeled correspondingly. The band appearing around 37 kD corresponds to partially purified CtLpxG. Elute fractions 2 and 3 were pooled to obtain the LpxG sample used in further analysis. (B) Identical purification as described above, except beginning with cell-free extract from D59A_t10. Elute fractions 2 and 3 were pooled to yield final D59A sample employed in later experiments.

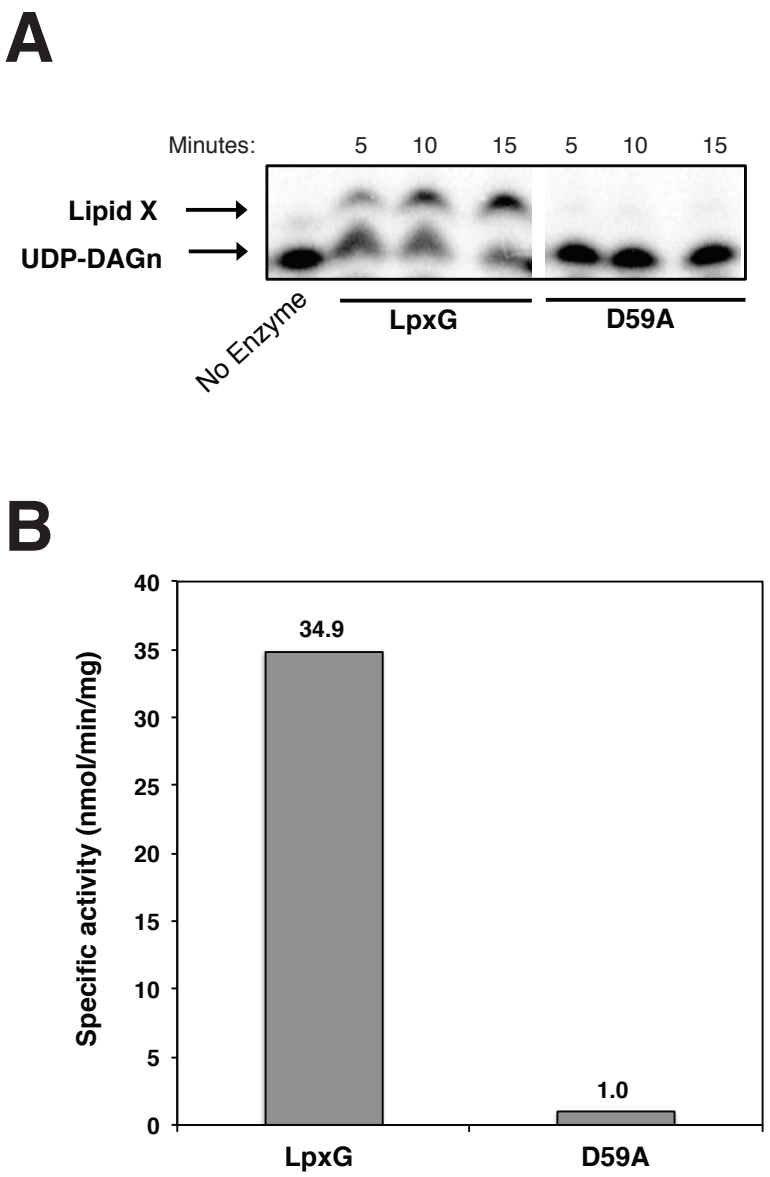

Figure 33: Activity Analysis of Purified LpxG

(A) Scan of phosphoscreen exposed to silca TLC plate from an assay of LpxG and D59A isolated from NiNTA purification. Protein concentration in each reaction was ~0.05 mg/mL. Reaction lacking protein sample (No enzyme) was included as a negative control. Bands corresponding to UDP-DAGn substrate and lipid X product are denoted with arrows. (B) Comparison of the specific UDP-DAGn hydrolase activity for the samples described in (A). The determined value for LpxG was 47.0 nmol/min/mg and for D59A, 1.3 nmol/min/mg, both of which were calculated from autoradiographic assay data as previously described.

5.3.2 Determination of LpxG Hydrolytic Attack Mechanism by Mass Spectrometry

While the other known UDP-DAGn hydrolases both catalyze the formation of lipid X, they do so through different methods: LpxH attacks the α phosphate of the substrate (40) whereas LpxI attacks at the β position (41). To confirm which hydrolytic mechanism LpxG employs, purified enzyme was used to convert UDP-DAGn to lipid X in the presence of $H_2{}^{16}O$ as well as an $H_2{}^{18}O/H_2{}^{16}O$ mixture (70:30, v/v). The lipid X and UMP products were extracted using an acidic single-phase Bligh-Dyer system (126), as was reported for analysis of CcLpxI reaction products (41). A sample of the LpxG reaction extraction was separated by reverse-phase liquid chromatography, and then analyzed by ESI-MS in the negative ion mode. The UMP product, with a predicted $[M-H]^-$ at m/z 332.029, was detected between minutes 2.2 and 2.5. For the $H_2{}^{18}O$-labeled reaction, ~70% of the UMP product contained ^{18}O, as shown by the presence of a much more intense peak at m/z 335.031 versus m/z 332.027 (lower panel, Fig. 34A). The lipid X product, predicted to have a $[M-H]^-$ at m/z 710.424, also eluted between minutes 2.2 and 2.5. No mass shift in the lipid X peak was observed in the reaction carried out in the presence of $H_2{}^{18}O$ (Fig. 34B). Thus, we conclude that CtLpxG catalyzes the attack of water exclusively on the α–phosphorus atom of UDP-DAGn.

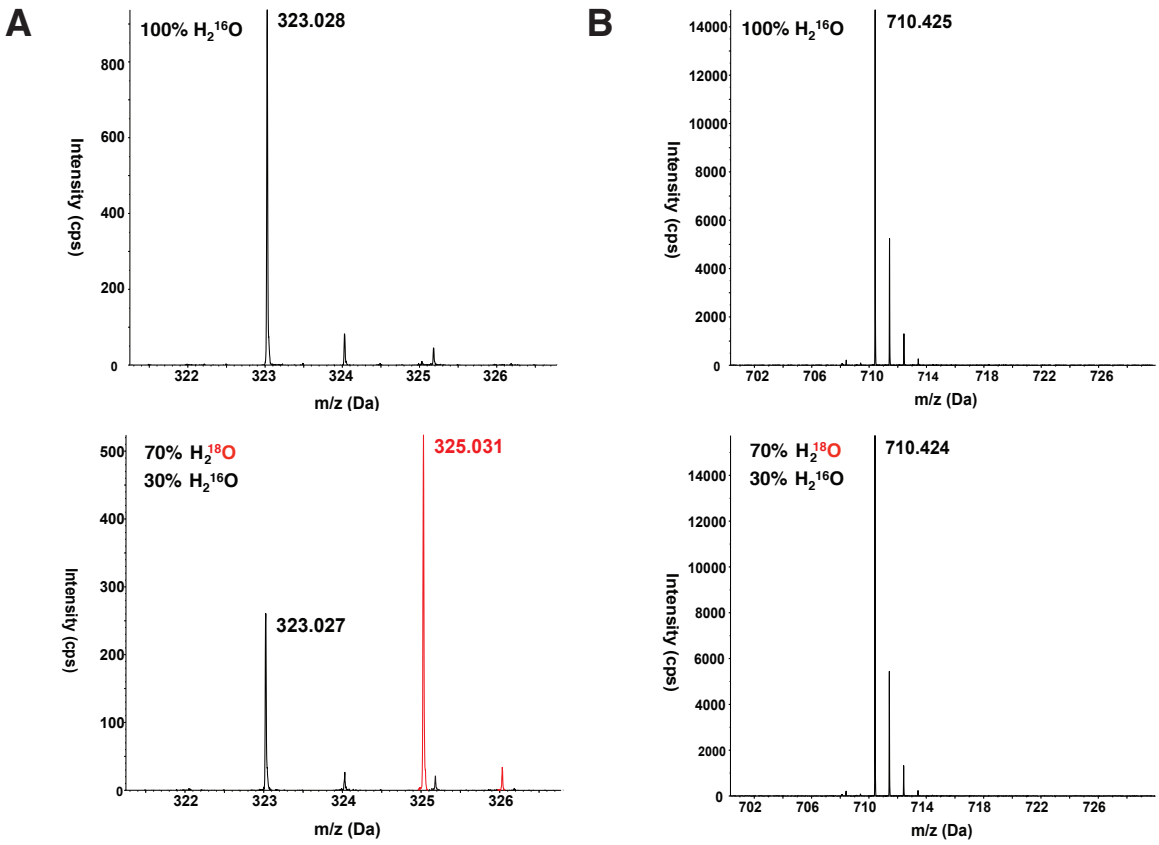

Figure 34: Mass Spectrometric Characterization of LpxG Reaction Products

An LpxG-catalyzed UDP-DAGn hydrolysis reaction was carried out in the presence of 70% $H_2{}^{18}O$. Results were analyzed by LC/MS and compared those obtained in the presence of 100% $H_2{}^{16}O$. (A) UMP generated by LpxG in the presence 100% $H_2{}^{16}O$ was detectable at m/z 323.0328 (upper panel). This peak was also present in the isotopically labeled reaction (lower panel), however a second peak corresponding to incorporation of ^{18}O into UMP was also observed at 325.031 (red trace). (B) Lipid X generated by LpxG appeared the same m/z value of 710.42 in both labeled (upper panel) and unlabeled (lower panel) reactions.

5.3.3 CtLpxG Displays Mn^{2+} Dependence *In Vitro*

All activity assessments in initial LpxG discovery were carried out in the presence of Mn^{2+}, however we sought to further investigate the metal dependence of CtLpxG. Sample of the purified enzyme were incubated with EDTA to chelate any

metal co-purifying with the protein. LpxG was then diluted into autoradiographic assay conditions in which the 1 mM MnCl2 was replaced with the following chloride salts: Ca^{2+}, Co^{2+}, Cu^{2+}, Fe^{3+}, Mg^{2+}, Mn^{2+}, Ni^{2+}, and Zn^{2+}. Assay conditions where the di- or trivalent metal salt was replaced by 2 mM NaCl or no metal additive were also included as controls. The remaining assay protocol was carried out as previously described and specific activity was calculated for each reaction. The Mn^{2+} assay condition showed activity that was 35-fold greater than the condition with no metal (Fig. 35). The Co^{2+} condition also enhanced activity; however, the increase (3 fold) was substantially lower than that seen when Mn^{2+} was present. The activity of the enzyme showed no increase in the presence of NaCl, indicating that the ionic strength of the reaction was not responsible for any stimulation observed. Overall, results indicated that Mn^{2+} was the most efficient and thus most likely cofactor for LpxG activity.

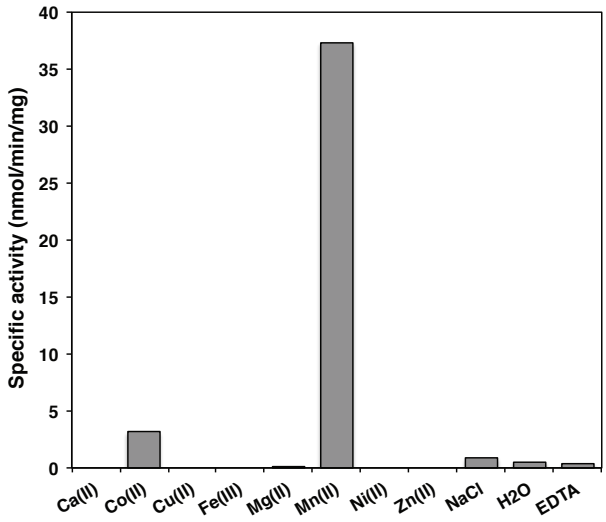

Figure 35: *In vitro* Metal Dependence of LpxG

LpxG treated with EDTA was assayed under standard conditions supplemented with either metal, NaCl, or no metal. Resulting specific activity was calculated and compared to the specific activity of the no metal control.

5.3.4 Point Mutation of a Conserved Residue Abrogates LpxG Activity

A protein-protein BLAST search of other Chlamydia species reveals LpxG orthologs in several other organisms (Fig. 36). Alignments of these sequences reveal a clear DXH(X)$_{\sim 25}$GDXXDR(X)$_{\sim 25}$GNHD motif (with X indicating any amino acid) (highlighted in black, Fig. 36) that is characteristic of the enzymes in the calicinuerin-like phosphoesterase (CLP) superfamily (103,105). Proteins with this classification utilize a cluster of two metal ions to facilitate hydrolysis, with the residues of the conserved motif coordinating the cofactors (103). Additionally present in LpxG is a UUXGHXH motif (Fig. 36), with U representing hydrophobic residues, also present in a sub-class of CLP

enzymes (102,145). Alanine mutations of motif amino acids have been shown to severely abrogate activity (106), confirming their importance in enzyme function.

To assess the classification of LpxG as a CLP enzyme, a point mutant of one of the aforementioned conserved motif residues was generated and tested for activity. The mutation, D59A (star, Fig. 36), substituted the aspartate in the block I DXH motif for alanine. A sample of LpxG containing this mutation was overexpressed in *E. coli* and purified using the same procedure described for wild-type protein (Fig. 32B). When the D59A from of CtLpxG was assayed for *in vitro* hydrolysis of UDP-DAGn, it exhibited extremely reduce levels of lipid X production compared to the wild-type protein (D59A, Fig. 33A). This corresponded to nearly a 40-fold decrease in specific activity compared to LpxG (Fig. 33B).

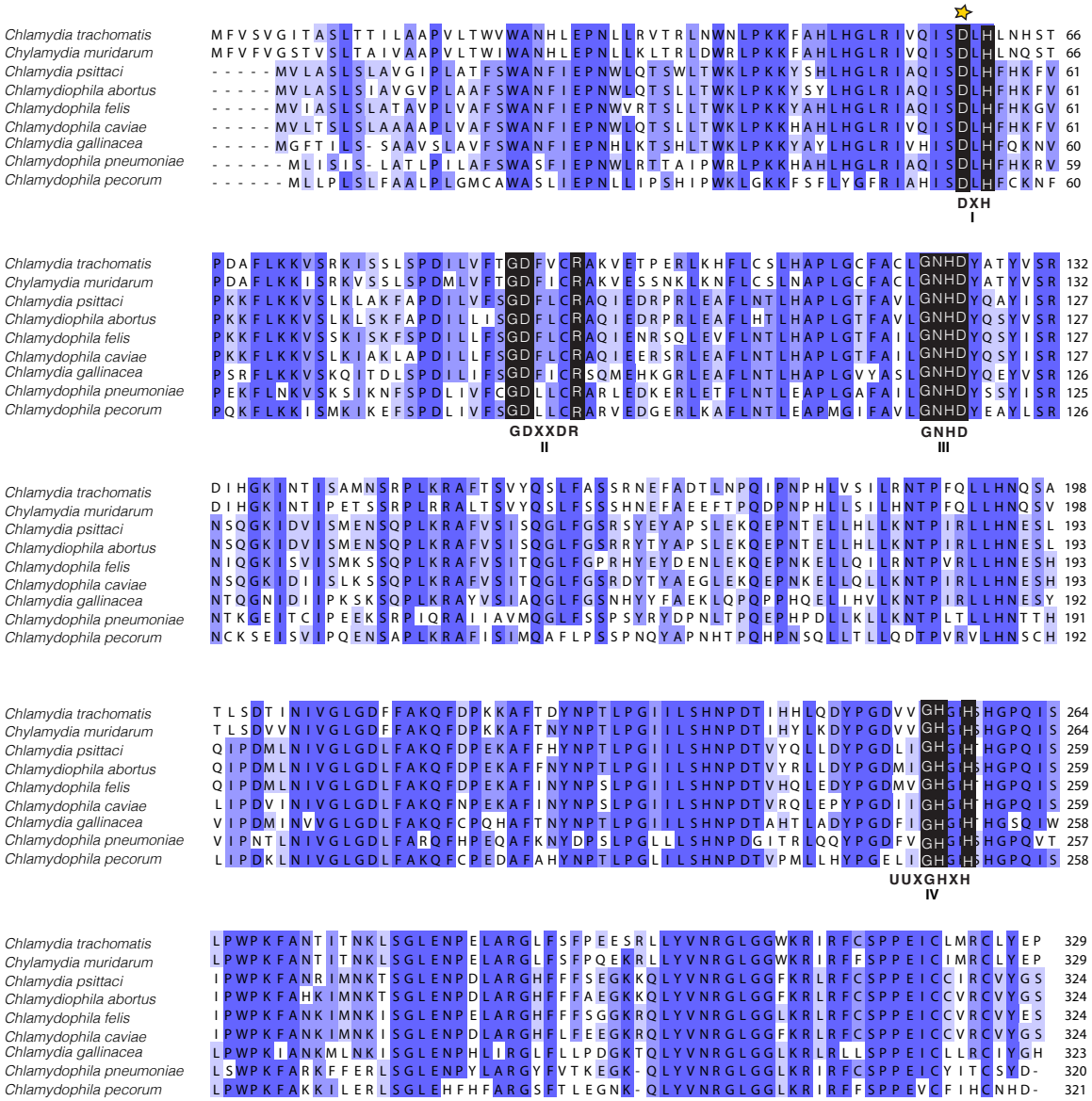

Figure 36: Alignment of LpxG Orthologs

Listed are the LpxG orthologs found in the Chlamydiacae family. Residues are colored by percent identity, with darkness of shade corresponding to degree of conservation. The four blocks of the CLP motif are marked in black, with the specific amino acid patterns and block numbers denoted below. "X" represents any amino acid and "U" denotes any hydrophobic residue. Sequences were obtained from the NCBI server and alignment was carried out using Clustal W (163).

5.3.5 Comparison of CtLpxG, CcLpxI, and EcLpxH UDP-DAGn Hydrolase Complementation in *E. coli*

Autogradiographic assay provides an efficient method for comparing the *in vitro* activity of LpxG to the previously characterized UDP-DAGn hydrolases, LpxH and LpxI (Fig. 37A). To compare the *in vivo* efficiencies of these enzymes, Ct*lpxG*, Ec*lpxH*, and Cc*lpxI* were assessed for their relative abilities to complement an *lpxH* deletion in *E. coli* W3110A. The UDP-DAGn hydrolase genes were ligated into pBAD33 vectors capable of arabinose-enhanced expression (see Chapter 4)(41). After P1 transduction removed the chromosomal copy *lpxH*, the resulting W3110AΔHCtG, W3110AΔHEc, and W3110AΔHCc were all able to maintain viability, albeit at differing degrees. When grown on LB-agar supplemented with no arabinose, W3110AΔHEc exhibited much more robust growth than in the presence of 0.02% (w/v) arabinose (Fig. 37B). This indicates that increase in Ec*lpxH* expression can be toxic in the background tested. In contrast, W3110AΔHCtG grew better when supplemented with 0.02% arabinose (Fig. 37B), suggesting increase in Ct*lpxG* levels helps cells better compensate for the *lpxH* deletion. The phenotype of W3110AΔHCc was relatively consistent regardless of arabinose concentration (Fig. 37B): cells deficient in *lpxH* are insensitive to alternations in Cc*lpxI* expression levels.

A

UDP-DAGn Hydrolase	Organism	Assay Cofactor	Range of Specific Acitivty µmol/min/mg
LpxG	*C. trachomatis*	Mn^{2+}	0.01
LpxH	*H. influenzae*	Mn^{2+}	10000
LpxI	*C. crescentus*	Mg^{2+}	10

B

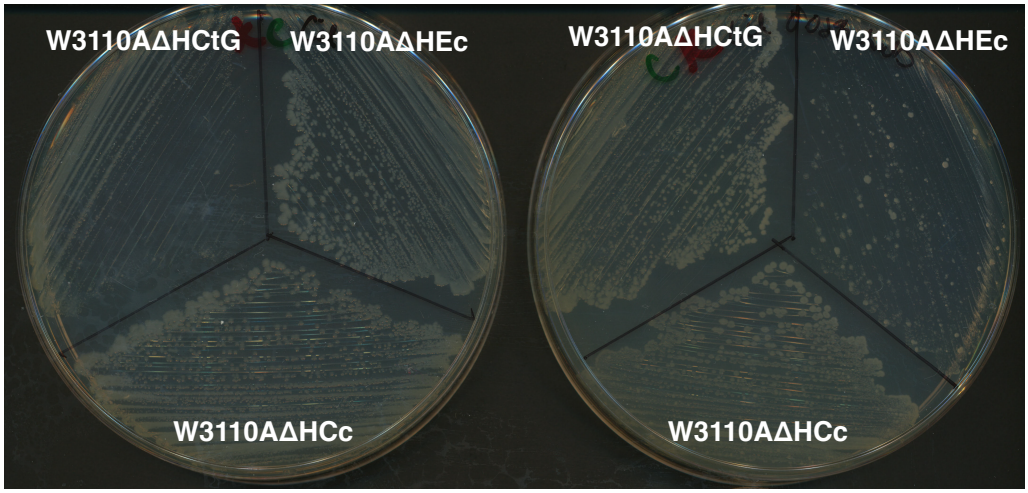

Figure 37: *In vivo* Comparison of UDP-DAGn Hydrolase Activity

(A) Comparison of reported *in vitro* activity for orthologs of LpxG, LpxH, and LpxI. Range of specific activity reflects reported V_{max} values for LpxH and LpxI, and the highest observed specific activity for LpxG (reported above). (B) Survival of *E. coli* W3110A harboring *lpxH:kan* insertions, rescued with each individual UDP-DAGn hydrolase. W3110AΔHCtG, W3110AΔHEc, and W3110AΔHCc were grown at 37°C after streaking on LB agar supplemented with ampicillin and chloramphenicol. In the right panel, growth medium has been additionally supplemented with 0.02 % (w/v) arabinose to stimulate expression of the pBAD33-derived plasmid harboring the complementing UDP-DAGn hydrolase in all tested strains.

5.4 Discussion

While the product of UDP-DAGn hydrolysis, lipid X (164), was the first lipid A biosynthetic intermediate to be isolated, an enzyme capable of producing lipid X was the last to be discovered (40). Even when the gene for LpxH, the UDP-DAGn hydrolase in *E. coli,* was identified, orthologs of the enzyme were missing in a variety of other lipid-A production bacteria (40). Discovery of a second UDP-DAGn hydrolase, LpxI (41), added some pieces to the puzzle of lipid X production in Gram-negative organisms. LpxH and LpxI have been characterized for their enzymatic properties (40,41) and have a very unique relationship, as they perform the same function but share no sequence homology and are never found in the same organism. Despite the amassing details about the known UDP-DAGn hydrolases, there was still an incomplete understanding lipid X formation, as several groups of lipid A-producing bacteria contain neither LpxH nor LpxI (81). Recent discovery of LpxG in *C. trachomatis* helped to elucidate how these bacteria are capable of lipid A biosynthesis despite containing orthologs for the known UDP-DAGn hydrolases (see Chapter 4).

5.4.1 Membrane Domain of LpxG Compels Purification Optimization and Hypotheses on Localization of *C. trachomatis* Lipid A Pathway

In the work described in this chapter, we show that CtLpxG can be purified from *E. coli* with use of NiNTA chromatography, resulting in nearly a 40-fold increase in observed UDP-DAGn hydrolase specific activity than seen in cell free extracts. Furthermore, a point mutation in a conserved residue of LpxG abrogates activity,

indicating the specificity of observed lipid X production. While evidence of active purified protein is clear, the low yield of protein and contaminating impurities merits further optimization of isolation procedures.

One difficulty in expression and purification of CtLpxG is the existence of a single N-terminal transmembrane domain. This makes it necessary to include detergent during all steps of purification, which may alter the stability of the protein during isolation. Interestingly, while a truncated version of LpxG lacking the N-terminal domain is still able to complement *lpxH in vivo* (see Chapter 4), over-expression of this construct did not yield properly folded LpxG (data not shown). The addition of a stabilizing tag or moiety to the N-terminal region of the truncated construct, such as maltose-binding protein, may alleviate expression problems creating opportunities for further purification and enzymatic studies.

The existence of a transmembrane domain is a feature not seen in the other UDP-DAGn hydrolases (40,41), as evident by the plot of membrane probability in Fig. 38. Lipid X production is hypothesized to take place at the periphery of the inner membrane due to the hydrophobic nature of the molecule and the location of subsequent pathway enzymes (6). In fact, structural evidence suggests that the macromolecular mechanism of LpxI involves interaction with the membrane for deposition (96) (Fig. 11). Despite this observation, LpxI can be stably purified without use of detergent and does not display surface dilution kinetics (41), indicating that membrane interaction is transient.

LpxH has slightly more hydrophobic character than LpxI, as protein yield is increased when a detergent solublization step is used in purification (157). Nonetheless, LpxH shows no evidence of surface dilution kinetics *in vitro* (157), once again suggesting temporary membrane association. This makes LpxG the first UDP-DAGn hydrolase that has permanent association with the membrane.

The unique nature of the integration of LpxG into the inner membrane is especially intriguing when assessing the characteristics of the other lipid A biosynthetic enzymes in *C. trachomatis.* While the *C. trachomatis* orthologs for LpxA, LpxC, and LpxD, and LpxK all are predicted to have topologies similar to those found in *E. coli*, the hyrdopathy plot for LpxB, the fifth enzyme in the pathway, differs greatly among the bacteria. *E. coli* LpxB is 382 amino acids in length and shows no evidence of transmembrane regions, as indicated by the low probability of membrane-bound residues (Fig. 38). *C. trachomatis* LpxB is 607 amino acids, 200 of which are predicted to make up a 6 N-terminal transmembrane domains (Fig. 38). This feature appears to be unique to the family Chlamydiaceae, as the N-terminal membrane domain is not seen in LpxB orthologs within the Chlamydiae phylum. The membrane integration of *C. trachomatis* LpxB may explain why a similar feature is observed in LpxG. Furthermore, the bilayer localization of the fourth and fifth biosynthetic enzymes may play an important role in the physiology of lipid A production in *C. trachomatis.*

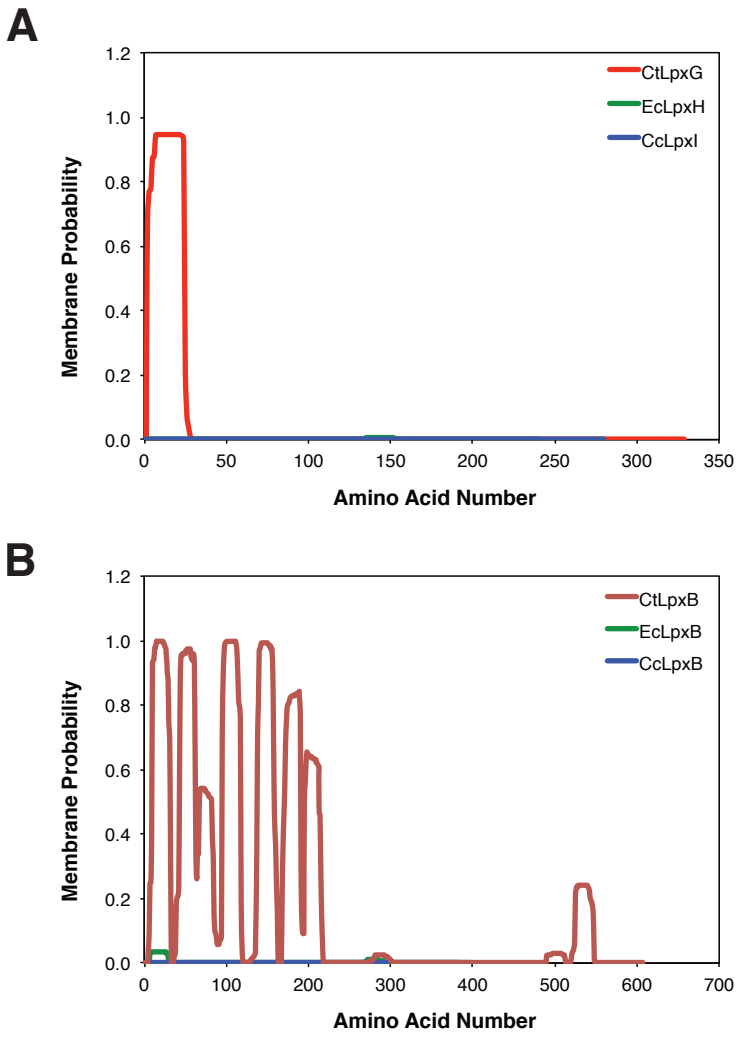

Figure 38: Topology of Fourth and Fifth Lpx Enzymes

(A) Probability of transmembrane localization (Membrane Probability) versus amino acid number for the UDP-DAGn hydrolases that catalyze the fourth step of lipid A biosynthesis in *E. coli, C. trachomatis,* and *C. crescentus*. Values were determined using the TMHMM Server 2.0 on the Center for Biological Sequence Analysis website (http://www.cbs.dtu.dk/services/TMHMM/). (B) The same data as described in (A), except for LpxB orthologs that are responsible for the fifth step of lipid A biosynthesis in the aforementioned bacterial species. Sequences for both sets of predictions were obtained from the NCBI server.

5.4.2 Hydrolytic Mechanism Suggests Conservation of α-attack in CLP Enzymes

It had been previously established that LpxH and LpxI have different methods of hydrolysis, with LpxH attacking the α phosphate (40) and LpxI the β phosphate (41) of UDP-DAGn. Employing the mass spectrometry strategy used for identifying the hydrolytic mechanism for LpxI, we determined the method of attack for LpxG. As evident by the deposition of water on the UMP group, LpxH appears to proceed through the same α attack as LpxH (Fig. 39). This is not surprising, as both LpxH and LpxG appear to be members of the CLP superfamily. Hydrolysis of pyrophosphate bonds, as seen in the formation of lipid X, was a type of chemistry not previously attributed to CLP enzymes until recently, when EPR spectroscopy and mutagenesis were used to confirm the classification of LpxH as part of this superfamily (Chapter 3)(157). The discovery of LpxG and elucidation of its hydrolytic mechanism provides further information about this subclass of CLP pyrophosphatase enzymes and suggests a conserved hydrolytic method for catalysis.

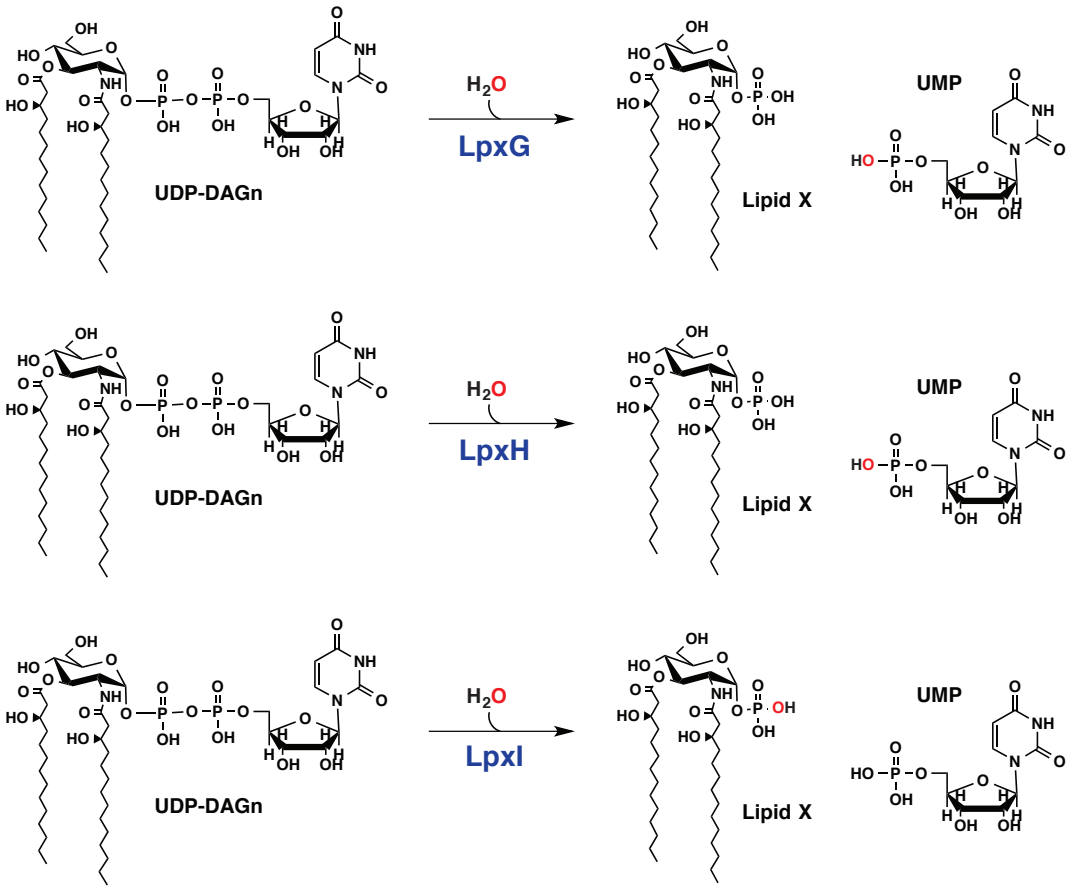

Figure 39: Hydrolytic Mechanisms of Known UDP-DAGn Hydrolases

5.4.3 LpxG's Identification as a CLP Enzyme Allows for Direct Comparison with LpxH

LpxG displays a clear CLP motif indicative of enzymes that employ divalent cations to facilitate catalysis (103,105). Moreover, LpxG activity appears to be dependent on a metal cofactor, as negligible *in vitro* UDP-DAGn hydrolysis is detected when no such species is present. Specific activation in lipid X production is observed when LpxG is assayed in the presence of Mn^{2+}, making it the most likely candidate for the enzyme's

cofactor *in vivo*. This is a property shared between LpxG and LpxH, as the latter enzyme shows significant activation in the presence of Mn^{2+} and contains two closely spaced Mn^{2+} binding sites (157). Metal-dependent hydrolysis is also observed with LpxI, albeit with Mg^{2+}(41).

The CLP motif in LpxG can be clearly detected through alignment of orthologs from various *Chlamydia* species as well as *Chlamydiacea* family members. As previously discussed, these conserved residues have been shown to serve as a scaffold for the metal cofactors and ordered water molecules that are vital to hydrolysis in other CLP enzymes. A mutation in first residue in the N-terminal section of this motif abolished LpxG activity, suggesting that it also relies on the conserved CLP residues to carry out enzymatic function. This corresponding mutation in LpxH, which also displays a CLP motif, reduced activity by 200,000-fold, speaking to the importance of the first aspartate in the CLP-mediated hydrolysis of UDP-DAGn (Chapter 3)(157). In other CLP enzymes, the residue in this position of the motif directly coordinates one of the metal cofactors (150,152).

The metal dependence of LpxG and importance of a motif residue for activity further corroborates the classification of LpxG as member of the CLP family. It should be noted that despite this family similarity with LpxH, the two proteins are distinct, as evident by the high E-value (0.8) of their alignment (Table 13). A specific difference between LpxG and LpxH is seen in one of the blocks of the conserved CLP motif. LpxH

orthologs display a unique LpxH-specific GNRD sequence in block III of the motif (Chapter 3)(157) while LpxG orthologs display GNHD, which is canonical in other CLP enzymes (157). Structural studies of a well-known CLP enzyme, bacteriophage λ serine-threonine protein phosphatase, indicate the histidine in the GNHD motif coordinates the Mn-bridging water molecule (Fig. 23)(150). Mutation to an arginine would retain this functionality and may even increase stability of the metal complex. Additionally, as an arginine residue has been shown to be imperative in binding uridine in deoxyuridine triphosphate pyrophosphatase (dUTPase) (165,166), it is possible the variance of the LpxH motif increases substrate affinity. Interestingly, the block III histidine is also seen in LpxH2, a hypothesized ancestor of LpxH (81). While LpxH2 from *Pseudomonas aeruginosa* does not have UDP-DAGn hydrolase function *in vivo* in *E. coli (82),* it is thought that *lpxH* is a product of a gene duplication of *lpxH2* within the Proteobacteria lineage before the β and γ divergence (81). Mutation of histidine to arginine in the third block of the CLP motif may have facilitated the optimization of LpxH for UDP-DAGn hydrolysis. Study of the effect of a similar mutation in LpxG would aid in determining if such a substitution enhances catalysis.

5.4.4 LpxG is Distinct from Other YkuE Related Proteins

Within the CLP family, LpxG is characterized as a member of the YkuE-related proteins. YkuE is a metallophosphoesterase originally characterized in *Bacillus subtilis* that has been reported to have monophosphoesterase activity and co-purify with equal

molar ratios of Mn^{2+} and Zn^{2+}(167). YkuE also displays a twin arginine motif and studies indicate it is transported to the cell wall of *B. subtilius* through the Tat system (167). Its function is not known, however the enzyme is hypothesized to play a role in phosphate acquisition from the extracellular environment (167). A homolog of YkuE, YaeI, exists in *E. coli*; it also displays a RR motif (Fig. 40). CtLpxG is very homologous to both YkuE and YaeI, with their alignments having an E-value of 4×10^{-26} and 7×10^{-22} respectively; furthermore, LpxG is annotated as YaeI in some *C. trachomatis* genomes. Yet, CtLpxG lacks the twin arginine motif, as does every LpxG ortholog in the *Chlamydiales* family (Fig. 36), making it very unlikely the protein serves the same functionality as YkuE and YaeI. The ability of LpxG to complement *lpxH* in *E. coli* corroborates that the protein is not transported, as lipid A biosynthesis takes place in the cytosol and in the inner leaflet of the inner membrane (6). Moreover, because of the essential nature of *lpxH* in *E. coli*, it can be assumed that YaeI, which is not essential, has no UDP-DAGn hydrolase function *in vivo*. Thus, despite bioinformatic annotation and sequence similarity, LpxG is a unique protein in the YkuE sub-family that functions as an UDP-DAGn hydrolase.

```
YaeI    1 -MMISRRRFLQ-----AATATLAAGSGFGYIHYLEPGWLELTHQHIA--FFKDKAAPFKILFLADLH 59
YkuE    1 MKKMSRRQFLKGMFGALAAGALTAGGGYGYARYLEPHMIETTEHTIKSSLIPHGFDGFKIVQFSDAH 67
CtLpxG  1 -MFVSVGITAS-----LTTILAAPVLTWVWANHLEPNLLRVTRLNWNLPKKFAHLHGLRIVQISDLH 54
```

Figure 40: N-terminal Alignment of YkuE-Related Proteins

Alignment of the first ~60 amino acids of *E. coli* YaeI, *B. subtilus* YkuE, and *C. trachomatis* LpxG. The twin arginine motif, signature of substrates of the Tat secretion system, is highlighted in green. Block I of the CLP family motif is highlighted in orange. Sequences were obtained from the NCBI server and alignment was carried out using Clustal W (163).

5.4.5 Evaluation of Differences in LpxG, LpxH, and LpxI May Reveal Variances in Lipid A Pathway Across Bacteria

The unique characteristics of the known UDP-DAGn hydrolases extend to their observed catalytic capabilities. Comparison of the *in vitro* hydrolysis of the three proteins reveals orders of magnitude differences, with EcLpxH exhibiting a 10^3 enhancement in activity over CcLpxI, and CcLpxI exhibiting another 10^3 enhancement over CtLpxG (Fig. 37). This may reflect assay optimization, as *E. coli* activity was originally reported in the range of LpxI (40). However, optimization of UDP-DAGn hydrolysis for LpxH was mainly attributed to presence of metal (Chapter 2), which has been accounted for in LpxG and LpxI. The variation in catalytic activities may also be accredited to substrate specificity of the enzymes for the type of lipid A seen in their representative bacteria. Specifically, the *in vitro* substrate utilized in the experiments was obtained from *E. coli* and contains two hydroxymyristate acyl chains whereas the UDP-DAGn from *C. trachomatis* contains a 20- and a 14-carbon acyl chain, with only the former being hydroxylated. It has been shown that Lpx enzymes can be extremely attuned to such differences, particularly in acyl chain length (168-170).

Variation of observed *in vitro* activity may explain the difference in phenotypes of W3110AΔH strains complemented with *ara*-controlled LpxH, LpxI, or LpxG. Hydrolytic proficiency seemed to positively correlate with cell viability in the absence of arabinose and negatively correlate in its presence. It is likely that abundance of a more proficient EcLpxH results in toxicity (seen in other lipid A biosynthetic enzymes, such as

LpxC) whereas a greater amount of CtLpxG is necessary to sustain pathway flux due to its lower activity. This observation may be due to issues with protein expression of CcLpxI and CtLpxG, however, paired with the *in vitro* disparity, it may hint at the nature of the lipid A pathway in their respective parental bacteria. In fact, it has been proposed that *E. coli* and other organisms containing LpxH orthologs (Proteobacteria) resemble the most optimized form of the pathway (81), thus making it unsurprising these organisms contains the most proficient UDP-DAGn hydrolase. Additionally, as *C. trachomatis* do not rely on lipid A biosynthesis for replication (20), it is not unreasonable that there would be less pressure on this organism to develop a highly efficient UDP-DAGn hydrolase.

5.4.6 LpxG: Ancestral or Adaptive?

Casting LpxG in the role of UDP-DAGn hydrolase in *C. trachomatis* is an intriguing one to ponder from an evolutionary standpoint. First to consider is its similarity to LpxH. It has been proposed that LpxH evolved from LpxH2, as discussed above. It might be possible that LpxG is part of this lineage, representing an ancestor of LpxH2. This hypothesis is supported by the evolutionary age of *Chlamydia* compared to other bacterial phyla. Early lipid A biosynthesis may have been carried out by LpxG. Modifications to the pathway on the molecular and biological level could have necessitated more efficient chemistry at the fourth step, leading to evolution of LpxH2. As lipid A biosynthesis is not essential in *Chlamydia,* selective pressure for optimization

of synthesis may not have occurred, thus causing the bacteria to retain LpxG. Crucial to this hypothesis of a three-part lineage would be identifying LpxH2 orthologs that are capable of UDP-DAGn hydrolysis *in vivo.* Currently, only the ortholog from *Pseudomonas aeruginosa* has been assessed for complementation activity. As this organism also contains LpxH, the LpxH2 ortholog may have evolved a different function, thus making it necessary to evaluate an LpxH2 ortholog from a bacterium lacking a known UDP-DAGn hydrolase. Mutational studies in conjunction with detailed bioinformatic analysis of all three orthologs could be used to further dissect their relation.

A second possibility in the evolution of LpxG as a UDP-DAGn hydrolase is genome condensation. *C. trachomatis* contains a very small genome (~1 MB) with signs of incomplete biosynthetic pathways. Many of these pathways have been found to be functional, either through acquisition of intermediates from the host cell or presence of distinct enzymes specialized to fill metabolic gaps (115). It is possible that the evolutionary-conserved UDP-DAGn hydrolase was lost in *C. trachomatis* due to genome condensation, causing another hydrolase to adapt to produce lipid X. LpxI is the most likely candidate for the original hydrolase in *C. trachomatis* ancestors, as homologs for the protein are found within *Simkaniaceae*, another family in the *Chlamydiae* phylum. In the case of this 're-purposing' of LpxG as an UDP-DAGn hydrolase, it is possible that the protein retains a secondary function *in vivo*. The similarity between YaeI and LpxG

(discussed above) may indicate a possible ancestral relationship, with the later diverging from the former in *C. trachomatis* due to need for a UDP-DAGn hydrolase. Interestingly, the strength of LpxG orthologs correlates with presence of a membrane-bound ortholog of LpxB. These could reflect the evolutionary similarity of the bacteria as a whole, or it may indicate that development of a membrane-embedded LpxB necessitated development or recruitment of a membrane-bound UDP-DAGn hydrolase.

5.4.7 Conservation of LpxG in Other Bacterial Groups: More Pieces to the Puzzle?

LpxG is found throughout the family Chlamydiaceae, as well as other members of the Chlamydia phylum (Fig. 41), completing the puzzle of lipid biosynthesis is this particular family. Orthologs for the protein are also seen in in other bacteria containing lipid A biosynthetic enzymes but lacking a known UDP-DAGn hydrolases (Figs. 7, 8), such as *Brachyspira hyodysenteriae*, and *Synechococcus* sp. PCC 6312 (Fig. 42). These orthologs are annotated as uncharacterized metallophosphoesterases and lack the twin-arginine motifs seen in YkuE orthologs as discussed above.

A more detailed bioinformatic analysis is necessary to determine if the discovery of LpxG fills in the absence of necessary pathway enzymes in all lipid-A producing Gram-negative bacteria. This could be complicated by the ubiquitous nature of the CLP motif, the likeness of LpxG to other proteins with difference functions (as discussed above with YaeI), and the lack of clustering with other biosynthetic enzymes. Such problems were avoided with the other hydrolases. As LpxH seems to be a distinct CLP

enzyme with a specific modification to a portion of the motif (GNRD versus GNHD), it is easy to discern between general family members and actual orthologs. Furthermore, LpxH was detected in organisms in the Proteobacteria phylum, which contain highly conserved lipid A biosynthetic enzymes. Likewise, LpxI is a completely distinct protein of a unique family; this facilitates ortholog identification. Moreover, *lpxI* is found clustered in the same region of the genome as other lipid A biosynthetic enzymes (41). If LpxG is not the final answer to the question of lipid X production in Gram-negative bacterial, it is possible an additional UDP-DAGn hydrolases exist. Alternatively, LpxB orthologs in bacterial lacking a UDP-DAGn hydrolase may be bifunctional and thus capable of both the hydrolysis and condensation that is required to synthesize the disaccharide backbone of lipid A.

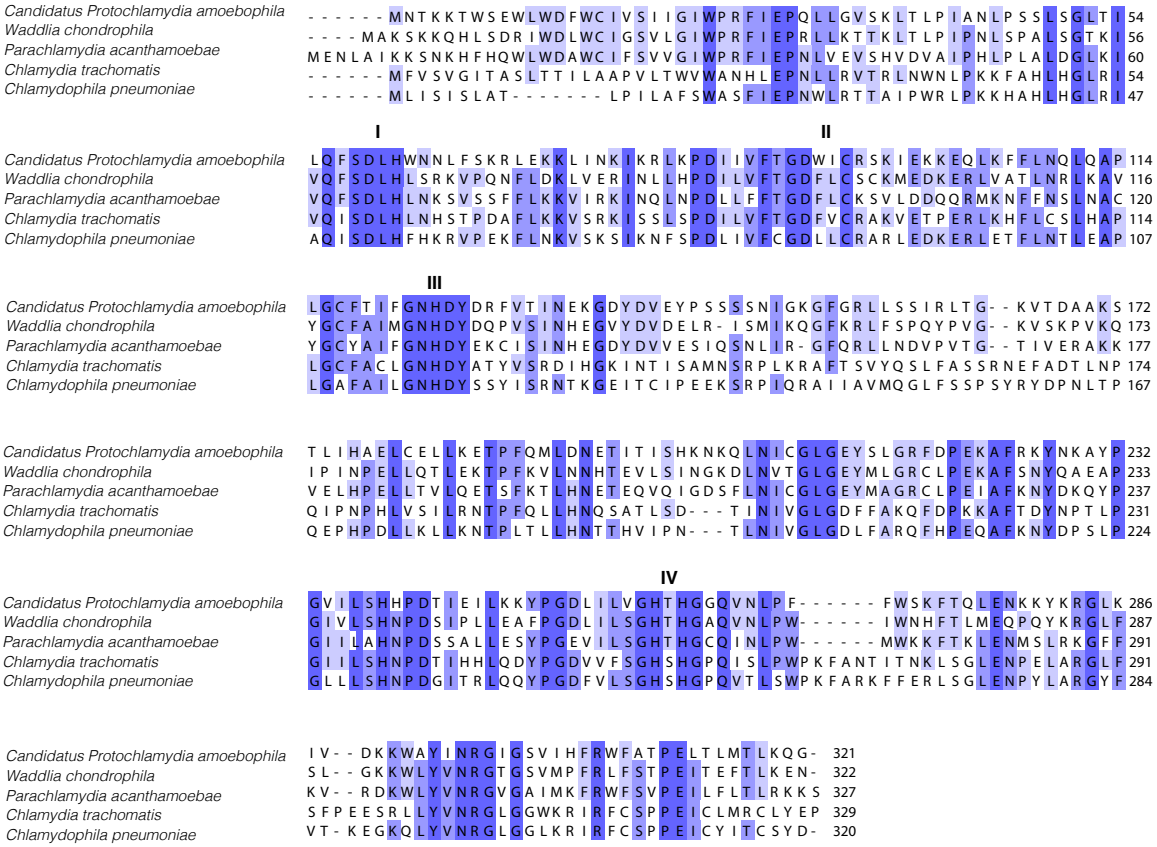

Figure 41: Alignment of LpxG Orthologs in Chlamydia Phylum

Aligned sequences of LpxG orthologs found across the phylum of Chlamydia. Residues are colored by percent identity, with darkness of shade corresponding to degree of conservation. The four blocks of the CLP motif are marked with Roman numerals. Sequences were obtained from the NCBI server and alignments were carried out with Clustal W (163).

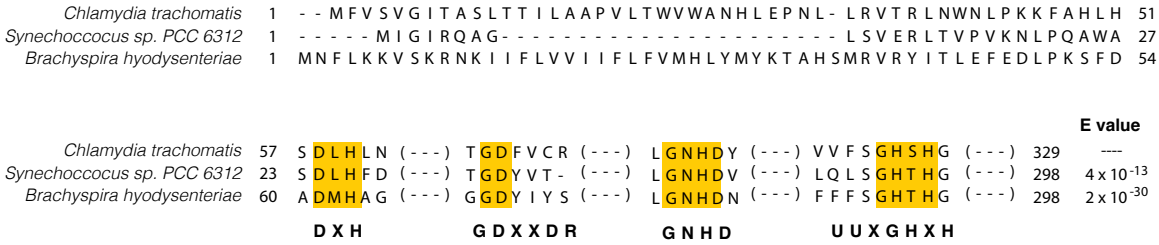

Figure 42: LpxG Orthologs Found Outside of Chlamydia

Alignment of N-terminal region and CLP motifs found in LpxG orthologs of *Brachyspira hyodysenteriae*, and *Synechococcus sp*. PCC 6312. E-values listed are in reference to *C. trachomatis* LpxG were calculated from protein-protein BLAST search on the NCBI website. Sequences were obtained from the NCBI server and alignments were carried out with Clustal W (163).

5.4.7 Conclusion

The existence of multiple enzymes being utilized for the fourth step of the Raetz pathway speaks to the universal nature of phosphoester hydrolysis in biology. Specifically, the observation that other proteins not thought to function as UDP-DAGn hydrolases *in vivo* are still capable of lipid X production *in vitro,* such as Cdh (40,82,89,91,92), reiterates how enzymatic scaffolds can conform to various substrates to perform chemistry. Despite this ubiquity, only particular enzymes have evolved to function as UDP-DAGn hydrolases *in vivo* (41,82), making complementation a necessary tool by which to assess enzyme function.

Even with the discovery of LpxG, questions about the fourth step of the lipid A biosynthetic pathway still remain. Namely, why is so much diversity seen at this step when the third and fifth steps are both extremely conserved? One possible explanation may be the nature of the reaction carried out to produce lipid X. Hydrolysis of pyrophosphate bonds, especially those in nucleotides, is extremely ubiquitous and

important in biology. Thus, over time, highly efficient mechanisms for such reactions have evolved. The lipid A pathway may have adopted these optimized enzyme scaffolds carry out biosynthesis. In bacteria in which there was not significant selective pressure for highly efficient lipid A metabolism, earlier versions of the UDP-DAGn hydrolase exist, as discussed above.

The relationship of LpxG, LpxH and LpxI make a very intriguing model system by which to study enzyme evolution from biochemical, structural, and bioinformatic approaches. Such investigations would yield important information about lipid A biosynthesis as well as the plasticity of metabolic processes in nature.

References

1. Whitman, W. B., Coleman, D. C., and Wiebe, W. J. (1998) Prokaryotes: the unseen majority. *Proceedings of the National Academy of Sciences of the United States of America* **95**, 6578-6583

2. de Lorenzo, V. (2008) Systems biology approaches to bioremediation. *Current opinion in biotechnology* **19**, 579-589

3. Abed, R. M., Dobretsov, S., and Sudesh, K. (2009) Applications of cyanobacteria in biotechnology. *Journal of applied microbiology* **106**, 1-12

4. Malone, D. L., Genuit, T., Tracy, J. K., Gannon, C., and Napolitano, L. M. (2002) Surgical site infections: reanalysis of risk factors. *The Journal of surgical research* **103**, 89-95

5. Tasota, F. J., Fisher, E. M., Coulson, C. F., and Hoffman, L. A. (1998) Protecting ICU patients from nosocomial infections: practical measures for favorable outcomes. *Critical care nurse* **18**, 54-65; quiz 66-57

6. Raetz, C. R., Reynolds, C. M., Trent, M. S., and Bishop, R. E. (2007) Lipid A modification systems in gram-negative bacteria. *Annual review of biochemistry* **76**, 295-329

7. Raetz, C. R., and Whitfield, C. (2002) Lipopolysaccharide endotoxins. *Annual review of biochemistry* **71**, 635-700

8. Kahler, C. M., and Stephens, D. S. (1998) Genetic basis for biosynthesis, structure, and function of meningococcal lipooligosaccharide (endotoxin). *Critical reviews in microbiology* **24**, 281-334

9. Weiss, J., Hutzler, M., and Kao, L. (1986) Environmental modulation of lipopolysaccharide chain length alters the sensitivity of Escherichia coli to the neutrophil bactericidal/permeability-increasing protein. *Infection and immunity* **51**, 594-599

10. Whitfield, C., Kaniuk, N., and Frirdich, E. (2003) Molecular insights into the assembly and diversity of the outer core oligosaccharide in lipopolysaccharides from Escherichia coli and Salmonella. *Journal of endotoxin research* **9**, 244-249

11. McGrath, B. C., and Osborn, M. J. (1991) Localization of the terminal steps of O-antigen synthesis in Salmonella typhimurium. *Journal of bacteriology* **173**, 649-654

12. Rund, S., Lindner, B., Brade, H., and Holst, O. (1999) Structural analysis of the lipopolysaccharide from Chlamydia trachomatis serotype L2. *The Journal of biological chemistry* **274**, 16819-16824

13. Schnaitman, C. A., and Klena, J. D. (1993) Genetics of lipopolysaccharide biosynthesis in enteric bacteria. *Microbiological reviews* **57**, 655-682

14. Walsh, A. G., Matewish, M. J., Burrows, L. L., Monteiro, M. A., Perry, M. B., and Lam, J. S. (2000) Lipopolysaccharide core phosphates are required for viability and intrinsic drug resistance in Pseudomonas aeruginosa. *Molecular microbiology* **35**, 718-727

15. Ferguson, A. D., Braun, V., Fiedler, H. P., Coulton, J. W., Diederichs, K., and Welte, W. (2000) Crystal structure of the antibiotic albomycin in complex with the outer membrane transporter FhuA. *Protein science : a publication of the Protein Society* **9**, 956-963

16. Kramer, R. A., Brandenburg, K., Vandeputte-Rutten, L., Werkhoven, M., Gros, P., Dekker, N., and Egmond, M. R. (2002) Lipopolysaccharide regions involved in the activation of Escherichia coli outer membrane protease OmpT. *European journal of biochemistry / FEBS* **269**, 1746-1752

17. Haurat, M. F., Aduse-Opoku, J., Rangarajan, M., Dorobantu, L., Gray, M. R., Curtis, M. A., and Feldman, M. F. (2011) Selective sorting of cargo proteins into bacterial membrane vesicles. *The Journal of biological chemistry* **286**, 1269-1276

18. Kadurugamuwa, J. L., and Beveridge, T. J. (1995) Virulence factors are released from Pseudomonas aeruginosa in association with membrane vesicles during normal growth and exposure to gentamicin: a novel mechanism of enzyme secretion. *Journal of bacteriology* **177**, 3998-4008

19. Steeghs, L., den Hartog, R., den Boer, A., Zomer, B., Roholl, P., and van der Ley, P. (1998) Meningitis bacterium is viable without endotoxin. *Nature* **392**, 449-450

20. Nguyen, B. D., Cunningham, D., Liang, X., Chen, X., Toone, E. J., Raetz, C. R., Zhou, P., and Valdivia, R. H. (2011) Lipooligosaccharide is required for the generation of infectious elementary bodies in Chlamydia trachomatis. *Proceedings of the National Academy of Sciences of the United States of America* **108**, 10284-10289

21. Moffatt, J. H., Harper, M., Harrison, P., Hale, J. D., Vinogradov, E., Seemann, T., Henry, R., Crane, B., St Michael, F., Cox, A. D., Adler, B., Nation, R. L., Li, J., and Boyce, J. D. (2010) Colistin resistance in Acinetobacter baumannii is mediated by complete loss of lipopolysaccharide production. *Antimicrobial agents and chemotherapy* **54**, 4971-4977

22. Garcia-Quintanilla, M., Pulido, M. R., Moreno-Martinez, P., Martin-Pena, R., Lopez-Rojas, R., Pachon, J., and McConnell, M. (2014) Activity of host antimicrobials against multidrug resistant Acinetobacter baumannii acquiring colistin resistance through loss of lipopolysaccharide. *Antimicrobial agents and chemotherapy*

23. Miller, S. I., Ernst, R. K., and Bader, M. W. (2005) LPS, TLR4 and infectious disease diversity. *Nature reviews. Microbiology* **3**, 36-46

24. Andra, J., Gutsmann, T., Muller, M., and Schromm, A. B. (2009) Interactions between lipid A and serum proteins. *Advances in experimental medicine and biology* **667**, 39-51

25. Bryant, C. E., Spring, D. R., Gangloff, M., and Gay, N. J. (2010) The molecular basis of the host response to lipopolysaccharide. *Nature reviews. Microbiology* **8**, 8-14

26. Park, B. S., Song, D. H., Kim, H. M., Choi, B. S., Lee, H., and Lee, J. O. (2009) The structural basis of lipopolysaccharide recognition by the TLR4-MD-2 complex. *Nature* **458**, 1191-1195

27. O'Neill, L. A., and Bowie, A. G. (2007) The family of five: TIR-domain-containing adaptors in Toll-like receptor signalling. *Nature reviews. Immunology* **7**, 353-364

28. Casella, C. R., and Mitchell, T. C. (2008) Putting endotoxin to work for us: monophosphoryl lipid A as a safe and effective vaccine adjuvant. *Cellular and molecular life sciences : CMLS* **65**, 3231-3240

29. Needham, B. D., and Trent, M. S. (2013) Fortifying the barrier: the impact of lipid A remodelling on bacterial pathogenesis. *Nature reviews. Microbiology* **11**, 467-481

30. Sassi, N., Paul, C., Martin, A., Bettaieb, A., and Jeannin, J. F. (2009) Lipid A-induced responses in vivo. *Advances in experimental medicine and biology* **667**, 69-80

31. Kong, Q., Six, D. A., Liu, Q., Gu, L., Roland, K. L., Raetz, C. R., and Curtiss, R., 3rd. (2011) Palmitoylation state impacts induction of innate and acquired immunity by the Salmonella enterica serovar typhimurium msbB mutant. *Infection and immunity* **79**, 5027-5038

32. Kong, Q., Six, D. A., Liu, Q., Gu, L., Wang, S., Alamuri, P., Raetz, C. R., and Curtiss, R., 3rd. (2012) Phosphate groups of lipid A are essential for Salmonella enterica serovar Typhimurium virulence and affect innate and adaptive immunity. *Infection and immunity* **80**, 3215-3224

33. Hajjar, A. M., Ernst, R. K., Tsai, J. H., Wilson, C. B., and Miller, S. I. (2002) Human Toll-like receptor 4 recognizes host-specific LPS modifications. *Nature immunology* **3**, 354-359

34. Vacchelli, E., Galluzzi, L., Eggermont, A., Galon, J., Tartour, E., Zitvogel, L., and Kroemer, G. (2012) Trial Watch: Immunostimulatory cytokines. *Oncoimmunology* **1**, 493-506

35. Coleman, J., and Raetz, C. R. (1988) First committed step of lipid A biosynthesis in Escherichia coli: sequence of the lpxA gene. *Journal of bacteriology* **170**, 1268-1274

36. Sweet, C. R., Ribeiro, A. A., and Raetz, C. R. (2004) Oxidation and transamination of the 3"-position of UDP-N-acetylglucosamine by enzymes from Acidithiobacillus ferrooxidans. Role in the formation of lipid a molecules with four amide-linked acyl chains. *The Journal of biological chemistry* **279**, 25400-25410

37. Sweet, C. R., Williams, A. H., Karbarz, M. J., Werts, C., Kalb, S. R., Cotter, R. J., and Raetz, C. R. (2004) Enzymatic synthesis of lipid A molecules with four amide-linked acyl chains. LpxA acyltransferases selective for an analog of UDP-N-acetylglucosamine in which an amine replaces the 3"-hydroxyl group. *The Journal of biological chemistry* **279**, 25411-25419

38. Young, K., Silver, L. L., Bramhill, D., Cameron, P., Eveland, S. S., Raetz, C. R., Hyland, S. A., and Anderson, M. S. (1995) The envA permeability/cell division gene of Escherichia coli encodes the second enzyme of lipid A biosynthesis. UDP-3-O-(R-3-hydroxymyristoyl)-N-acetylglucosamine deacetylase. *The Journal of biological chemistry* **270**, 30384-30391

39. Kelly, T. M., Stachula, S. A., Raetz, C. R., and Anderson, M. S. (1993) The firA gene of Escherichia coli encodes UDP-3-O-(R-3-hydroxymyristoyl)-glucosamine

N-acyltransferase. The third step of endotoxin biosynthesis. *The Journal of biological chemistry* **268**, 19866-19874

40. Babinski, K. J., Ribeiro, A. A., and Raetz, C. R. (2002) The *Escherichia coli* gene encoding the UDP-2,3-diacylglucosamine pyrophosphatase of lipid A biosynthesis. *The Journal of biological chemistry* **277**, 25937-25946

41. Metzger, L. E., and Raetz, C. R. (2010) An Alternative Route for UDP-diacylglucosamine Hydrolysis in Bacterial Lipid A Biosynthesis. *Biochemistry*

42. Crowell, D. N., Anderson, M. S., and Raetz, C. R. (1986) Molecular cloning of the genes for lipid A disaccharide synthase and UDP-N-acetylglucosamine acyltransferase in Escherichia coli. *Journal of bacteriology* **168**, 152-159

43. Garrett, T. A., Kadrmas, J. L., and Raetz, C. R. (1997) Identification of the gene encoding the Escherichia coli lipid A 4'-kinase. Facile phosphorylation of endotoxin analogs with recombinant LpxK. *The Journal of biological chemistry* **272**, 21855-21864

44. Belunis, C. J., Clementz, T., Carty, S. M., and Raetz, C. R. (1995) Inhibition of lipopolysaccharide biosynthesis and cell growth following inactivation of the kdtA gene in Escherichia coli. *The Journal of biological chemistry* **270**, 27646-27652

45. White, K. A., Kaltashov, I. A., Cotter, R. J., and Raetz, C. R. (1997) A mono-functional 3-deoxy-D-manno-octulosonic acid (Kdo) transferase and a Kdo kinase in extracts of Haemophilus influenzae. *The Journal of biological chemistry* **272**, 16555-16563

46. Karow, M., Fayet, O., Cegielska, A., Ziegelhoffer, T., and Georgopoulos, C. (1991) Isolation and characterization of the Escherichia coli htrB gene, whose product is essential for bacterial viability above 33 degrees C in rich media. *Journal of bacteriology* **173**, 741-750

47. Doerrler, W. T., and Raetz, C. R. (2002) ATPase activity of the MsbA lipid flippase of Escherichia coli. *The Journal of biological chemistry* **277**, 36697-36705

48. Karow, M., and Georgopoulos, C. (1993) The essential Escherichia coli msbA gene, a multicopy suppressor of null mutations in the htrB gene, is related to the universally conserved family of ATP-dependent translocators. *Molecular microbiology* **7**, 69-79

49. Ward, A., Reyes, C. L., Yu, J., Roth, C. B., and Chang, G. (2007) Flexibility in the ABC transporter MsbA: Alternating access with a twist. *Proceedings of the National Academy of Sciences of the United States of America* **104**, 19005-19010

50. Reynolds, C. M., and Raetz, C. R. (2009) Replacement of lipopolysaccharide with free lipid A molecules in Escherichia coli mutants lacking all core sugars. *Biochemistry* **48**, 9627-9640

51. Mamat, U., Meredith, T. C., Aggarwal, P., Kuhl, A., Kirchhoff, P., Lindner, B., Hanuszkiewicz, A., Sun, J., Holst, O., and Woodard, R. W. (2008) Single amino acid substitutions in either YhjD or MsbA confer viability to 3-deoxy-d-manno-oct-2-ulosonic acid-depleted Escherichia coli. *Molecular microbiology* **67**, 633-648

52. Klena, J. D., Ashford, R. S., 2nd, and Schnaitman, C. A. (1992) Role of Escherichia coli K-12 rfa genes and the rfp gene of Shigella dysenteriae 1 in generation of lipopolysaccharide core heterogeneity and attachment of O antigen. *Journal of bacteriology* **174**, 7297-7307

53. Sperandeo, P., Cescutti, R., Villa, R., Di Benedetto, C., Candia, D., Deho, G., and Polissi, A. (2007) Characterization of lptA and lptB, two essential genes implicated in lipopolysaccharide transport to the outer membrane of Escherichia coli. *Journal of bacteriology* **189**, 244-253

54. Ruiz, N., Gronenberg, L. S., Kahne, D., and Silhavy, T. J. (2008) Identification of two inner-membrane proteins required for the transport of lipopolysaccharide to the outer membrane of Escherichia coli. *Proceedings of the National Academy of Sciences of the United States of America* **105**, 5537-5542

55. Sperandeo, P., Lau, F. K., Carpentieri, A., De Castro, C., Molinaro, A., Deho, G., Silhavy, T. J., and Polissi, A. (2008) Functional analysis of the protein machinery required for transport of lipopolysaccharide to the outer membrane of Escherichia coli. *Journal of bacteriology* **190**, 4460-4469

56. Okuda, S., Freinkman, E., and Kahne, D. (2012) Cytoplasmic ATP hydrolysis powers transport of lipopolysaccharide across the periplasm in E. coli. *Science* **338**, 1214-1217

57. Wu, T., McCandlish, A. C., Gronenberg, L. S., Chng, S. S., Silhavy, T. J., and Kahne, D. (2006) Identification of a protein complex that assembles lipopolysaccharide in the outer membrane of Escherichia coli. *Proceedings of the National Academy of Sciences of the United States of America* **103**, 11754-11759

58. Prost, L. R., and Miller, S. I. (2008) The Salmonellae PhoQ sensor: mechanisms of detection of phagosome signals. *Cellular microbiology* **10**, 576-582

59. Gunn, J. S. (2008) The Salmonella PmrAB regulon: lipopolysaccharide modifications, antimicrobial peptide resistance and more. *Trends in microbiology* **16**, 284-290

60. Jia, W., El Zoeiby, A., Petruzziello, T. N., Jayabalasingham, B., Seyedirashti, S., and Bishop, R. E. (2004) Lipid trafficking controls endotoxin acylation in outer membranes of Escherichia coli. *The Journal of biological chemistry* **279**, 44966-44975

61. Kato, A., Chen, H. D., Latifi, T., and Groisman, E. A. (2012) Reciprocal control between a bacterium's regulatory system and the modification status of its lipopolysaccharide. *Molecular cell* **47**, 897-908

62. Eguchi, Y., Itou, J., Yamane, M., Demizu, R., Yamato, F., Okada, A., Mori, H., Kato, A., and Utsumi, R. (2007) B1500, a small membrane protein, connects the two-component systems EvgS/EvgA and PhoQ/PhoP in Escherichia coli. *Proceedings of the National Academy of Sciences of the United States of America* **104**, 18712-18717

63. Lippa, A. M., and Goulian, M. (2009) Feedback inhibition in the PhoQ/PhoP signaling system by a membrane peptide. *PLoS genetics* **5**, e1000788

64. Kawasaki, K., Ernst, R. K., and Miller, S. I. (2005) Inhibition of Salmonella enterica serovar Typhimurium lipopolysaccharide deacylation by aminoarabinose membrane modification. *Journal of bacteriology* **187**, 2448-2457

65. Breazeale, S. D., Ribeiro, A. A., and Raetz, C. R. (2003) Origin of lipid A species modified with 4-amino-4-deoxy-L-arabinose in polymyxin-resistant mutants of Escherichia coli. An aminotransferase (ArnB) that generates UDP-4-deoxyl-L-arabinose. *The Journal of biological chemistry* **278**, 24731-24739

66. Bishop, R. E., Gibbons, H. S., Guina, T., Trent, M. S., Miller, S. I., and Raetz, C. R. (2000) Transfer of palmitate from phospholipids to lipid A in outer membranes of gram-negative bacteria. *The EMBO journal* **19**, 5071-5080

67. Lee, H., Hsu, F. F., Turk, J., and Groisman, E. A. (2004) The PmrA-regulated pmrC gene mediates phosphoethanolamine modification of lipid A and polymyxin resistance in Salmonella enterica. *Journal of bacteriology* **186**, 4124-4133

68. Gibbons, H. S., Kalb, S. R., Cotter, R. J., and Raetz, C. R. (2005) Role of Mg2+ and pH in the modification of Salmonella lipid A after endocytosis by macrophage tumour cells. *Molecular microbiology* **55**, 425-440

69. Reynolds, C. M., Kalb, S. R., Cotter, R. J., and Raetz, C. R. (2005) A phosphoethanolamine transferase specific for the outer 3-deoxy-D-manno-octulosonic acid residue of Escherichia coli lipopolysaccharide. Identification of the eptB gene and Ca2+ hypersensitivity of an eptB deletion mutant. *The Journal of biological chemistry* **280**, 21202-21211

70. Bishop, R. E. (2005) The lipid A palmitoyltransferase PagP: molecular mechanisms and role in bacterial pathogenesis. *Molecular microbiology* **57**, 900-912

71. Trent, M. S., Pabich, W., Raetz, C. R., and Miller, S. I. (2001) A PhoP/PhoQ-induced Lipase (PagL) that catalyzes 3-O-deacylation of lipid A precursors in membranes of Salmonella typhimurium. *The Journal of biological chemistry* **276**, 9083-9092

72. Reynolds, C. M., Ribeiro, A. A., McGrath, S. C., Cotter, R. J., Raetz, C. R., and Trent, M. S. (2006) An outer membrane enzyme encoded by Salmonella typhimurium lpxR that removes the 3'-acyloxyacyl moiety of lipid A. *The Journal of biological chemistry* **281**, 21974-21987

73. Gibbons, H. S., Lin, S., Cotter, R. J., and Raetz, C. R. (2000) Oxygen requirement for the biosynthesis of the S-2-hydroxymyristate moiety in Salmonella typhimurium lipid A. Function of LpxO, A new Fe2+/alpha-ketoglutarate-dependent dioxygenase homologue. *The Journal of biological chemistry* **275**, 32940-32949

74. Walsh, C. (2000) Molecular mechanisms that confer antibacterial drug resistance. *Nature* **406**, 775-781

75. Pop-Vicas, A., Tacconelli, E., Gravenstein, S., Lu, B., and D'Agata, E. M. (2009) Influx of multidrug-resistant, gram-negative bacteria in the hospital setting and the role of elderly patients with bacterial bloodstream infection. *Infect Control Hosp Epidemiol* **30**, 325-331

76. Pop-Vicas, A. E., and D'Agata, E. M. (2005) The rising influx of multidrug-resistant gram-negative bacilli into a tertiary care hospital. *Clin Infect Dis* **40**, 1792-1798

77. McClerren, A. L., Endsley, S., Bowman, J. L., Andersen, N. H., Guan, Z., Rudolph, J., and Raetz, C. R. (2005) A slow, tight-binding inhibitor of the zinc-dependent deacetylase LpxC of lipid A biosynthesis with antibiotic activity comparable to ciprofloxacin. *Biochemistry* **44**, 16574-16583

78. Cuny, G. D. (2009) A new class of UDP-3-O-(R-3-hydroxymyristol)-N-acetylglucosamine deacetylase (LpxC) inhibitors for the treatment of Gram-negative infections: PCT application WO 2008027466. *Expert Opin Ther Pat* **19**, 893-899

79. Clements, J. M., Coignard, F., Johnson, I., Chandler, S., Palan, S., Waller, A., Wijkmans, J., and Hunter, M. G. (2002) Antibacterial activities and characterization of novel inhibitors of LpxC. *Antimicrobial agents and chemotherapy* **46**, 1793-1799

80. Barb, A. W., Leavy, T. M., Robins, L. I., Guan, Z., Six, D. A., Zhou, P., Hangauer, M. J., Bertozzi, C. R., and Raetz, C. R. (2009) Uridine-based inhibitors as new leads for antibiotics targeting Escherichia coli LpxC. *Biochemistry* **48**, 3068-3077

81. Opiyo, S. O., Pardy, R. L., Moriyama, H., and Moriyama, E. N. (2010) Evolution of the Kdo2-lipid A biosynthesis in bacteria. *BMC Evol Biol* **10**, 362

82. Babinski, K. J., Kanjilal, S. J., and Raetz, C. R. (2002) Accumulation of the lipid A precursor UDP-2,3-diacylglucosamine in an *Escherichia coli* mutant lacking the lpxH gene. *The Journal of biological chemistry* **277**, 25947-25956

83. Zavaleta-Pastor, M., Sohlenkamp, C., Gao, J. L., Guan, Z., Zaheer, R., Finan, T. M., Raetz, C. R., Lopez-Lara, I. M., and Geiger, O. (2010) Sinorhizobium meliloti phospholipase C required for lipid remodeling during phosphorus limitation. *Proceedings of the National Academy of Sciences of the United States of America* **107**, 302-307

84. Rubin, E. J., O'Brien, J. P., Ivanov, P. L., Brodbelt, J. S., and Trent, M. S. (2014) Identification of a broad family of lipid A late acyltransferases with non-canonical substrate specificity. *Molecular microbiology* **91**, 887-899

85. Nishijima, M., Bulawa, C. E., and Raetz, C. R. (1981) Two interacting mutations causing temperature-sensitive phosphatidylglycerol synthesis in Escherichia coli membranes. *Journal of bacteriology* **145**, 113-121

86. Nishijima, M., and Raetz, C. R. (1981) Characterization of two membrane-associated glycolipids from an Escherichia coli mutant deficient in phosphatidylglycerol. *The Journal of biological chemistry* **256**, 10690-10696

87. Raetz, C. R., Purcell, S., Meyer, M. V., Qureshi, N., and Takayama, K. (1985) Isolation and characterization of eight lipid A precursors from a 3-deoxy-D-manno-octylosonic acid-deficient mutant of Salmonella typhimurium. *The Journal of biological chemistry* **260**, 16080-16088

88. Strain, S. M., Armitage, I. M., Anderson, L., Takayama, K., Qureshi, N., and Raetz, C. R. (1985) Location of polar substituents and fatty acyl chains on lipid A precursors from a 3-deoxy-D-manno-octulosonic acid-deficient mutant of Salmonella typhimurium. Studies by 1H, 13C, and 31P nuclear magnetic resonance. *The Journal of biological chemistry* **260**, 16089-16098

89. Bulawa, C. E., and Raetz, C. R. (1984) The biosynthesis of gram-negative endotoxin. Identification and function of UDP-2,3-diacylglucosamine in Escherichia coli. *The Journal of biological chemistry* **259**, 4846-4851

90. Ray, B. L., Painter, G., and Raetz, C. R. (1984) The biosynthesis of gram-negative endotoxin. Formation of lipid A disaccharides from monosaccharide precursors in extracts of Escherichia coli. *The Journal of biological chemistry* **259**, 4852-4859

91. Bulawa, C. E., and Raetz, C. R. (1984) Isolation and characterization of Escherichia coli strains defective in CDP-diglyceride hydrolase. *The Journal of biological chemistry* **259**, 11257-11264

92. Raetz, C. R., Hirschberg, C. B., Dowhan, W., Wickner, W. T., and Kennedy, E. P. (1972) A membrane-bound pyrophosphatase in Escherichia coli catalyzing the hydrolysis of cytidine diphosphate-diglyceride. *The Journal of biological chemistry* **247**, 2245-2247

93. Raetz, C. R., Dowhan, W., and Kennedy, E. P. (1976) Partial purification and characterization of cytidine 5'-diphosphate-diglyceride hydrolase from membranes of Escherichia coli. *Journal of bacteriology* **125**, 855-863

94. Icho, T., Bulawa, C. E., and Raetz, C. R. (1985) Molecular cloning and sequencing of the gene for CDP-diglyceride hydrolase of Escherichia coli. *The Journal of biological chemistry* **260**, 12092-12098

95. Anderson, M. S., Bulawa, C. E., and Raetz, C. R. (1985) The biosynthesis of gram-negative endotoxin. Formation of lipid A precursors from UDP-GlcNAc in extracts of Escherichia coli. *The Journal of biological chemistry* **260**, 15536-15541

96. Metzger, L. E. t., Lee, J. K., Finer-Moore, J. S., Raetz, C. R., and Stroud, R. M. (2012) LpxI structures reveal how a lipid A precursor is synthesized. *Nat Struct Mol Biol* **19**, 1132-1138

97. Doolittle, R. F. (1994) Convergent evolution: the need to be explicit. *Trends Biochem Sci* **19**, 15-18

98. Omelchenko, M. V., Galperin, M. Y., Wolf, Y. I., and Koonin, E. V. (2010) Non-homologous isofunctional enzymes: a systematic analysis of alternative solutions in enzyme evolution. *Biol Direct* **5**, 31

99. Gherardini, P. F., Wass, M. N., Helmer-Citterich, M., and Sternberg, M. J. (2007) Convergent evolution of enzyme active sites is not a rare phenomenon. *Journal of molecular biology* **372**, 817-845

100. Ago, H., Oda, M., Takahashi, M., Tsuge, H., Ochi, S., Katunuma, N., Miyano, M., and Sakurai, J. (2006) Structural basis of the sphingomyelin phosphodiesterase activity in neutral sphingomyelinase from *Bacillus cereus*. *The Journal of biological chemistry* **281**, 16157-16167

101. Zhuo, S., Clemens, J. C., Stone, R. L., and Dixon, J. E. (1994) Mutational analysis of a Ser/Thr phosphatase. Identification of residues important in phosphoesterase substrate binding and catalysis. *The Journal of biological chemistry* **269**, 26234-26238

102. Aravind, L., and Koonin, E. V. (1998) Phosphoesterase domains associated with DNA polymerases of diverse origins. *Nucleic acids research* **26**, 3746-3752

103. Mitic, N., Smith, S. J., Neves, A., Guddat, L. W., Gahan, L. R., and Schenk, G. (2006) The catalytic mechanisms of binuclear metallohydrolases. *Chem Rev* **106**, 3338-3363

104. Battistuzzi, G., Dietrich, M., Locke, R., and Witzel, H. (1997) Evidence for a conserved binding motif of the dinuclear metal site in mammalian and plant purple acid phosphatases: 1H NMR studies of the di-iron derivative of the Fe(III)Zn(II) enzyme from kidney bean. *The Biochemical journal* **323 (Pt 3)**, 593-596

105. Cleland, W. W., and Hengge, A. C. (2006) Enzymatic mechanisms of phosphate and sulfate transfer. *Chem Rev* **106**, 3252-3278

106. White, D. J., Reiter, N. J., Sikkink, R. A., Yu, L., and Rusnak, F. (2001) Identification of the high affinity Mn2+ binding site of bacteriophage lambda phosphoprotein phosphatase: effects of metal ligand mutations on electron paramagnetic resonance spectra and phosphatase activities. *Biochemistry* **40**, 8918-8929

107. Dismukes, G. C. (1996) Manganese Enzymes with Binuclear Active Sites. *Chem Rev* **96**, 2909-2926

108. Liechti, G. W., Kuru, E., Hall, E., Kalinda, A., Brun, Y. V., VanNieuwenhze, M., and Maurelli, A. T. (2014) A new metabolic cell-wall labelling method reveals peptidoglycan in Chlamydia trachomatis. *Nature* **506**, 507-510

109. Bastidas, R. J., Elwell, C. A., Engel, J. N., and Valdivia, R. H. (2013) Chlamydial intracellular survival strategies. *Cold Spring Harbor perspectives in medicine* **3**, a010256

110. Bavoil, P., Ohlin, A., and Schachter, J. (1984) Role of disulfide bonding in outer membrane structure and permeability in Chlamydia trachomatis. *Infection and immunity* **44**, 479-485

111. Hatch, T. P., Allan, I., and Pearce, J. H. (1984) Structural and polypeptide differences between envelopes of infective and reproductive life cycle forms of Chlamydia spp. *Journal of bacteriology* **157**, 13-20

112. Caldwell, H. D., Kromhout, J., and Schachter, J. (1981) Purification and partial characterization of the major outer membrane protein of Chlamydia trachomatis. *Infection and immunity* **31**, 1161-1176

113. Belland, R. J., Zhong, G., Crane, D. D., Hogan, D., Sturdevant, D., Sharma, J., Beatty, W. L., and Caldwell, H. D. (2003) Genomic transcriptional profiling of the developmental cycle of Chlamydia trachomatis. *Proceedings of the National Academy of Sciences of the United States of America* **100**, 8478-8483

114. Andersson, J. O., and Andersson, S. G. (1999) Insights into the evolutionary process of genome degradation. *Current opinion in genetics & development* **9**, 664-671

115. McCoy, A. J., Adams, N. E., Hudson, A. O., Gilvarg, C., Leustek, T., and Maurelli, A. T. (2006) L,L-diaminopimelate aminotransferase, a trans-kingdom enzyme shared by Chlamydia and plants for synthesis of diaminopimelate/lysine. *Proceedings of the National Academy of Sciences of the United States of America* **103**, 17909-17914

116. Binet, R., Fernandez, R. E., Fisher, D. J., and Maurelli, A. T. (2011) Identification and characterization of the Chlamydia trachomatis L2 S-adenosylmethionine transporter. *mBio* **2**, e00051-00011

117. Demars, R., Weinfurter, J., Guex, E., Lin, J., and Potucek, Y. (2007) Lateral gene transfer in vitro in the intracellular pathogen Chlamydia trachomatis. *Journal of bacteriology* **189**, 991-1003

118. DeMars, R., and Weinfurter, J. (2008) Interstrain gene transfer in Chlamydia trachomatis in vitro: mechanism and significance. *Journal of bacteriology* **190**, 1605-1614

119. Wang, Y., Kahane, S., Cutcliffe, L. T., Skilton, R. J., Lambden, P. R., and Clarke, I. N. (2011) Development of a transformation system for Chlamydia trachomatis: restoration of glycogen biosynthesis by acquisition of a plasmid shuttle vector. *PLoS pathogens* **7**, e1002258

120. Wickstrum, J., Sammons, L. R., Restivo, K. N., and Hefty, P. S. (2013) Conditional gene expression in Chlamydia trachomatis using the tet system. *PloS one* **8**, e76743

121. Sisko, J. L., Spaeth, K., Kumar, Y., and Valdivia, R. H. (2006) Multifunctional analysis of Chlamydia-specific genes in a yeast expression system. *Molecular microbiology* **60**, 51-66

122. Subtil, A., Parsot, C., and Dautry-Varsat, A. (2001) Secretion of predicted Inc proteins of Chlamydia pneumoniae by a heterologous type III machinery. *Molecular microbiology* **39**, 792-800

123. Nguyen, B. D., and Valdivia, R. H. (2013) Forward genetic approaches in Chlamydia trachomatis. *Journal of visualized experiments : JoVE*, e50636

124. Lucast, L. J., Batey, R. T., and Doudna, J. A. (2001) Large-scale purification of a stable form of recombinant tobacco etch virus protease. *Biotechniques* **30**, 544-546, 548, 550 passim

125. Miroux, B., and Walker, J. E. (1996) Over-production of proteins in Escherichia coli: mutant hosts that allow synthesis of some membrane proteins and globular proteins at high levels. *Journal of molecular biology* **260**, 289-298

126. Bligh, E. G., and Dyer, W. J. (1959) A rapid method of total lipid extraction and purification. *Can J Biochem Physiol* **37**, 911-917

127. Radika, K., and Raetz, C. R. (1988) Purification and properties of lipid A disaccharide synthase of *Escherichia coli*. *The Journal of biological chemistry* **263**, 14859-14867

128. Mildvan, A. S., Xia, Z., Azurmendi, H. F., Saraswat, V., Legler, P. M., Massiah, M. A., Gabelli, S. B., Bianchet, M. A., Kang, L. W., and Amzel, L. M. (2005) Structures and mechanisms of Nudix hydrolases. *Arch Biochem Biophys* **433**, 129-143

129. Belford., A. I. S. a. R. L. (1995) Rapid quantitation from inhomogeneously broadened EPR spectra by a fast convolution algorithm. *Journal of Magnetic Resonance A* **113**, 65-73

130. Rusnak, F., Yu, L., Todorovic, S., and Mertz, P. (1999) Interaction of bacteriophage lambda protein phosphatase with Mn(II): evidence for the formation of a [Mn(II)]2 cluster. *Biochemistry* **38**, 6943-6952

131. Golombek, A. P., and Hendrich, M. P. (2003) Quantitative analysis of dinuclear manganese(II) EPR spectra. *J Magn Reson* **165**, 33-48

132. Epel, B., Schafer, K. O., Quentmeier, A., Friedrich, C., and Lubitz, W. (2005) Multifrequency EPR analysis of the dimanganese cluster of the putative sulfate thiohydrolase SoxB of *Paracoccus pantotrophus*. *J Biol Inorg Chem* **10**, 636-642

133. Blanchard, S., Blain, G., Riviere, E., Nierlich, M., and Blondin, G. (2003) Temperature dependence of X- and Q-band EPR spectra of the dinuclear manganese(II) complex [(NO2Bpmp)Mn2(mu-OAc)2]+: determination of the exchange constant and of the spin parameters for the S=1, 2, and 3 spin states. *Chemistry* **9**, 4260-4268

134. P. Mathur, M. C., and G. C. Dismukes. (1987) Dimanganese(II) complexes of a septadentate ligand. Functional analogs of the manganese pseudocatalase. *Journal of the American Chemical Society* **109**, 5227-5233

135. Howard, T., Telser, J., and DeRose, V. J. (2000) An electron paramagnetic resonance study of Mn2(H2O)(OAc)4(tmeda)2 (tmeda = N,N,N',N'-tetramethylethylenediamine): a model for dinuclear manganese enzyme active sites. *Inorganic chemistry* **39**, 3379-3385

136. Reed, G. H. M., G. D. . (1984). in *Biological Magnetic Resonance*, Plenum Press, New York. pp 73-135

137. Blanchard, S., Blondin, G., Riviere, E., Nierlich, M., and Girerd, J. J. (2003) X- and Q-band EPR studies of the dinuclear Mn(II) complex [(Bpmp)Mn2(mu-OAc)2]+. Determination of the spin parameters for the S = 1 and S = 2 spin states. *Inorganic chemistry* **42**, 4568-4578

138. Partha Chakraborty, S. K. C. (1994) Synthesis, structure, EPR and electrochemical studies of a μ2-phenoxo bridged manganese(II) dimer afforded by a binucleating macrocylic ligand. *Polyhedron* **13**, 683-687

139. Dimitris P. Kessissoglou, X. L., William M. Butler, and Vincent L. Pecoraro. (1987) Mononuclear manganese(IV) complexes of hydroxyl-rich Schiff base ligands. *Inorganic chemistry* **26**, 2487-2492

140. Bouchra Mabad, P. C., Jean Pierre Tuchagues, and David N. Hendrickson. (1986) Manganese(II) complexes of polydentate Schiff bases. 1. Synthesis, characterization, magnetic properties, and molecular structure. *Inorganic chemistry* **25**, 1420-1431

141. P. Mathur, G. C. D. (1983) Models for the photosynthetic water oxidizing enzyme. 2. Electronic, magnetic, and EPR characterization of a binuclear manganese(II) semiquinone complex. *Journal of the American Chemical Society* **105**, 7093-7098

142. Hayden, J. A., and Hendrich, M. P. (2010) EPR spectroscopy and catalase activity of manganese-bound DNA-binding protein from nutrient starved cells. *J Biol Inorg Chem* **15**, 729-736

143. Gelasco, A., Kirk, M. L., Kampf, J. W., and Pecoraro, V. L. (1997) The [Mn(2)(2-OHsalpn)(2)](2-,-,0,+) System: Synthesis, Structure, Spectroscopy, and Magnetism of the First Structurally Characterized Dinuclear Manganese Series Containing Four Distinct Oxidation States. *Inorganic chemistry* **36**, 1829-1837

144. Theodora D. Tzimaa, E. F. D. M., Vasilios S. Melissas, Yiannis Sanakis, Panayotis Kyritsis (2013) Electronic and magnetic properties of the binuclear [Mn2{(OPPh2)2N}4] complex, as revealed by magnetometry, EPR and density functional broken-symmetry studies *Polyhedron* **52**, 706–712

145. Sharples, G. J., and Leach, D. R. (1995) Structural and functional similarities between the SbcCD proteins of *Escherichia coli* and the RAD50 and MRE11 (RAD32) recombination and repair proteins of yeast. *Molecular microbiology* **17**, 1215-1217

146. Wehenkel, A., Bellinzoni, M., Schaeffer, F., Villarino, A., and Alzari, P. M. (2007) Structural and binding studies of the three-metal center in two mycobacterial PPM Ser/Thr protein phosphatases. *Journal of molecular biology* **374**, 890-898

147. Su, J., Schlicker, C., and Forchhammer, K. (2011) A third metal is required for catalytic activity of the signal-transducing protein phosphatase M tPphA. *The Journal of biological chemistry* **286**, 13481-13488

148. Rantanen, M. K., Lehtio, L., Rajagopal, L., Rubens, C. E., and Goldman, A. (2007) Structure of *Streptococcus agalactiae* serine/threonine phosphatase. The subdomain conformation is coupled to the binding of a third metal ion. *FEBS J* **274**, 3128-3137

149. Goldberg, J., Huang, H. B., Kwon, Y. G., Greengard, P., Nairn, A. C., and Kuriyan, J. (1995) Three-dimensional structure of the catalytic subunit of protein serine/threonine phosphatase-1. *Nature* **376**, 745-753

150. Voegtli, W. C., White, D. J., Reiter, N. J., Rusnak, F., and Rosenzweig, A. C. (2000) Structure of the bacteriophage lambda Ser/Thr protein phosphatase with sulfate ion bound in two coordination modes. *Biochemistry* **39**, 15365-15374

151. Schenk, G., Carrington, L. E., Hamilton, S. E., de Jersey, J., and Guddat, L. W. (1999) Crystallization and preliminary X-ray diffraction data for a purple acid phosphatase from sweet potato. *Acta crystallographica. Section D, Biological crystallography* **55**, 2051-2052

152. Hopfner, K. P., Karcher, A., Craig, L., Woo, T. T., Carney, J. P., and Tainer, J. A. (2001) Structural biochemistry and interaction architecture of the DNA double-strand break repair Mre11 nuclease and Rad50-ATPase. *Cell* **105**, 473-485

153. Qureshi, N., Kaltashov, I., Walker, K., Doroshenko, V., Cotter, R. J., Takayama, K., Sievert, T. R., Rice, P. A., Lin, J. S., and Golenbock, D. T. (1997) Structure of

the monophosphoryl lipid A moiety obtained from the lipopolysaccharide of Chlamydia trachomatis. *The Journal of biological chemistry* **272**, 10594-10600

154. Miller, J. H. (1972) *Experiments in molecular genetics*, Cold Spring Harbor Laboratory Press, Plainview, NY

155. Doerrler, W. T., Reedy, M. C., and Raetz, C. R. (2001) An Escherichia coli mutant defective in lipid export. *The Journal of biological chemistry* **276**, 11461-11464

156. Hamilton, C. M., Aldea, M., Washburn, B. K., Babitzke, P., and Kushner, S. R. (1989) New method for generating deletions and gene replacements in Escherichia coli. *Journal of bacteriology* **171**, 4617-4622

157. Young, H. E., Donohue, M. P., Smirnova, T. I., Smirnov, A. I., and Zhou, P. (2013) The UDP-diacylglucosamine pyrophosphohydrolase LpxH in lipid A biosynthesis utilizes Mn2+ cluster for catalysis. *The Journal of biological chemistry* **288**, 26987-27001

158. Roan, N. R., Gierahn, T. M., Higgins, D. E., and Starnbach, M. N. (2006) Monitoring the T cell response to genital tract infection. *Proceedings of the National Academy of Sciences of the United States of America* **103**, 12069-12074

159. Metzger, L. E. t., and Raetz, C. R. An alternative route for UDP-diacylglucosamine hydrolysis in bacterial lipid A biosynthesis. *Biochemistry* **49**, 6715-6726

160. McCoy, A. J., Sandlin, R. C., and Maurelli, A. T. (2003) In vitro and in vivo functional activity of Chlamydia MurA, a UDP-N-acetylglucosamine enolpyruvyl transferase involved in peptidoglycan synthesis and fosfomycin resistance. *Journal of bacteriology* **185**, 1218-1228

161. Anderson, M. S., and Raetz, C. R. (1987) Biosynthesis of lipid A precursors in Escherichia coli. A cytoplasmic acyltransferase that converts UDP-N-acetylglucosamine to UDP-3-O-(R-3-hydroxymyristoyl)-N-acetylglucosamine. *The Journal of biological chemistry* **262**, 5159-5169

162. Anderson, M. S., Robertson, A. D., Macher, I., and Raetz, C. R. (1988) Biosynthesis of lipid A in Escherichia coli: identification of UDP-3-O-[(R)-3-hydroxymyristoyl]-alpha-D-glucosamine as a precursor of UDP-N2,O3-bis[(R)-3-hydroxymyristoyl]-alpha-D-glucosamine. *Biochemistry* **27**, 1908-1917

163. Larkin, M. A., Blackshields, G., Brown, N. P., Chenna, R., McGettigan, P. A., McWilliam, H., Valentin, F., Wallace, I. M., Wilm, A., Lopez, R., Thompson, J. D., Gibson, T. J., and Higgins, D. G. (2007) Clustal W and Clustal X version 2.0. *Bioinformatics* **23**, 2947-2948

164. Takayama, K., Qureshi, N., Mascagni, P., Nashed, M. A., Anderson, L., and Raetz, C. R. (1983) Fatty acyl derivatives of glucosamine 1-phosphate in Escherichia coli and their relation to lipid A. Complete structure of A diacyl GlcN-1-P found in a phosphatidylglycerol-deficient mutant. *The Journal of biological chemistry* **258**, 7379-7385

165. Tarbouriech, N., Buisson, M., Seigneurin, J. M., Cusack, S., and Burmeister, W. P. (2005) The monomeric dUTPase from Epstein-Barr virus mimics trimeric dUTPases. *Structure* **13**, 1299-1310

166. Homma, K., and Moriyama, H. (2009) Crystallization and crystal-packing studies of Chlorella virus deoxyuridine triphosphatase. *Acta crystallographica. Section F, Structural biology and crystallization communications* **65**, 1030-1034

167. Monteferrante, C. G., Miethke, M., van der Ploeg, R., Glasner, C., and van Dijl, J. M. (2012) Specific targeting of the metallophosphoesterase YkuE to the bacillus cell wall requires the twin-arginine translocation system. *The Journal of biological chemistry* **287**, 29789-29800

168. Wyckoff, T. J., and Raetz, C. R. (1999) The active site of Escherichia coli UDP-N-acetylglucosamine acyltransferase. Chemical modification and site-directed mutagenesis. *The Journal of biological chemistry* **274**, 27047-27055

169. Williams, A. H., Immormino, R. M., Gewirth, D. T., and Raetz, C. R. (2006) Structure of UDP-N-acetylglucosamine acyltransferase with a bound antibacterial pentadecapeptide. *Proceedings of the National Academy of Sciences of the United States of America* **103**, 10877-10882

170. Bartling, C. M., and Raetz, C. R. (2009) Crystal structure and acyl chain selectivity of Escherichia coli LpxD, the N-acyltransferase of lipid A biosynthesis. *Biochemistry* **48**, 8672-8683

Biography

Hayley Elizabeth Young was born August 6, 1986 in Atwood, Kansas. She spent her childhood in Bird City, Kansas, attending Cheylin USD 103 from kindergarten through high school. During this time, Hayley developed a curiosity in the world around her; this interest in science was nurtured by her teachers and especially by her father. After graduating Cheylin High School in 2004, Hayley began her collegiate education at Creighton University in Omaha, Nebraska. There, she was able to take her scientific pursuits from the classroom into the laboratory, completing organic synthesis research with Dr. Martin Hulce in the Department of Chemistry. Hayley also worked as a research technician in the lab of Dr. Lucy Wrenshall and Dr. John Miller at the University of Nebraska Medical Center in Omaha. Hayley graduated from Creighton in 2008 with a B.S. in Chemistry and subsequently began her doctoral studies in the Department of Biochemistry at Duke University. She joined the lab of Dr. Christian R. H. Raetz in 2009. After the passing of Dr. Raetz, Hayley continued her Ph.D. under the supervision of Dr. Pei Zhou.

Hayley's publications at Duke University include:

Young, H. E., Donohue, M. P., Smirnova, T. I., Smirnov, A. I., Zhou, P. (2013). The UDP-diacylglucosamine pyrophosphohydrolase LpxH in lipid A biosynthesis utilizes a Mn2+ cluster for catalysis. J Biol Chem 288 (38), 26987-27001.

Young, H. E., Valdivia, R. H., Zhou, P. Identification of the UDP-2,3-diacylglucosamine hydrolase in *C. trachomatis. (in preparation)*